AD-A043 304 TORONTO UNIV (ONTARIO) INST FOR AEROSPACE STUDIES F/G 20/4
PRESSURE MEASUREMENTS AT THE FOCUS OF COMBUSTION-DRIVEN IMPLOSI--ETC(U)
APR 77 B VASUDEVAN AF-AFOSR-3303-77
UNCLASSIFIED UTIAS-TN-209 AFOSR-TR-77-0949 NL

| OF |
AD
A043 304

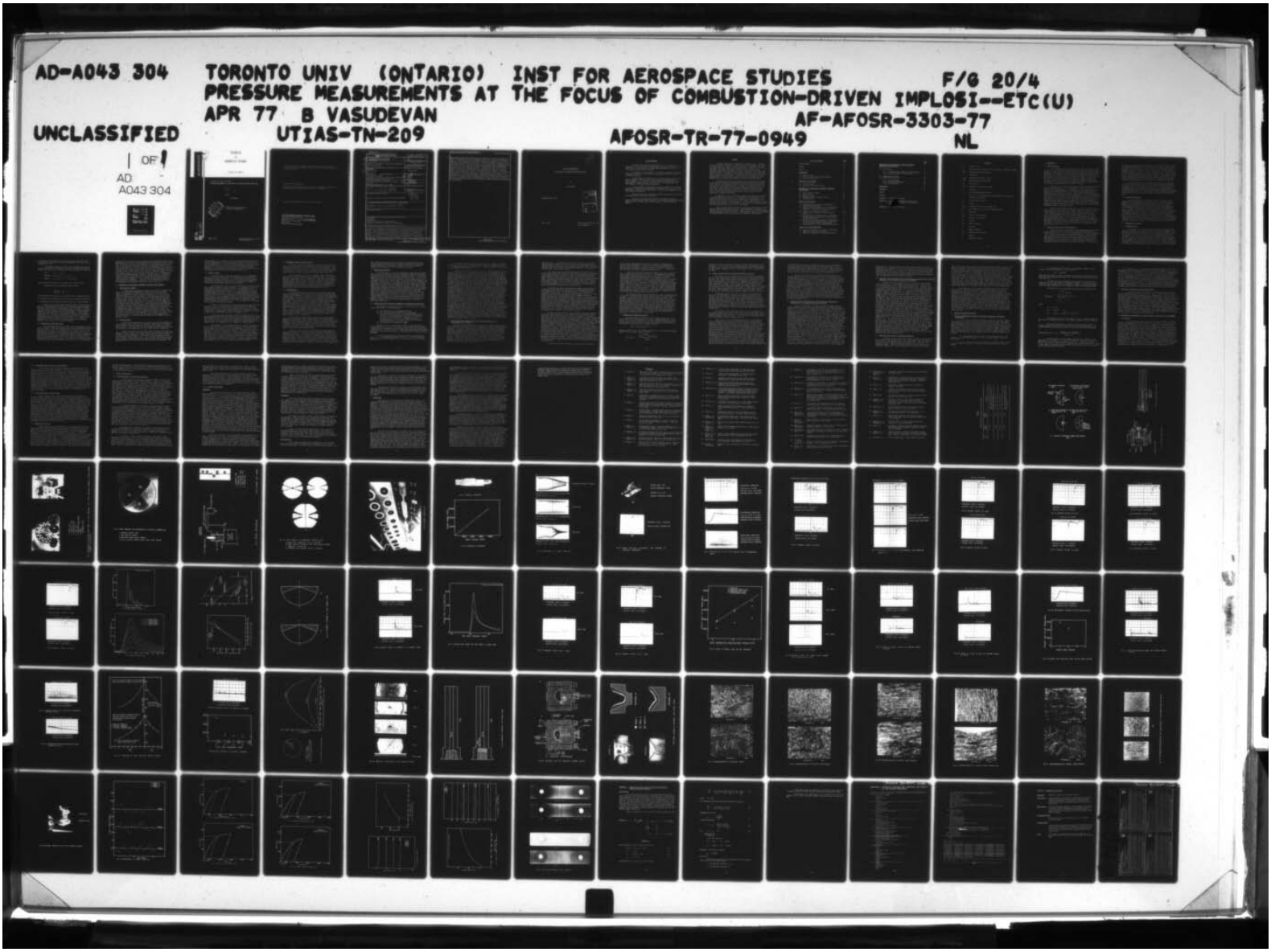

INSTITUTE
FOR
AEROSPACE STUDIES

UNIVERSITY OF TORONTO

AFOSR-TR- 77-0949

PRESSURE MEASUREMENTS AT THE FOCUS OF COMBUSTION-DRIVEN IMPLOSIONS

by

B. Vasudevan

April, 1977

UTIAS Technical Note No. 209
CN ISSN 0082-5263

Qualified requestors may obtain additional copies from the Defense Documentation Center, all others should apply to the National Technical Information Service.

Conditions of Reproduction:

Reproduction, translation, publication, use and disposal in whole or in part by or for the United States Government is permitted.

Approved for public release; distribution unlimited.

AIR FORCE OFFICE OF SCIENTIFIC RESEARCH (AFSC)
NOTICE OF TRANSMITTAL TO DDC
This technical report has been reviewed and is approved for public release IAW AFR 190-12 (7b).
Distribution is unlimited.
A. D. BLOSE
Technical Information Officer

UNCLASSIFIED

SECURITY CLASSIFICATION OF THIS PAGE (When Data Entered)

REPORT DOCUMENTATION PAGE	READ INSTRUCTIONS BEFORE COMPLETING FORM
1. REPORT NUMBER (14) AFOSR-TR-77-0949	2. GOVT ACCESSION NO. / 3. RECIPIENT'S CATALOG NUMBER (9)
4. TITLE (and Subtitle) (6) PRESSURE MEASUREMENTS AT THE FOCUS OF COMBUSTION-DRIVEN IMPLOSIONS	5. TYPE OF REPORT & PERIOD COVERED INTERIM (rep.)
	6. PERFORMING ORG. REPORT NUMBER UTIAS Tch Not.No 209
7. AUTHOR(s) (10) B. VASUDEVAN	8. CONTRACT OR GRANT NUMBER(s) AFOSR 77-3303
9. PERFORMING ORGANIZATION NAME AND ADDRESS UNIVERSITY OF TORONTO INSTITUTE FOR AEROSPACE STUDIES/4925 DUFFERIN ST DOWNSVIEW, ONTARIO, CANADA, M3H 5T6	10. PROGRAM ELEMENT, PROJECT, TASK AREA & WORK UNIT NUMBERS (16) 2307A3 61102F
11. CONTROLLING OFFICE NAME AND ADDRESS AIR FORCE OFFICE OF SCIENTIFIC RESEARCH/NA (11) BLDG 410 BOLLING AIR FORCE BASE, D C 20332	12. REPORT DATE April 1977
	13. NUMBER OF PAGES 93
14. MONITORING AGENCY NAME & ADDRESS (if different from Controlling Office) (14) UTIAS-TN-209	15. SECURITY CLASS. (of this report) UNCLASSIFIED
	15a. DECLASSIFICATION/DOWNGRADING SCHEDULE

16. DISTRIBUTION STATEMENT (of this Report) (12) 96 p.

Approved for public release; distribution unlimited.

17. DISTRIBUTION STATEMENT (of the abstract entered in Block 20, if different from Report)

(15) AF-AFOSR-3303-77

18. SUPPLEMENTARY NOTES

19. KEY WORDS (Continue on reverse side if necessary and identify by block number)

IMPLOSIONS
DETONATIONS
PRESSURE MEASUREMENTS AT IMPLOSION FOCUS
CHANGES IN STRUCUTRE OF COPPER DUE TO IMPLOSIONS

20. ABSTRACT (Continue on reverse side if necessary and identify by block number)

A detailed experimental imvestigation was made of time-resolved pressure histories at the focus of combustion-driven implosions in the UTIAS 20 cm diam Implosion Chamber. Gaseous mixtures of stoichiometric hydrogen and oxygen were used in the initial pressure range 1.7 atm (25 psi) to 6.8 atm (100 psi). The gaseous mixtures were detonated using exploding wires. Extended records from a PCB 119M08, 6.3 mm diam piezoelectric pressure transducer gave detailed (averaged) pressure-time histories of initial and subsequent implosions. A 20-degree conical liner (normally used to protect the front plate of the implosion chamber

DD FORM 1 JAN 73 1473 EDITION OF 1 NOV 65 IS OBSOLETE

118 920

UNCLASSIFIED

SECURITY CLASSIFICATION OF THIS PAGE (When Data Entered)

from damaging off-centerd explosive-driven implosions) was used to determine its effect on the pressure histories obtained at the focus of gas-driven implosions. Owing to its deviation from a cone near the apex, the presence of such a liner reduced the peak pressures by about 45%. This fact allowed an indirect estimate of the peak pressure for a 6.8 atm (100 psi) initial pressure run. However, when the conical liner was accurately made, the peak pressures were identical with those without it, as expected from theory. The actual location of the focal point was determined by taking imprints of implosions on lead witness plates placed at the origin. The imprints were sharp and well-focussed. A maximum degree of off-centredness of about 3/4 mm from the origin, resulted in a reduction of only about 2% in average pressures. Copper witness plates, subjected to explosive-driven implosions were analyzed using metallurgical techniques. Photomicrographs were taken of the imploded specimen which illustrated the changes in grain size and shape arising from the passage of strong shock waves. Microhardness changes were determined to yield approximate values of peak pressures reached in the specimens.

(12)

PRESSURE MEASUREMENTS

AT THE FOCUS OF COMBUSTION-DRIVEN IMPLOSIONS

by

B. Vasudevan

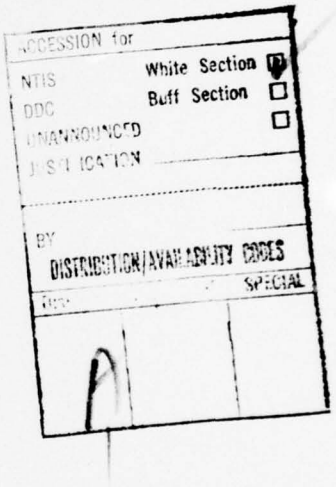

Submitted April, 1977.

April, 1977.

UTIAS Technical Note No. 209
CN ISSN 0082-5263

Acknowledgements

I should like to express my gratitude to Dr. I. I. Glass, my supervisor, for providing me the opportunity to work on this project. His supervision, advice, interest and understanding throughout the course of this project are very much appreciated.

I should also like to thank Dr. G. Nuffield, Department of Geology, University of Toronto, for many helpful discussions and advice on X-ray diffraction analysis.

Sincere thanks are offered to Dr. R. A. Roig for his active contributions, helpful discussions and critical reading of the manuscript. I wish to thank Dr. J. J. Gottlieb for stimulating discussions and friendly encouragement. Thanks are also extended to Mr. N. N. Wabka and Mr. Ole Holst-Jensen for many interesting discussions.

I wish to thank our technician Mr. Reinhard Gnoyke for his valuable assistance in developing new exploding-wire techniques and carrying out the experiments. Thanks are due to the staff of the U.T.I.A.S. machine shop for their technical assistance.

The moral support and stimulation provided by my parents and brothers were helpful and are very much appreciated.

This work was financially supported by the National Research Council of Canada and the United States Air Force Office of Scientific Research under Grant No. AF-AFOSR 77-3303; this assistance is acknowledged with thanks.

Summary

A detailed experimental investigation was made of time - resolved pressure histories at the focus of combustion-driven implosions in the UTIAS 20 cm diam Implosion Chamber. Gaseous mixtures of stoichiometric hydrogen and oxygen were used in the initial pressure range 1.7 atm (25 psi) to 6.8 atm (100 psi). The gaseous mixtures were detonated using exploding wires. Extended records from a PCB 119M08, 6.3 mm dia piezoelectric pressure transducer gave detailed (averaged) pressure-time histories of initial and subsequent implosions. The effects were determined of diluting the stoichiometric mixture with hydrogen and helium. The critical dilution index was found experimentally. It represents the amount of helium or hydrogen dilution at which the present ignition system failed to produce a detonation wave.

A 20-degree conical liner (normally used to protect the front plate of the implosion chamber from damaging off-centered explosive-driven implosions) was used to determine its effect on the pressure histories obtained at the focus of gas-driven implosions. Owing to its deviation from a cone near the apex, the presence of such a liner reduced the peak pressures by about 45%. This fact allowed an indirect estimate of the peak pressure for a 6.8 atm (100 psi) initial pressure run. However, when the conical liner was accurately made, the peak pressures were identical with those without it, as expected from theory.

A numerical analysis of off-centre implosions predicted the decrease of average pressures as a function of the degree of off-centredness. The actual location of the focal point was determined by taking imprints of implosions on lead witness plates placed at the origin. The imprints were sharp and well-focussed. A maximum degree of off-centredness of about 3/4 mm from the origin, resulted in a reduction of only about 2% in average pressures. This was well within the accuracy of the experiments.

Copper witness plates, subjected to explosive-driven implosions, were analyzed using metallurgical techniques. Photomicrographs were taken of the imploded specimen which illustrated the changes in grain size and shape arising from the passage of strong shock waves. Microhardness changes were determined to yield approximate values of peak pressures reached in the specimens.

Table of Contents

		Page
	Acknowledgement	ii
	Summary	iii
	Notation	vi
1.	INTRODUCTION	1
	1.1 Historical Note	1
	1.2 Extent of Earlier Pressure Measurements	1
	1.3 Scope of Present Work	2
2.	COMBUSTION WAVE DYNAMICS	2
	2.1 Detonation Phase	2
	2.2 Implosion and Reflection Phase	3
3.	DESCRIPTION OF EXPERIMENTAL EQUIPMENT, APPARATUS AND PROCEDURE	4
	3.1 UTIAS Implosion Chamber	4
	3.2 Explosive Liner	4
	3.3 Ignition System	5
	3.4 Combustion Chamber Loading Procedure	6
	3 5 Instrumentation	6
4.	RESULTS AND DISCUSSION	7
	4.1 Initial Conditions Leading to Detonating or Deflagrating Combustion	7
	4.2 Records of Pressure-Time History for Detonating Combustion of Stoichiometric H_2-O_2 Mixtures	8
	4.3 Comparison with Numerical Results	10
	4.4 Effect of Conical Liners on Pressure History at Focus	11
	4.5 Records of Pressure-Time History for Detonating and Deflagrating Combustions of H_2-O_2 Mixtures Diluted with Helium	12
	4.6 Records of Pressure-Time History for Detonating, Deflagrating and Transition-Type of Combustion of H_2-O_2 Mixtures Diluted with Hydrogen	13
	4.7 Cycle Time and Records of Subsequent Implosions	13
5.	STUDY OF OFF-CENTRE IMPLOSIONS	14
	5.1 Numerical Computations of Effects of Off-Centre Implosions on Pressure at Origin	14
	5.2 Imprints of Implosions on Lead Witness Plates	16

		Page
6.	METALLURGICAL CORROBORATION OF PEAK PRESSURES AT IMPLOSION FOCUS AND BEYOND	16
	6.1 Introduction	16
	6.1.1 Some Metallurgical Effects of Shock Loading	17
	6.1.2 Brief Description of Present Work	17
	6.2 Experimental Procedure	17
	6.3 Results and Discussion	18
	6.3.1 Photomicrographs	18
	6.3.2 Hardness Measurements	19
	6.3.3 X-ray Pictures	20
7.	CONCLUSIONS	21
	REFERENCES	24
	TABLES	
	FIGURES	
	APPENDIX A: Low-Pass Filter Design	
	APPENDIX B: Listing of the Computer Program used for Computation of the Effect of Off-Centre Impacts	
	APPENDIX C: Metallurgical Glossary	

Notation

a	Speed of sound
a'	Distance between implosion focus and origin of combustion chamber
BCC	Body-centered cubic structure
C	Capacitance
d_{hkl}	Spacing between (h,k,l) planes
FCC	Face-centered cubic structure
g	Acceleration
HCP	Hexagonal close packed structure
L	Inductance
n	Molar helium/hydrogen dilution
n	Power index describing pressure distribution as a function of position of shock wave
n_c	Critical molar dilution
p	Pressure
P_{ave}	Average pressure (over the gauge area)
Q	Heat addition per unit mass of gaseous mixture
R	Resistance
R_g	Radius of pressure gauge
V_s	Position of shock wave
V	Voltage
VH	Vickers hardness
v	Velocity
ω_n	Natural frequency
ω_d	Damped natural frequency
ρ	Density
ξ	Damping coefficient

1. INTRODUCTION

1.1 Historical Note:

The UTIAS Implosion-Driven Hypervelocity Launcher conceived in 1959 by Prof. I. I. Glass (Ref. 1) was developed in the early 60's to facilitate simulation studies of meteoroid impact and a spacecraft entry into a planetary atmosphere. Half-calibre, 0.5 cm (0.22 in) dia. titanium projectiles were accelerated to velocities of about 0.5 cm/μsec and recovered intact (Ref. 2). In the late 60's, the facility was modified to accomodate a 2.54 cm (1.0 in) dia. shock tube. Planar shock waves of about 2.0 cm/μsec were produced (Ref. 3). In 1974, the explosive-driven implosion chamber facility was successfully used to transform solid graphite into diamond by shock compression (Ref. 4). Presently, studies are being carried out to use the device as a plasma source for diagnostics of fusion reactions.

The principle of operation of the UTIAS Implosion-Driven Hypervelocity Launcher is shown in Fig. 1. The hemispherical cavity is filled with a mixture of stoichiometric H_2-O_2 . The mixture is then ignited at the geometric centre of the hemisphere by an exploding wire thereby generating a hemispherical detonation wave (Fig. 1a). This outgoing detonation wave collides with an explosive liner placed against the wall of the hemispherical cavity detonating it simultaneously and uniformly, thus creating an implosion wave (Fig. 1b). The strength of this implosion wave increases as it travels toward the centre (Fig. 1c) at which large (ideally infinite) pressures and temperatures can be generated. As the implosion wave reflects from the origin, it leaves behind a region of high-pressure and high-temperature gas which accelerates the projectile along the barrel (Fig. 1d). The projectile subsequently leaves the barrel and enters a range tank where the ambient gas conditions simulate an atmospheric entry.

While the concept seems rather simple, to bring it into reality however involves quite a number of problems. Significant amounts of research and development were expended in the various stages of the project: the study of the properties of hydrogen - oxygen - helium reactions (Refs. 5, 6, 7, 8), spherical deflagration, detonation and implosion wave phenomena (Refs. 9,10), initiation of explosive liners both in planar as well as spherical geometries (Regs. 11, 12, 13), study of explosion and implosion wave systems (Refs. 12, 13, 16, 17, 18, 19, 20), spectroscopic studies of the high-pressure, high-temperature plasmas (Refs. 14, 15), the theoretical performance calculations of the launchers (Refs. 16, 19, 21, 22, 23) and the design and construction of the various models of the implosion-driven launcher (Refs. 24, 25, 26, 27).

1.2 Extent of Earlier Pressure Measurements:

While the region of high-pressure, high-temperature gas left behind by the reflected implosion was used extensively for accomplishing many different tasks (Sec. 1.1), an accurate measurement of the physical quantities in the vicinity of the origin was relatively difficult. Unlike the planar case, analytical solutions do not exist for a reflected spherical shock. Numerical solutions were available but their validity had to be verified experimentally. In the course of the launcher project, temperatures were measured spectroscopically (Refs. 14, 15) and at least two investigators attempted to measure pressures for gas-driven implosions. In 1963, Benoit

(Ref. 9) successfully measured time-resolved pressures for constant-volume or deflagrating combustion of H_2-O_2-He mixtures. However, he was unable to measure the pressure-time history for detonating combustions as suitable transducers were not available. In 1967, Watson (Ref. 19) made further attempts to measure pressures in gaseous detonations. His results for the pressure jump across detonation waves exhibited substantial scatter. Also, it was hard to distinguish between gauge ringing and actual pressure variations. Nevertheless, the average behaviour seems to be consistent with the classical Chapman-Jouguet theory. However, from an overall point of view, his pressure measurements were not satisfactory. Moreover, he could not measure the high pressures behind the reflected implosion at the origin.

Over the past decade, considerable improvements have taken place in transducer technology and now a pressure transducer with a rise-time of about 0.7 μsec and a pressure range of 0-8500 atm (0-125,000 psi) with good compensation for acceleration is available. In addition many of the problems arising from off-centered implosions were solved by improving the ignition system (Ref. 15) and developing a better technique of assembling the exploding wire. This, together with the availability of a reasonably good transducer warranted a detailed study of pressures at the implosion focus.

1.3 Scope of Present Work:

As an introduction to the present work, a brief review of the classical theory of detonation and implosion waves is outlined in Sec. 2. Details of the experimental equipment, operation of the UTIAS Implosion Chamber and the instrumentation used are given in Sec. 3. Section 4 describes the results of pressure measurements in detonating combustions of stoichiometric hydrogen-oxygen mixtures at various filling pressures (1.7 - 6.8 atm). Presentations are made of the effects of hydrogen or helium dilution, the introduction of a 20-degree conical liner on pressure-time histories at the focus and detailed time-resolved pressure histories of subsequent implosions. Section 5 presents a theoretical analysis of the effects of off-centered implosions on peak pressures generated at the focus. Included in this section are discussions of imprints of implosions obtained on lead witness plates for four successive runs. Section 6 contains corroborative pressure results from metallurgical analysis of the implosion craters in copper witness plates. Concluding remarks are made in Sec. 7.

2. COMBUSTION WAVE DYNAMICS

2.1 Detonation Phase:

The present work is directed towards the study of high-pressure spherical detonation waves produced in the UTIAS Implosion Chamber. Such high pressure spherical detonation waves are extremely thin compared with the typical detonation wave radii. Hence they can be treated using classical theory. It is assumed that there is a sharply defined wave front sweeping over the unburnt gas which changes it instantaneously into burnt gas. The transition across such a front is analougous to the transition across a shock front. The major difference is in the chemical kinetics of the detonation wave and the attached rarefaction wave. Planar, cylindrical and spherical detonation waves can be considered as one-dimensional fronts with different flow fields behind them. A brief description will be given

of detonation and deflagration waves observed during the present work. A more detailed discussion of the theory of combustion waves can be found elsewhere (Ref. 28).

Disregarding dissipative effects, the one-dimensional equations of motion are written in stationary coordinates with respect to the combustion wave moving into an unburnt gas (1) and producing a new state (2).

Mass: $\rho_1 v_1 = \rho_2 v_2$

Momentum: $p_1 + \rho_1 v_1^2 = p_2 + \rho_2 v_2^2$

Energy: $h_1 + 1/2\, v_1^2 + Q = h_2 + 1/2\, v_2^2$

where Q is the heat addition per unit mass in the reaction front.

Combining the mass and momentum equation yields:

$$\frac{p_2 - p_1}{\rho_2 - \rho_1} = \frac{\rho_1}{\rho_2} v_1^2$$

which indicates the existance of two different types of combustion waves:

1) Detonation waves through which both pressure and density increase and

2) Deflagration waves through which both pressure and density decrease.

While the present experiments were conducted to study the waves of the first category, the second type of combustion waves were nevertheless observed. The detonation waves produced in the UTIAS implosion chamber were identified as classical Chapman-Jouguet waves (Ref. 19). Such waves travel at constant velocity for a given composition of combustible mixture regardless of the geometry of the combustion chamber. Pressure jumps across such detonation waves as well as their velocities were measured by Watson (Ref. 19). The present work assumes his results to be valid and consequently deals with higher pressures existing at the origin during the implosion and reflection phases of the wave motion. It is therefore appropriate to review briefly some available analytical and numerical solutions to the implosion and reflection problem.

2.2 Implosion and Reflection Phase:

The outgoing detonation wave reflects from the hemispherical wall of the combustion chamber and implodes back into the preheated high pressure reaction products. The most important part of the entire process is the implosion and reflection of the shock wave at the origin. This is due to the generation of extremely high temperatures and pressures at the focus just after the reflection. An exact solution for the various thermodynamic quantities at the origin after reflection is complex. However, Guderley (Ref. 29) solved the problem in 1942 for the case of an infinitely strong imploding shock wave in an ideal gas. His solution is valid only very close to the origin where continuum concepts are still valid. His self-similar

solution for the flow field behind an implosion gives the pressure and velocity distribution as a function of radial position of the shock wave. Later, Chester (Ref. 30), Chisnell (Ref. 31) and Whitham (Ref. 32) developed analytical solutions to the problem of imploding shock waves of moderate strength. However, they are of limited use since they don't give any information on flow properties. These analytical solutions are discussed in some detail by Elsenaar (Ref. 16). At UTIAS, several authors (Refs.13, 18, 20, 22, 23, 33) have developed numerical solutions to the various phases of flow inside the implosion chamber. Of the many numerical models, the one developed by Elsenaar (Ref. 16) overcomes many of the difficulties encountered by others. The model assumes a reasonably realistic equation of state with boundary conditions of zero velocity at the origin and at the hemispherical wall. Further, the shock wave maintains a spherical geometry throughout. Since the present experimental conditions closely match his assumptions, a comparison of the results is made in Sec. 4. The development of the numerical model can be found in Ref. 16.

3. DESCRIPTION OF EXPERIMENTAL EQUIPMENT, APPARATUS AND PROCEDURE:

3.1 UTIAS Implosion Chamber:

The UTIAS Implosion Chamber essentially consists of two massive steel discs, one containing the hemispherical cavity and the other the barrel. Figure 2 illustrates the various parts of the facility. The front disc contains a segmented cone which supports the barrel, a liner disc, the gas inlet and the electrode used for ignition. The barrel has a cavity at its centre. A steel insert is placed in this cavity which serves as the mount for the pressure transducer as shown in Fig. 3. A conical liner disc can be fastened by four screws to the front disc to protect it from any damage due to undesirable off-centered implosions. During the present investigations involving gas-driven implosions at low initial pressures, this protector disc was not used. However, some experiments were done with this disc in place to determine its effect on pressure histories obtained at the implosion focus. The massive back disc has a machined 20 cm dia. hemispherical cavity to accomodate both explosive gases and a PETN explosive liner, if used. Both the front and rear discs are fastened together by thirty-two 3.18 cm (1.25 in) dia. bolts. The front disc, the segmented cone, the barrel, the steel insert with the transducer at its centre, the liner disc and the protector disc are shown in Fig. 4. The entire implosion chamber in the assembled position appears in Fig. 5.

3.2 Explosive Liner:

Direct pressure measurements were made only for gas-driven implosions and consequently solid explosives were not used. However, a few experiments were conducted to study the effects of explosive-driven implosions on copper witness blocks. The explosive liners were prepared following the method used by Chan (Ref. 34) and Sharma (Ref. 35) and is given here for completeness.

Figure 6 illustrates the four major steps involved in the process of making the explosive liner. The copper liner is first polished with sand paper and then a plastic foam is glued to the polished surface. Time is allowed for the glue to dry thoroughly. A PETN slurry is then prepared and pressed into the plastic foam to form a liner. As the superfine PETN explosive powder does not possess sufficient mechanical binding strength to form a solid hemispherical shell, it is first mixed with fine cotton linters and water. The

resulting PETN slurry consisting of fine powdered PETN (80 g),water (200 g) and fine cotton linters (1.5 g) is prepared carefully to ensure that the slurry is homogeneous. The wet PETN slurry is pushed into the plastic foam as carefully as possible to achieve a uniform thickness and density. The explosive liner is then allowed to dry very slowly usually overnight. Obtaining a uniform thickness and homogeneous density of the PETN liner are very important otherwise off-centered implosions may result.

3.3 Ignition System:

In order to induce a spherical detonation wave in a combustible mixture, sufficiently large amounts of energy must be released exactly at the origin as quickly as possible. For a given amount of stored energy of the ignition system, this criterion could be satisfied by keeping the resistance of the exploding wire as high as possible and the impedance of the rest of the ignition system as low as possible.

During the present work, a 0.127 mm (5 mil) dia. 1.0 mm long nickel wire was used to ignite the explosive gases. The transmission line in the high-voltage circuit was changed from RG-8 (52 Ω impedance) to a low-inductance (16 Ω impedance) cable (Ref. 15). This considerably increased the energy dumped into the exploding wire and simultaneously reduced the discharge time significantly. Further, the thyratron/capacitive discharge system was replaced by the spark gas/capacitive discharge system which is shown in Fig. 7. The spark gap essentially consists of two brass electrodes, a plexiglass tube and an automobile spark plug. The operating cycle of the system consists of dehumidifying the spark gap with compressed nitrogen and then charging the capacitor to 22 Kv. A 5 Kv trigger pulse to the spark plug is used to initiate the discharge.

The pressure transducer used in the present work is just over 3 mm in radius. Thus, in order to achieve repeatable results, the imploding shock wave should be focussed very close to the origin each time. This would be possible only if the outgoing detonation wave started out exactly at the origin. I am grateful to our technician Mr. R. Gnoyke for providing a simple and straightforward procedure to accomplish this.

A self-stick copper tape about 2 mm wide was placed onto a 15 x 10 mm polyethylene sheet and about 1 mm of the tape was removed near the centre. The exploding wire was then placed across this gap and soldered to the copper tape. Two pieces of No. 20 tinned solid copper wire were soldered to the opposite ends of the copper tape to be connected to the high-voltage circuit and the ground. An exploding wire thus assembled is shown in Fig. 8.

Once assembled, the exploding wire has to be placed such that its centre coincides with the centre of the transducer. Figure 9 illustrates the three main steps involved. First, the transducer is secured in its position at the centre of the barrel (Fig. 9a). Three layers of electrical tape are placed over the transducer to protect it from the heat of the implosion. The centre of the barrel is then located using a centre-marker and a drop of white ink (liquid paper) is placed over it for easy identification (Fig. 9b). Finally, the exploding wire assembly is glued to the electrical tape with 5-minute epoxy such that the centre of the exploding wire coincides with the white dot (Fig. 9c). By using a magnifying glass, the exploding wire can be placed to within 0.1 mm of the centre.

3.4 Combustion Chamber Loading Procedure:

The barrel, with the exploding wire positioned at the centre, is fitted to the front disc and the exploding wire leads are soldered to the electrodes. The front and rear discs are then fastened together. With all accessories connected, the doors leading to the blast room are closed. All further operations are carried out remotely from a control room for safety reasons. A picture of the control room is shown in Fig. 10.

The vacuum pump is first put in operation until a pressure of the order of 2 torr is obtained in the combustion chamber. The explosive gases are then admitted into the chamber with oxygen first followed by hydrogen. When helium wasused as diluting gas, the gases were introduced in the following sequence: oxygen - helium - hydrogen. If the diluting gas was hydrogen, the loading was done in two steps only: oxygen first, then hydrogen. The procedures were adopted just to be consistent and earlier reports indicate that the loading sequence has no effect on the peak pressures obtained for constant-volume combustion (Ref. 9).

3.5 Instrumentation:

All time-resolved pressure histories were obtained using high-pressure quartz piezoelectric transducers of the type PCB 119M08, 119M09 supplied by PCB Piezoetronics, Buffalo, N.Y. The 0.63 cm dia. transducers contain 4 quartz crystals, two of which act to compensate for accelerations up to 20,000 g. The quartz crystals have been pre-stressed to give a good linear response (within 1%) in the entire operating range of the transducer. The transducers have a calibrated pressure range of 0-8500 atm (0-125,000 psi) and a good frequency response up to 500 KHz. A picture of the transducer is shown in Fig. 11. Figure 12 shows a typical static calibration curve supplied by the manufacturer. The output charge from the transducer was amplified using a Kistler 504E type charge amplifier. . In the early stages of the experimental work, it was noticed that the Kistler charge amplifier had a flat response only up to 150 KHz due to a low-pass filter. To extend the operating range, a new filter with a cut-off frequency of about 800 KHz was designed. Details of the filter design are given in Appendix A.

Using a Signal Generator (IEC F34 Type), a sine wave of 400 mV amplitude at continuously varying frequencies was fed into the charge amplifier system and the output recorded. Figure 13 illustrates the results obtained. The charge amplifier with the 150 KHz filter starts rolling off at about 100 KHz and the output amplitude falls to one-half of the input at 225 KHz. The improved performance of the new filter is evident from Fig. 13b. In Fig. 13c, the roll off starts around 750 KHz and the output falls to 50% of the input at about 925 KHz.

The time response of the pressure transducer, charge amplifier system was obtained in a 1 m long x 5 cm dia. plexiglass shock tube at PCB Piezotronics, Buffalo. The transducer was mounted "face on" at the end wall of the channel which was pumped down to about 15 torr. With the room itself acting as a driver, the aluminum - foil diaphragm was opened with a mechanical breaker. Figure 14 shows the pressure jump recorded behind the reflected shock wave. The transducer rise-time was thus found to be about 0.8 μsec. However, rise-times as fast as 0.65 μsec. were obtained with the same transducer for the reflected implosion. The manufacturer suggested that

the transducers may respond faster at higher pressures because of their integral type of construction (no conventional diaphgram) and indeed the pressures generated in the implosion chamber are 4 orders of magnitude greater than those obtained in the calibration shock tube.

4. RESULTS AND DISCUSSION

In the course of the present investigations, time-resolved pressure histories have been obtained in the UTIAS implosion chamber which indicate the occurrence of three different types of combustion waves. A good oscillograph trace of each of these three processes appears in Fig. 15. Figure 15a shows the pressure history for the detonation of stoichiometric $2H_2 + O_2$ at an initial pressure of 3.4 atm (50 psi). The picture shows the implosion and reflection process which occurs at about 80 μsec from the time the gases were detonated. Upon reflection of the implosion from the origin, the pressure rises sharply to about 5440 atm (80,000 psi) and then decays rather quickly. Figure 15b illustrates a typical deflagration process. The pressure rises slowly as the combustion wave moves toward the hemispherical wall and attains a peak value when the wave reaches the wall dropping down slowly thereafter. A third type of combustion wave system developed in a few experiments (Fig. 15c) in which the multiple pressure jumps were found to be much too high to be a deflagration wave and too low to be a detonation wave. The present experimental set up with only one transducer located at the origin of the combustion chamber is not sufficient to accurately describe this process. Several transducers mounted at different radii in the front wall might be necessary to follow the wave system developed in this type of transitional combustion.

4.1 Initial Conditions Leading to Detonation or Deflagrating Combustion:

Upon ignition of the mixture, either a detonation wave or a deflagration wave develops. This depends upon:

a) the constituents of the combustible mixture
b) the initial conditions of pressure and temperature
c) the characteristic features of the ignition system such as the amount of energy released at the source (the exploding wire), the rate of release, the dimensions of the source, the form of source energy (i.e., thermal, electrical, energetic photons, etc.,) and the extraneous mass released to the medium by the source (Ref. 36).
d) the geometry of the combustion chamber.

With (b), (c) and (d) remaining the same, it was found that for initial mixtures $(2H_2 + O_2) + n\,x$ where 'x' represents helium or hydrogen, a detonation wave developed when the dilution index n, was less than a certain critical value n_c. Above this value, a smooth deflagration type of combustion took place. At the critical values n_c, a transition type of combustion system developed.

For helium diluted mixtures, detonating combustions developed for $0 \leq n \leq 2$ and deflagrating combustion for $n = 3$. The critical helium dilution was not exactly determined but can be expected to lie in the range $2 < n < 3$.

For hydrogen diluted mixtures, detonating type of combustion took place of $0 \leq n \leq 1$. For $n_c = 2$, a transition type of combustion developed and for $n = 3$, deflagrating combustion was observed. Detailed experiments were not made in the range $1 < n < 2$ and $2 < n < 3$.

Results obtained earlier by Benoit (Ref. 9) indicated that the critical dilution index was $n = 3$ for helium dilution and $n = 7$ for hydrogen dilution for initial pressures above 6.8 atm (100 psi). The present experiments were conducted at an initial pressure of 3.4 atm (50 psi) and with a different ignition system. This might be the reason for the difference. It may be noted that the present ignition system failed to initiate a detonation wave in a stoichiometric mixture of $2H_2 + O_2$ at initial pressures of 1.02 atm (15 psi) or less. From what is understood at the present time, the initiation process can be described as the intimate coupling between the shock hydrodynamic flow structure generated by the igniter and the chemical kinetic processes of the exothermic reactions that occur in the transient flow in the wake of the shock front (Ref. 36). However, no quantitative theory nor empirical correlation of experimental results of sufficient generality exist to date that link the properties of igniter, the kinetics and the exothermicity of the explosive to the critical energy required for direct initiation. Perhaps, the only conclusive result obtained so far is the demonstration of the dependence of the critical energy on the properties of the explosive gas (such as induction delay) and initial thermodynamic conditions (such as loading pressure). For example, the critical energy required to initiate a detonation wave (in cylindrical geometry) in stoichiometric oxy-acetelene mixtures increased from about 1 joule/cm for an initial pressure of 100 torr to about 30 joules/cm for an initial pressure of 20 torr (Ref. 37). Thus, a five-fold decrease of loading pressure increased the critical energy by a factor of 30. Further, for a given explosive at fixed initial conditions, experimental evidence indicates that the critical energy can differ by as much as a few orders of magnitude for different ignition sources (Ref. 38). This strongly supports the contention that the critical energy depends not only on the properties of the explosive and the initial conditions but also on the characteristic features of the igniter such as the detailed time history of the energy deposition at the source (exploding wire, spark gap, etc.,), the dimensions of the source, the form of the source energy (i.e, thermal, electrical, energetic photons, etc) and the extraneous mass released to the medium by the source (Ref. 36). Attempts have been made to link the properties of the igniter to that of the explosive and some details can be found in Refs. 36 to 39.

4.2 Records of Pressure-Time History for Detonating Combustions of Stoichiometric H_2-O_2 Mixtures:

Detailed pressure histories at the origin of the UTIAS implosion chamber were obtained for the detonation of $2H_2 + O_2$ mixtures at varying initial pressures (1.7 - 6.8 atm). The upper figure (6.8 atm) was limited by the pressure transducer. Electrical pick-up from the exploding wire prevented any pressure measurements during the first 30-40 μsec. However, high pressure of interest occur only around 80 μsec when the implosion reflects from the origin. A good pressure-time trace for an initial pressure of 3.4 atm (75 psi) is shown in Fig. 16. Figure 16a illustrates the electrical noise present for the first 30 μsec and actual pressures thereafter. At about 80 μsec when the first implosion occurs, the trace goes off scale but is picked by another oscilloscope and shown in Fig. 16b. The pressure rises sharply to about 8500 atm (125,000 psi) when the implosion wave reflects

from the origin. As the hemispherical shock wave moves out, the pressure drops quickly and remains at a low value until it is raised again by the imploding shock wave arriving at the origin for the second time. The process continues until all the energy evolved through combustion is dissipated via viscosity, heat conduction and radiation.

The pressure histories measured during the early stages of the project showed considerable scatter in peak pressures as well as rise times. It was suspected that the scatter could be due to off-centered implosions as the transducer radius is just over 3 mm. As described in Sec.5, the effects of off-centered implosions can cause large errors in pressure measurements. Typically an off-centre implosion of about 2 mm from the origin of the combustion chamber reduces the peak pressures by about 10%. If other errors such as calibration error of the oscilloscope, non-linear response of the charge amplifier (see Fig. 13), non-linearity in the transducer output are included the variations can be as high as 20%.

To overcome the problem of large-scale scattering of the data, an attempt was made to improve the symmetry of the outgoing detonation wave. Any asymmetry in this wave would undoubtedly cause the imploding wave to focus away from the origin. As described earlier, a new procedure for preparing and mounting the exploding wire was developed. Several runs were carried out using this simple technique and the repeatability of the pressure measurements was remarkably improved. Figure 17 shows the pressure records for three runs conducted at an initial pressure of 1.7 atm (25 psi). Figures 18 to 25 present detonation records for initial pressures between 1.7 atm (25 psi) and 6.8 atm (100 psi). The measured peak pressures increased from about 1360 atm (20,000 psi) for an initial pressure of 1.7 atm (25 psi) to about 9865 atm (145,000 psi) for an initial pressure of 6.8 atm (100 psi). Also, the measured rise-times decreased from about 1 μsec for an initial pressure of 1.7 atm (25psi) to about 0.65 μsec for an initial pressure of 6.8 atm (100 psi). It may be noted that the rise-time of the transducer as obtained from a shock tube run was about 0.8 μsec.

The pressure-time histories of all detonation runs show substantial oscillation after the implosion. The reflection of the shock wave within the crystals may explain the presence of such oscillations. The number of small peaks after the first implosion (average 10 peaks in 20 μsec) corresponds with the 2 μsec time interval for an acoustic pulse to travel back and forth once through the quartz crystals inside the transducer. If this was the only reason for the oscillations, the period of the waves should be constant (2 μsec) and also the magnitude should decay continuously. The observed oscillations are not so regular. Therefore, the oscillations are probably due to the superposition of the reflection phenomena and ringing of the charge amplifier occurring out of phase. Mechanical vibration of the transducer can be ruled out since the frequencies of oscillation are varying and are different from the natural frequency (500 KHz) of the transducer. Further, it is known that the transducer-charge amplifier system has a reasonably flat response for a 1.7 atm (25psi) initial pressure run. Since all pressure traces have a very similar oscillation pattern after the implosion, it can be concluded that mechanical vibrations were absent. The decay portions of the pressure-time histories were obtained by drawing continuous curves through the mean value of the oscillations. Figure 26 shows such a trace for an initial pressure of 5.1 atm (75 psi).

The pressure histories obtained for various initial pressures of

$2H_2 + O_2$ show a self-similar pattern when the times are normalized with respect to the time taken for the pulse to reach 50% of the peak pressure and drop back to 50% again. Figure 27 shows such normalized plots. It may be noted that the peak pressures are obtained when $\tau \sim 1$. Consequently, the rise time of any pulse is approximately equal to τ.

A plot of the measured peak pressures against the initial stoichiometric filling pressure is shown in Fig. 28. The maximum error involved for 5.1 atm (75 psi) initial pressure run is indicated. The absolute error was calculated assuming appropriate values for calibration error of oscilloscopes ($\pm$ 2%), non-linear output of the transducers ($\pm$ 1%), non-linear output of the charge amplifier (-5%) and lowering of pressures due to off-centre implosions (-2% - see Sec. 5.1). The peak pressures measured during a total of five runs (with two different transducers) at 5.1atm (75 psi) initial pressure varied by a little over 3%, well within the estimated error limits. However, one of the transducers { (119 M09 type) + ve signal} generally gave higher output at lower filling pressures. Sufficient number of experiments were not made to assess this variation. Apart from this variation, the peak pressures measured using transducers of 119 M08 type gave a maximum error of $\pm$ 5% in the entire operating range of the transducer.

The relationship between peak pressures and initial filling pressures is linear for initial pressures from 1.7 atm (25 psi) to 5.1 atm (75 psi). Thereafter, the pressures fall rapidly below the linear extension. This decrease in peak pressure may arise from the fact that for a 5.1 atm (75 psi) initial pressure run, the peak pressure reaches the maximum rated pressure (8500 atm, 125,000 psi) of the transducer. For pressures larger than this value, the transducer may be saturated. Another reason for the drop could be due to the fact that the transducer may have been subjected to frequencies above its natural frequency where the output is attenuated. The response of the transducer for pressures above 8500 atm (125,000 psi) as well as its transfer function are not known. In the absence of these data, the attenuation, if any, cannot be estimated. An indirect method of assessing the attenuation is described later in this section.

4.3 Comparison with Numerical Results:

The peak pressures measured at varying initial pressure (1.7 - 6.8 atm, 25-100 psi) are compared with the results of Elsenaar (Ref. 16) as shown in Fig. 29. A best fit straight line was drawn through his numerical result to get a simple relation between the final pressure after the reflection and the position of the shock from the origin as follows:

$$p(r) = (2390)\ p_i/(r_s)^{1.30}$$

where r_s is given in mm. The average pressures over a 6.3 mm dia. area (gauge diameter) was calculated using the equation

$$P_{(average)} = \frac{\int_0^{2\pi} \int_0^{R_{gauge}} p(r)\ r\ dr\ d\theta}{\pi\ R_{gauge}^2}$$

This yields a linear relationship of final to initial pressure and is shown in Fig. 28. At very low values of initial pressures, the agreement is poor. At higher initial pressures, the experimental results seem to be overtaking the numerically calculated pressures. The reasons for this discrepancy are not known.

4.4 Effect of Conical Liners on Pressure History at the Focus:

The conical liner is a protector disc used to prevent any damage to the top plate of the implosion chamber that may result from off-centered implosions. The effects of the presence of the liner on conditions existing near the origin after the reflection of the implosion were not known. Therefore, a few experiments were conducted to investigate the effects in gas-driven implosions. Ideally, if the conical liner were perfectly conical with its apex at the origin of the hemispherical chamber, conditions at the focus should not differ from those with the conical liner absent. In actuality, the conical liner is truncated such that there is a finite size hole around its apex. When assembled, the focus of the conical liner falls exactly at the origin of the hemispherical combustion chamber as shown in Fig. 30a.

A 20-degree conical liner with a 4 cm dia. hole at the apex was chosen for the investigation. Figure 31 illustrates the effects of the conical liner on the pressure history for an initial pressure of 3.4 atm (50 psi). Compared to the pressure history obtained without the liner, the peak pressures dropped by about 45%. The presence of the liner decreased the decay rate of the pressure pulse considerably. This is shown in Fig. 32, where the decay part of the traces are drawn through the mean of the trace oscillation. The decrease in peak pressure as well as a spreading out of the pulse may be attributed to the loss of spherical geometry of the imploding shock wave while it diffracts over the curved surface (see Fig. 30a) of the conical liner.

The experiment with the 20 degree conical liner was repeated at an initial pressure of 5.1 atm (75 psi). Figure 33 shows the result. Again, the peak pressures dropped to about 57% of the value that would have been normally obtained without the liner . The decay rate of the pressure pulse has a trend similar to the 3.4 atm (50 psi) run.

Earlier in Sec. 4.2, it was mentioned that for initial pressures above 5.1 atm (75psi), the peak pressures obtained behind the reflected implosion dropped away from the linear trend. Further, the behaviour was attributed to the possible saturation of the transducer. Since the presence of the conical liner reduced the peak pressures obtained by about 45% for both the 3.4 atm (50 psi) and 5.1 atm (75 psi) initial pressure runs, a pressure measurement with the liner at an initial pressure of 6.8 atm (100 psi) could be used to check the value of peak pressure obtained earlier without a liner. The result thus obtained is shown in Figs. 34 and 35. Referring to Fig.35, the straight line relationship extended from low pressure measurement indicates the probable true pressures existing near the origin of the chamber in the absence of any conical liner. Peak pressures measured in the absence of the liner for 3.4 atm, 5.1 atm and 6.8 atm (50, 75 and 100 psi) initial pressure runs are shown. Also shown inthe same figure are the measured peak pressures for these three runs in the presence of the 20-degree conical liner. The boosted values (by 45%) of the peak pressures obtained in the presence of the liner are included. This clearly indicates that

the peak pressures for the 6.8 atm initial pressure run in the absence of the conical liner is indeed much higher than that was measured. It also substantiates the earlier suggestion that the transducer output may not be linear for peak pressures above 8500 atm (125,000 psi). However, it should be noted that the boosted value of the peak pressure obtained for the 6.8 atm (100 psi) run still falls short of the linear trend by about 6%.

Earlier in this section, the 45% drop in peak pressures in the presence of the conical liner was attributed to the loss of sphericity of the imploding shock wave. To confirm this, a decisive experiment was planned in which the 20-degree conical liner was extended up to the periphery of the transducer as shown in Fig. 30b. The very small space at the origin provided some difficulties in insulating the ignition lead from the conical liner. However, the problem was easily solved by modifying the exploding wire assembly and the mounting procedure. Figure 36 shows the results obtained with the new linear for two successive runs conducted at an initial pressure of 5.1 atm (75 psi). For comparison, a pressure-time trace obtained in the absence of the liner for the same initial conditions is also shown. The peak pressure, rise-time decay rate and even the oscillations seem to be following the same pattern. The experiment conclusively indicates that the presence of the conical liner makes no difference in the pressure-time history as long as the conical liner is perfectly conical and does not change the spherical geometry of the imploding shock wave. This result was expected from theoretical considerations(Ref. 40).

4.5 Records of Pressure-Time History for Detonating and Deflagrating Combustions of H_2-O_2 Mixtures Diluted with Helium:

It is well known (Ref. 41) that the release of chemical energy through detonation waves produce appreciable pressure and temperature jumps across the wave front and thus produce high enthalpy gases. If the detonation products are to be used as driver gases for hypervelocity facilities, it is essential to keep their acoustic impedance as low as possible in order to obtain the greatest particle velocities for a given expansion ($du = dp/\rho a$) and a high escape speed ($u = 2\, a_o/(\gamma_o - 1)$) (see Ref. 42). A technique commonly used for producing such driving gases in the shock tube work consists of using the heat released by deflagrating combustion of hydrogen and oxygen to preheat the driving gases containing up to 70% of unburned hydrogen or helium. It is of interest to study the thermodynamic characteristics of such reaction products especially when the combustion wave is a fully developed Chapman-Jouguet detonation wave. This section presents the results of experimental studies on final pressures obtained for detonations of stoichiometric hydrogen-oxygen mixtures diluted with helium. Figure 27 illustrates the pressure history obtained for a helium molar dilution index n = 1 at a total initial pressure of 3.4 atm (50 psi). As a result of the reduced acoustic impedance, the waves moved faster and the imploding shock wave arrived at the origin 5 μsec earlier. The observed peak pressures increased by about 22%., when compared to the case in which no helium was added. The rise-time and decay rate of the pressure pulse did not show a noticeable difference owing to the addition of helium. When the dilution index was increased to n = 2, the peak pressure dropped back to almost the same as that obtained for n = 0. Figure 38 illustrates this point. Again, there was no resolvable change in the rise-time or the decay rate of the pulse. As the dilution index was raised to n = 3, the mixture failed to produce a detonation wave. Instead, a deflagrating combustion took place. The pressure rise and the flame velocity measured for this run compare well with the results of

Benoit (Ref. 9). Figure 39 shows the pressure history obtained for this deflagration run. The peak pressure of 34 atm (500 psi) coincides with the value predicted by Benoit (Ref. 5). The effect of helium dilution on peak pressures achieved at the focus is shown in Fig. 40. The present results indicate that for dilutions of stoichiometric hydrogen-oxygen mixtures with up to 2 moles of helium produce higher pressures than that obtained by detonating stoichiometric ($2H_2 + O_2$) mixtures at the same initial conditions.

4.6 Records of Pressure-Time History for Detonating, Deflagrating and Transition Combustion of H_2-O_2 Mixtures Diluted with Hydrogen:

Dilution of the stoichiometric ($2H_2 + O_2$) mixtures with hydrogen showed the same trend as that obtained for helium dilution. As shown in Fig. 41, the waves produced in the chamber moved faster for m = 1 compared with n = 1, as hydrogen has less acoustic impedance than helium. The peak pressures increased for a molar dilution index m = 1, but the increase was not as much as that obtained for helium with n = 1. There was no substantial difference in the rise-time or the decay rate of the pressure pulse introduced by the dilution. When the dilution index was increased to m = 2, a combustion wave system resulted which neither had the features of a detonation wave nor of a deflagration wave. Figure 42 illustrates the pressure-time history obtained for this run. It is definitely not a deflagrating type of combustion. For the initial conditions used, the flame should have reached the hemispherical wall only after 1-1.5 μsec (Ref. 9). Neither does this run indicate the formation of a fully developed detonation wave since there was no indication of the arrival of a strong imploding shock wave indicated by the jump in pressure associated with it. This transition type of combustion may have been the result of the initial deflagration wave accelerating sufficiently to form a detonation wave near the walls of the hemispherical combustion chamber. This type of transition, induced by the presence of the wall was observed by Pluckebaum et al (Ref. 43) and by Watson (Ref. 19). On increasing the dilution index to m = 3, it was found that an almost typical deflagration wave developed as shown in Fig. 43. Some oscillations are still present in the trace. The peak pressure obtained was about 5% less than that calculated by Benoit and Galipeau (Ref. 44). It may be noted that the critical dilution index was found to be m = 2 for the present studies while Benoit (Ref. 9) had obtained a value of m = 7. The fact that Benoit used initial pressures of 6.8 atm (100 psi) and higher as opposed to present experiments conducted at 3.4 atm (50 psi) was initially attributed to this difference. However, two runs conducted with $2H_2 + O_2 + 7H_2$ at 6.8 atm (100 psi) failed to ignite the mixture. This is quite surprising and a detailed study of the effects of the changes brought about in the new ignition system is required to account for the discrepancy. Finally, it should be noted that the present results indicate that small amounts of hydrogen and helium (about 2 moles of helium and 1 mole of hydrogen) when added to the stoichiometric ($2H_2 + O_2$) mixtures produce higher peak pressures at the implosion focus.

4.7 Cycle Time and Records of Subsequent Implosions:

Cycle time, in the context of the present studies, is defined as the time elapsed between the generation of the outgoing detonation wave and the arrival of the first imploding shock wave at the origin. This time interval was detected by the pressure transducer positioned at the origin of the combustion chamber. Figure 44 shows the variation of the cycle time with initial gas composition. Earlier experimental results obtained by Watson

(Ref. 19) as well as one calculated by Brode and mentioned in Ref. 19 are also shown. Watson's points were obtained with cycle time being defined as the time interval between the passage of the outgoing detonation wave at the inner probe (at a 6.35 cm radius from the origin) to the passage of the next outgoing wave at this probe. For the detonation wave of a stoichiometric ($2H_2 + O_2$) mixture , the cycle time is about 81 sec. To the accuracy with which the records could be read, the cycle time is independent of the initial pressure at low initial pressures 1.7 - 6.8 atm (25-100 psi). Watson's results substantiate the present work and extend it to higher pressures as well. For a mixture of helium dilution such as the case computed by Brode ($2H_2 + O_2 + 7$ He at 6.8 atm), the cycle time is only 51 sec or about five-eighth the value of the stoichiometric case. Since this cycle time is in a sense a representation of the average sound speed in the chamber, a plot of the cycle time based on the equilibrium sound speed immediately behind the detonation wave versus initial gas composition is included in the figure to illustrate a similar trend.

An extended record of the pressure transducer was used to follow the shock wave as it travelled back and forth inside the chamber. Each time the imploding shock wave hit the origin, the pressure rose sharply. Figure 45 a illustrates this phenomenon for a run conducted at an initial pressure of 3.4 atm (50 psi). It is interesting to note that the initial implosion pressure of 5440 atm (80,000 psi) is 1600-fold greater than the initial pressure and even the fifth implosion caused the pressure to rise to about 1020 atm (15,000 psi) or 300-fold the initial loading pressure. The peak pressures obtained for the first five implosions are shown in Fig. 45b. Another interesting feature which was not predicted from numerical results but was observed in the present experiments is the fact that the cycle times for first (80 μ sec) and third (82 μ sec) cycles are considerably less than that for second (88 μ sec) and fourth (92 μ sec) cycles. The same trend was observed by Roberts (Ref. 14) in his spectroscopic work at higher initial pressures. His comparable values for 13.6 atm (200 psi) initial pressure ($2H_2 + O_2$) run are as follows: first (76 μ sec), third (80 μ sec), second (85 μ sec), fourth (83 μ sec).

5. STUDY OF OFF-CENTRE IMPLOSIONS

5.1 Numerical Computation of Effect of Off-Centre Implosions on Pressure at the Focus:

In view of the fact that the pressure transducer used in the present experiments is of relatively small size (3.18 mm radius), any off-centre implosion would undoubtedly result in lower measured pressures at the origin. The actual pressures measured for such off-centered implosions would definitely depend on the degree of off-centerdness or in other words, the actual location of the focal point with respect to the origin of the hemispherical combustion chamber. The greater this distance, the lower will be the measured pressures. A simple method is presented of predicting the pressures for off-centre implosions as a function of the degree of off-centeredness. The assumptions made in the present analysis are as follows:

1) The imploding shock wave which is focussed away from the origin maintains a pressure distribution which is still radially symmetric about the focal point.

2) For a given set of initial conditions, this radial pressure distribution is always the same and is independent of the location of the focal point itself.

3) The pressure at any radius of the combustion chamber is only a function of the radial position r , and is given by

$$p(r) = \text{const}/(r)^n$$

where the power index n, is mainly dependent on γ,the specific heats ratio of the gas ahead of the imploding shock wave. This relation follows classical considerations (Ref. 45).

The first and second assumptions are probably true for focal points lying quite close to the origin of the combustion chamber. At least, the errors involved in these assumptions can be assumed to be small as a first approximation for focal points lying with 3% of the combustion chamber radius from the origin.

Referring to Fig. 46, the average pressure over the transducer area

$$P_{(\text{average})} = \frac{\int_0^2 \int_0^{r(\theta)} p(r)\, dA}{\int_0^{2\pi} \int_0^{r(\theta)} dA} \qquad 5.1$$

where

$$dA = r\,dr\,d\theta$$

$$p(r) = \text{const}/r^n \quad \text{and}$$

$$r(\theta) = -a'\cos\theta + \{ (a'\cos\theta)^2 - (a^2 - R^2) \}^{1/2}$$

The integral was solved using Simpson's Rule in an IBM 370 system and the results are presented in Fig. 47. The computer program is listed in Appendix B.

The term percentage error is defined as the percentage reduction of average pressures as seen by the transducer due to off-centered implosions. For a given location of the focal point, this was calculated by using the following

$$(\text{Percentage Error})_{a'} = 100 \left[\frac{(P_{ave})_{a'=0} - (P_{ave})_{a'}}{(P_{ave})_{a'=0}} \right]$$

The percentage error thus obtained was plotted as a function of the power index n, for three (a' = 1,2, and 3 mm) different locations of focal points. The values of n were chosen in the range $0.1 \leq n \leq 1.9$. Any value of n less than 0.1 would be too unrealistic for a spherical wave near its focal point. Further, n cannot take on values of 2.0 or more or the average pressures over the transducer area would theoretically be infinite.

From Fig. 47, it is seen that for an implosion 1 mm off centre (a' = 1), the maximum error involved is only about 2.5% and occurs at about n = 1.0. As a' increases to 2 mm, the maximum error rises to about 10% and the corresponding value of n increases to 1.1. As the focal point moves out to 3 mm, just 0.2 mm from the edge of the transducer, the maximum error shoots up to about 32% and occurs at n = 1.2. Essentially, the errors are low when n is relatively small since the pressure distribution is more or less uniform. For intermediate values of n ($0.6 < n < 1.4$), the errors are considerable and are very sensitive to the location of the focal point (a'). It may be noted that the value of this index as calculated from Elsenaar's work (Ref. 16) is n = 1.3 and hence relatively large errors can occur for significantly large (a' > 2 mm) off-centered implosions. For large values of n, however, the pressures are very much concentrated near the focus which results in lower values of errors as long as the focal point lies within the transducer.

5.2 Imprints of Implosions on Lead Witness Plates:

To actually determine the degree of off-centeredness, the transducer at the origin was replaced by 3.2 cm (1.25 in) dia, 1.3 cm (0.5 in) thick lead witness plates and imprints of implosions were obtained for the initial conditions used in the pressure measurements (typically 6.8 atm, 100psi). Figure 48 shows the imprints obtained for four successive runs. The focussing is sharp and the focal point lies within 3/4 mm from the origin in all the runs. This fact indicates that the hemispherical waves generated in the implosion chamber are symmetrical, well focussed and stable in the low pressure range in which the pressure measurements were carried out. Further, comparing with the numerical computations, it is seen that the average maximum error in the pressure measurements resulting from off-centre implosions is only about 2%. Table 1 lists the dimensions of the craters which were measured using a micrometer gauge. Runs 2 and 3 produced almost identical craters. The fourth run was conducted with the lead block recessed by about 0.5 mm from the barrel surface due to a machining error which significantly reduced the crater size and was therefore an uncontrolled run.

6. METALLURGICAL CORROBORATION OF PEAK PRESSURES AT IMPLOSION FOCUS AND BEYOND

6.1 Introduction:

It is interesting to speculate that there may be a number of unknown materials that might be stable under atmospheric pressure, if they could only be produced by exceeding some critical stress. A number of unusual materials have been produced in recent years by using intense shock waves. Some of them are diamond, cubic boron nitride, dense silicon and germanium, coesite and stishovite, metallic indium antimonide and omega titanium (Ref.46). Most of these materials were completely unknown before the invention of high-pressure, high-temperature facilities, with the possible exception of diamond. It should be noted that most of these newly created materials are highly resistant to chemical reactions and extremely hard. For example, cubic boron nitride has almost the same density and hardness as that of diamond and has considerably more resistance to oxidation at high temperatures in air than diamond. Some tests have indicated that there are some grinding applications in which cubin boron nitride performs better than diamond (Ref. 47). It is very encouraging to note that the UTIAS implosion chamber facility is well within the range of pressures and temperatures that are required to produce any of the above-mentioned new materials. The facility has already demonstrated its capability of transforming graphite to diamond (Ref. 4).

6.1.1 Some Metallurgical Effects of Shock Loading:

Intense shock waves ireversibly change many physical properties of a material such as hardness, yield strength, resistance, conductivity, etc. Also, the shock loaded materials exhibit changes in the crystal structure, grain size, shape and orientation depending on shock strength, pulse-duration, and direction of shock-wave motion with respect to the crystal axis. Moreover, as the shock wave enters the material, the dislocation sources are continuously activated and dislocation loops are generated (Ref. 48). The formation of these dislocations and their growth plays an important role in the ultimate value of the hardness of the recovered sample. Some percentage (less than 10%) of the energy involved in the shock loading is retained permanently by the material in various forms and this energy would be released on annealing. At fairly high shock pressures (above 200,000 atm - 200k bars) multiple twins (Appendix C) are formed (Ref. 48). Finally, it is to be noted that high-velocity dislocations in a shock front are expected to be efficieint producers of point defects (Ref. 49). In this section, some of the phenomena just described will be discussed in some detail with special emphasis on hardness and microstructural changes.

6.1.2 Brief Description of Present Work:

Copper witness plates, subjected to explosive-driven implosions in the UTIAS Implosion Chamber, were analyzed from a metallurgical point of view. Two witness plates,shock loaded under two different boundary conditions were chosen for the present study. Figure 49 illustrates the two different boundary conditions. The experiment with conditions shown in Fig. 49a was conducted by Chan (Ref. 2) in 1969. In this case, the witness plate had free access to move into the barrel upon loading. In the present investigation a solid steel plate prevented any such movement of the witness plate (Fig. 49b). After shock loading, the copper witness plates were sliced into specimens using a metallurgical cut-off wheel apparatus at the Materials Science Laboratory (University of Toronto). Subsequently, each specimen was polished, etched and examined using a microhardness tester, by X-ray back reflection techniques and by studying the grain structure and defects from photomicrographs. The resultant data thus obtained were sufficient to provide distributions of hardness change and therefore work-hardened zones as a function of radial position away from the implosion focus and the depth of the specimen. A study of the grain size, shape and orientation after implosion was undertaken and together with the microhardness results, an attempt was made to roughly determine the pressures involved in the implosion process.

6.2 Experimental Procedure:

Figure 50a shows the configuration of the experimental set up used by Chan. About 88 g of PETN explosive, placed against the hemispherical cavity was detonated by the H_2-O_2 gaseous detonation wave moving into stoichiometric H_2-O_2 mixture at an initial pressure of 27.2 atm (400 psi). It should be noted that Chan did not use a conical liner for this particular experiment. Figure 50b illustrates the present experimental arrangement. Only about 70 g of PETN was used and a 20 degree conical liner was included. A detailed description of the operation of the facility can be found in Sec. 3. After shock loading, both specimens were cut into two halves as shown in Fig. 51. A special metallurgical cut-off wheel was used which consisted of a steel plate with the specimen mounted over it, traversed by a rotating silicon carbide abrasive wheel. The plate, the specimen and the lower half of the wheel were totally immersed in a bath of coolant which was continuously filtered and recirculated. This process helped to reduce the surface work hardening due to cutting to a minimum. The two cut faces were each ground on abrasive wheels

and then electropolished to an optical finish. Phosphoric acid diluted with water was used as an electrolyte. One of the polished surfaces was used to test the hardness changes while the other was etched in a solution containing 50 ml of water, 5 ml of sulphuric acid, 1 g of potassium dichromate and 2 drops of hydrochloric acid to reveal the grain structure.

6.3 Results and Discussion:

6.3.1 Photomicrographs of Shock Loaded Specimens:

A casual inspection of the etched specimens through an optical microscope revealed the existance of three distinct regions. Figure 52 is a schematic representation of these three regions. The differences in grain size and shape are very apparent as shown in Figs. 53-57. Region 3 of both specimens A and B (Fig. 57) has a microstructure which is very similar to the corresponding unimploded specimens (Fig. 53). At a magnification of 240, specimen A has in this region an average of 0.6 grains/cm^2 (4 grains/in^2) and specimen B, an average of 0.3 grains/cm^2 (2 grains/in^2). However, at the same magnification, region 1 of specimen A (Fig. 54a) which was exposed to high temperatures (~ 20,000°K) and high pressures has an average of 12 grains/cm^2 (80 grains/in^2). Thus, a 20-fold increase in the number of grains per unit area is observed very near the implosion surface (Region 1). Specimen B showed a similar increase. The number of grains increased from 0.3 grain/cm^2 (2 grains/in^2) to about 9 grains/cm^2 (60 grains/in^2), a 30-fold jump (Fig. 54b). The large increase in the number of grains near the crater surface will be discussed later. Region 2 of both the specimens (Fig. 55 & 56) had been squeezed and deformed by the passage of the shock wave. In the following, a physical interpretation as to the formation of the different regions is proposed.

As a crystalline material is deformed, its hardness increases as the dislocations become more tangled, and its ductility decreases. Typical changes for a cold-worked metal are shown in Fig. 58. The grains in the material elongate in the direction of deformation as shown in Fig. 58a. If the material is now heated to a slightly elevated temperature, the dislocations of opposite sign begin to annihilate each other, the point defects disappear, and physical properties such as resistivity approach the values of the undeformed material (Ref. 50). The microstructure, as viewed in the optical microscope remains unchanged until, at a higher temperature, the elongated grains transform to fine, equiaxed grains as shown in Fig. 58b. This nucleation of new strain-free grain in a deformed material is called re-crystallization (Ref. 50). If, after full re-crystallization, the material is heated further, the size of the grain increases and the driving force for this grain growth is the reduction in surface energy by the reduction in grain boundary area (Ref. 50). This grain growth is shown in Fig. 58c.

The phenomena just described can be applied to the deformation process in the shock loaded case for a qualitative comparison. It should be noted that durations in the shock loaded case are many orders of magnitude lower but the amplitude of the pressure and temperature pulses are many orders of magnitude higher than the corresponding cold-worked case.

At the onset of high pressures at the origin, the material starts deforming in both regions 1 and 2. At the same time, due to extensive heating of the material near the implosion surface, re-crystallization takes place on the top layers. The extent to which this layer is extended is dependent on the temperature pulse duration for a given material. This re-crystallization of copper is believed to have resulted in the formation of numerous grains (a 20-30 fold increase) in this region. However, temperatures in region 2 may not have reached high enough values and

hence the absence of any significant re-crystallization. Even in region 1, the temperatures may not have lasted long enough for any significant grain growth to take place. Region 3 was not affected at all from a microstructural point of view.

From the knowledge gained so far, microstructural studies are suited only for materials which undergo changes (such as a change in phase) during short pressure intervals. Further, changes in gain sizes are in general related to temperatures rather than pressures. But authors who worked on changes in material strength on shock loading have found that the hardness values can increase by several hundred percent (Refs. 47, 48, 51, 52). Hence, for a quantitative estimation of shock strength, hardness changes in all regions of the shocked specimens were determined.

6.3.2 Hardness Measurements:

SPECIMEN A:

The shock loaded specimen was mounted onto the base of a Leitz Miniload Hardness Tester as shown inFig. 59. Twenty points were chosen from each of the regions 1, 2 and 3 and the hardness values were determined and plotted in Fig. 60. Actual deviations of hardness values from the mean were much greater than the error involved in the determination of the hardness itself. Region 3, which was not affected from a microstructural point of view, had a Vickers hardness value of 86.5 Kg/mm^2. Region 2, which underwent large-scale plastic deformation and grain elongation had a value 108.2 Kg/mm^2. Region 1, which was subjected to large pressures as well as very high temperatures, had the lowest hardness value of just 64.0 Kg/mm^2. A fourth region, very near the corners around which the material had flowed into the barrel, had the highest hardness reading of 124.75 Kg/mm^2. For a proper interpretation of these results, it is necessary to know the hardness value of the unshocked specimen. This value is not given in Ref. 2. However, the compressive yield stress of the unshocked copper is reported as 2000 Kg/cm^2 (28,750 psi) (Ref.2). Therefore, a compressive test on 7.5 cm (3 in) long x 6.5 cm^2 (1 in^2) cross-sectional area copper block was carried out and the stress-strain curve plotted (Fig. 61). From this plot, the yield stress was determined to be 2400 Kg/cm^2 (34,400 psi) . Three different copper blocks of the same properties and dimensions as the previous one were annealed to temperatures of around $400^{\circ}F$ for varying periods of time and compressive tests were carried out for these specimens. The stress-strain relationships determined experimentally, were plotted for these specimens (Figs. 62 to 64). As expected, the yield stress decreased as the annealing period was increased. For each of the four specimens, mean value of Vickers Hardness was found and plotted in Fig. 65. A cross plot of yield stress vs. Vickers Hardness is shown in Fig. 66. From this plot, the hardness value for a yield stress of 2000 Kg/cm^2 (28,750 psi) was determined to be 84.7 Kg/mm^2.

The above result indicates that the hardness values changed in all regions after the shock loading. Apart from Region 1, the hardness value increased considerably in all regions. The reason for the very low hardness in region 1 might be due to the annealing effect caused by direct exposure to very high temperatures. Region 4, on the other hand,had been forced against the high strength steel barrel and worked severely. As a result, the hardness of this region reached the highest value. However, regions 2 and 3 were likely hardened only by the passage of the shock waves. In the following, the changes

in the hardness values are compared with available data (Ref. 48) to yield the peak pressures generated by the shock wave. It should be noted that the available data have been collected from one-dimensional plane shock wave experiments and therefore the comparison may only yield approximate values for nonstationary spherical implosions.

Figure 67 illustrates the effect of shock pressures on hardness of copper. This curve is unique and is independent of the hardness value of the unshocked specimen (Ref. 48). For example, a copper block of initial hardness 75 Kg/mm^2 (VH) will not undergo any change in hardness value up to a shock pressure of 62 k bars (see Fig. 67). From this figure, it is seen that region 2 which had a hardness value of 108.2 Kg/mm^2 must have been subjected to a shock pressure of about 155,000 atm (155 k bars). However, region 3 had been hardened to a much less degree and the estimated shock pressures are about 80,000 atm (~ 80 k bars) corresponding to a hardness value of 86 Kg/mm^2. The 50% drop in pressures (from 155,000 atm in region 2 to about 80,000 atm in region 3) can be attributed to the weakening of the main spherical shock wave through subsequent interactions from reflected waves from the edge of the copper block.

SPECIMEN B:

Figure 68 illustrates the hardness changes in the three regions 1-3. Region 2, which had been compressed severely by the shock, reached a mean hardness value of 110 Kg/mm^2. The corresponding shock pressures are estimated (from Fig. 69) to be 160,000 atm (~ 160 k bars). It should be noted that the peak pressures in the specimen are greater for this run (compared with Chan's run) in spite of the fact that 20 g less explosive (PETN) and a 20-degree conical liner were used in the present experiment. It may be noted that the presence of a 20-degree conical liner reduced the peak pressures by about 45% in gas-driven implosions. This increase in pressures reached in specimen B is a direct consequence of adding a steel backing plate for the copper specimen to prevent any plastic flow into the barrel.

The hardness of region 1 reached a very low value (~ 59 Kg/mm^2) as for specimen A. This result seems to be consistent and presently it is believed that lowering of hardness near the implosion surface is due to an annealing effect. Again, Region 3 showed very little change in the hardness values. Corresponding to a hardness value of about 87 Kg/mm^2, peak pressures of about 90,000 atm (~ 85 k bars) are reached in this region. The drop (160 to 85 k bars) can be attributed to weakening of the main shock wave as for specimen A.

Finally, it should be noted that Roig (Ref. 53), in one of his recent experiments under very similar conditions ($2H_2 + O_2$ at 400 psi, 70 g PETN) converted the α-type (body centered cubic) iron to the ϵ-type (hexagonal close packed) phase. This phase transition has been reported to occur at about 130 k bar (Ref. 47). This is in agreement with the present results for copper obtained from hardness measurements.

X-Ray Pictures:

Shocked materials undergo several changes (Sec. 6.1.1). Some of these like phase changes, stacking faults and twin faults can be detected from X-ray photographs. Pure copper does not undergo any phase change. Also,

large twin faults cannot be determined from X-ray powder photographs. To see if there are any general changes, copper powder samples were taken from each of the regions (1, 2 and 3) of the shocked specimen (B) and also from the unshocked copper. Figure 69 shows X-ray diffraction lines reflected from different crystal planes.

Twin faults, if present, will produce an asymmetry in the peaks of any given reflection line (Ref. 54). The difference between the peak position (in terms of intensity) and the centre of gravity for a given hkl reflection (Ref. 54) can only be determined from a densitometer trace of the X-ray film. This was not done since the result would not be of any use in determining physical quantities such as pressure or temperature associated with the shock loading.

Stacking faults, present in a material, produce peak shifts (Ref. 54)in the powder pattem . This was readily observed in X-ray pictures taken from regions 1 and 2. The shifts were estimated to be approximately (0.01 - 0.02) 20^{o} and they are present for all reflection lines. However, region 3, does not seem to have been affected at all and X-ray pictures do not show any change.

7. CONCLUSIONS

Time-resolved pressures have been measured at the origin of combustion-driven implosions. Gaseous mixtures of stoichiometric hydrogen - oxygen were used in the initial pressure range of 1.7 atm (25 psi) to 6.8 atm (100 psi). The peak pressures behind the reflected spherical implosion as measured by a PCB Piezoelectric transducer (6.3 mm dia, 0.8 μsec - rise time) increased from about 1360 atm (20,000 psi) for an initial loading pressure of 1.7 atm (25 psi) to approximately 9860 atm (145,000 psi) for an initial loading pressure of 6.8 atm (100 psi). The measured rise times decreased from about 1 μsec for the 1.7 atm (25 psi) runs to about 0.65 μsec for the 6.8 atm (100 psi) runs. The averaged pressures measured over the transducer area seem to have the profile previously calculated by Elsenaar (Ref. 16). A good comparison is not possible since the present results were obtained at fairly low initial loading pressures (6.8 atm and below) as opposed to his numerical results which were obtained for higher initial loading pressures (13.6 atm and above). The presently measured pressures exhibited substantial scatter in the early stages of the experimental work owing to off-centre implosions. An improved technique of mounting the exploding wire greatly improved the focussing and reduced the scatter. There is little doubt that actual point peak pressures are vastly greater than that obtained from a gauge of finite size.

The effect of diluting the stoichiometric ($2H_2 + O_2$) mixtures with helium or hydrogen on pressure histories at the focus have been determined. The results indicated that the addition of helium (up to 2 moles) or hydrogen (up to 1 mole) significantly increased the peak pressures. The effects of dilution with helium are more pronounced than those of hydrogen. Since substantial reduction in molecular weight and escape speed can be achieved while simultaneously generating significantly higher pressures, such gases make ideal drivers for hypervelocity launchers and shock tubes. Hydrogen or helium dilution decreased the cycle times (owing to higher sound speeds and shock velocities) which were found to be in good agreement with previous results for higher filling pressures. When the amounts of extra hydrogen or helium dilution was increased beyond a critical molar value (3 for the He and 2 for

H_2) deflagrating combustion developed. The peak pressures and the flame speeds obtained in the deflagration runs were in good agreement with computed results (Ref. 9).

For the first time, experimental evidence was obtained to show that an accurately made conical liner which extends right to the gauge periphery has no effect on the pressures generated at the implosion focus. The pressures are identical with those produced in a hemispherical chamber. In the present experiments, by using a 20-degree conical liner, the mass of explosive gases was reduced by 34%, but the final pressures were almost the same as for the hemispherical implosion chamber. For gas-driven implosions, a 20-degree conical liner that does not extend to the gauge, reduced the peak pressure by about 45% and decreased the pulse decay rate significantly. The fact that the peak pressures dropped by 45% was utilized to make an indirect estimate of the peak pressure for a 6.8 atm (100 psi) initial pressure run when the gauge becomes overloaded. The experiments indicated that the transducer output was not linear for peak pressures above 8500 atm (125,000 psi) [or an inlet pressure of 5.1 atm (75 psi)].

Lead witness-plates were used to produce imprint craters which showed that the gaseous implosions were well-focussed and reasonably well-centered. The results conclusively indicate that the present ignition system as developed by Roig (Ref. 15) together with the various exploding-wire-mounting procedures adopted in the course of the present work have improved the performance of the facility in terms of reproducible centered and well focussed implosions. A numerical calculation showed that the errors involved in the present measurements due to off-centre implosions was less than 2% for the observed locations of focal points. Perhaps the small shifts in focal points could be eliminated by pre-mixing the explosive gases before introducing them into the combustion chamber and by polishing the copper hemispheres before each run to obtain an accurate hemisphere with a uniform reflecting surface.

Copper witness-plates, subjected to explosively-driven implosions, were analyzed using metallurgical techniques. Photomicrographs were taken of the imploded specimen which illustrated the changes in grain size and shape arising from the passage of strong shock waves. Microhardness changes were measured to yield approximate values of peak pressures reached in the specimens. For a run conducted with stoichiometric ($2H_2 + O_2$) mixture at a loading pressure of 27.2 atm (400 psi) with about 70 gms of PETN, the peak pressure was estimated to be approximately 160,000 atm (~ 160 k bars).

Finally, extrapolating the present direct pressure measurements to higher initial pressures suggests that (averaged) peak pressures of the order of 10^5 atm can be achieved even with gas-driven implosions at an initial loading pressure of about 68 atm (1000 psi). Judging from the present results, such high pressures may not exist for more than a few-tenths ofa microsecond. High-pressure transducers such as manganin gauges have been developed at Stanford Research Institute to measure pressures in the megabar range (Ref. 55) with submicrosecond rise times. However, these gauges are of relatively large size (5-8 cm dia) and generally suitable for solid-solid impact experiments where ideal one-dimensional conditions can apparently be maintained. Miniaturizing a four-terminal-manganin gauge to suit our requirements may not be impossible but would definitely be a challenging task. Further, the response of such gauges to nonuniform pressures is not known. Hence,for gas-driven implosions at initial loading pressures above 6.8 atm (100 psi) and

explosive-driven implosions, an indirect method such as the metallurgical techniques might be developed and improved to provide values of peak pressures. Nevertheless, it is the pressure history that is most useful. For explosive runs to be conducted at UTIAS in the near future, this could only be provided by a transducer with submicrosecond rise times in the megabar range.

REFERENCES

1. Glass,I. I. — Appraisal of UTIAS Implosion-Driven Hypervelocity Launchers and Shock Tubes: Progress in Aerospace Sciences, Vol. 13, V, pp. 223-291, 1972, Pergamon Press, Oxford.

2. Chan, S. K.; Capelli, G.; Graf, W. O. — Performance Trials of the Eight-Inch Diameter UTIAS Implosion-Driven Hypervelocity Launcher MK II and MK III. UTIAS Tech. Note No. 161, 1971.

3. Glass, I. I.; Chan, S. K. — Radiative Relaxation Behind High Speed Shock Waves in Air. Phys. of Fluids, Vol. 17, No.4, pp.688-690, April,1974. Also UTIAS Report No. 191, August, 1973.

4. Glass, I. I.; Sharma, S. P. — Production of Diamonds from Graphite Using Explosive-Driven Implosions. AIAA Journal, Vol. 14, pp.402-404, March, 1976.

5. Benoit, A. — Thermodynamic and Composition Data for Constant Volume Combustion of Stoichiometric Mixtures of Hydrogen-Oxygen Diluted with Hydrogen or Helium, UTIAS Tech. Note No. 85, 1964.

6. Benoit, A. — Specific Heat Ratios and Isentropic Exponents for Constant-Volume Combustion of Stoichiometric Mixtures of Hydrogen - Oxygen Diluted with Helium or Hydrogen. UTIAS Tech. Note No. 102,1966.

7. Benoit, A. — Characteristics of Chapman-Jouguet Detonation Propagating in Stochiometric Hydrogen-Oxygen Mixtures Diluted with Helium and Hydrogen, UTIAS Tech. Note No. 104, 1966.

8. Benoit, A. — Equilibrium Thermodynamic Data for the H_2-O_2-He Systems. UTIAS Tech. Note No. 128, 1968.

9. Benoit, A. — An Experimental Investigation of Spherical Combustion for the UTIAS Implosion-Driven Launcher. UTIAS Tech. Note No. 71, 1963.

10. Benoit, A.; Glass, I. I. — An Experimental Study of Spherical Combustion Waves in a Hemispherical Chamber. Combustion and Flames, Vol. 12, No.2, Dec 1968, UTIAS Reprint No. 125.

11. Makomski, A.H. — Preliminary One-Dimensional Investigation of the Initiation of Low-Density PETN by Hydrogen-Oxygen Detonation Waves UTIAS Tech . Note No. 83, Feb, 1965.

12. Kennedy, J.E.; Glass, I. I. — Multipoint Initiated Implosions from Hemispherical Shells of Sheet Explosive. UTIAS Tech. Note No. 99, 1966.

13. Flagg, R. F. — Explosive-Driven, Spherical Implosion Waves. The Phys. of Fluids, Vol. 11, No. 10, pp.2282-2284, Oct, 1968. Also UTIAS Report No. 125, June,1967.

14. Roberts, D. E. A spectroscopic Investigation of Combustion-Driven Implosion Waves. UTIAS Tech. Note. No. 140, 1969.

15. Roig, R. A. A Spectroscopic Investigation of Combustion-Driven Implosions. UTIAS Report No. 214, 1977.

16. Elsenaar, A. A Numerical Modal for a Combustion-Driven Spherical Implosion Wave. UTIAS Tech. Note. No. 144, 1969.

17. Macpherson, A.K. A Preliminary Study of Spherical Detonation Wave Symmetry in Stoichiometric Hydrogen-Oxygen Mixtures. UTIAS Tech.Note No.154, 1970.

18. Macpherson,A.K. A Preliminary Monte-Carlo Analysis of the Reflection of an Imploding Hemispherical Shock Wave Similar to that Generated in the UTIAS Implosion-Driven Hypervelocity Launcher or Shock Tube. UTIAS Report No.152, 1970.

19. Watson, J. D. Implosion-Driven Hypervelocity Launcher Performance Using Gaseous Detonation Waves. UTIAS Tech. Note. No. 113, 1967.

20. Poinssot, J.C. A Preliminary Investigation of a UTIAS Implosion-Driven Shock Tube. UTIAS Tech. Note. No. 136, 1969.

21. Glass, I. I. Shock and Combustion Wave Dynamics in a Implosion-Driven Hypervelocity Launcher. UTIAS Review No.25, 1965.

22. Sevray, P. A. Performance Analysis of the UTIAS Implosion-Driven Hypervelocity Launcher. UTIAS Tech.Note No.121,1968.

23. Flagg, R. F.
Mitchell,G.P. An Optimization Study of the UTIAS Implosion-Driven Hypervelocity Launcher MKII. UTIAS Tech. Note. No.130, 1968.

24. Bremner, G.F.
Glass, I. I. Hypervelocity Launcher, UTIAS Progress Report, Sec. C-5, 1961.

25. Benoit, A.
Bremner,G.R.
Brode, H. L.
Glass, I.I. Implosion-Driven Hypervelocity Launcher. UTIAS Progress Report, Sec. C-1, 1962.

26. Dawson, V.C.D.
Waser, R.A.
Oakes, D.O. The MK II UTIAS Implosion-Driven Hypervelocity Launcher Design Analysis. UTIAS Tech.Note No.147, 1970.

27. Cherwinski,W. Structural Design and Development of UTIAS Implosion-Driven Launchers. UTIAS Report No.153, 1971.

28. Courant, R.
Friedrichs,K. Supersonic Flow and Shock Waves. Interscience Publishers, 1948.

29. Guderley, G. Strong Spherical and Cylindrical Shock Waves in the Neighbourhood of the Centre of the Sphere or the Axis of the Cylinder. Luftfahrtforschung, Vol. 19, No.9, pp.302-312, 1942.

30. Chester, W. The Propagation of Shock Waves in a Channel of Non-Uniform Width. Quarterly Journal of Mechanics and Applied Mathematics, Vol. Vl, Pt. 4, 1953.

31. Chisnell, R.F. The Motion of a Shock Wave in a Channel, with Application to Cylindrical and Spherical Shock Waves. Journal of Fluid Mechanics, Vol. 2, p.286, 1957.

32. Whitham, G.B. On the Propagation of Shock Waves Through Regions of Non-Uniform Area of Flow. Journal of Fluid Mechanics, Vol. 4, p.337, 1958.

33. Brode, H. L. Theoretical Description of the Performance of the UTIAS Hypervelocity Launcher - Proceedings of the Second International Colloquium on the Gasdynamics of Explosions and Reactive Systems, Astronautics Acta, Vol. 15, pp. 301-309, 1970.

34. Chan, S. K. An Analytical and Experimental Study of an Implosion-Driven Shock Tube. UTIAS Report no. 191, Aug, 1973.

35. Sharma, S.P. Production of Diamonds from Graphite Using Explosive -Driven Implosions. UTIAS Tech.Note.No.196, Dec, 1975.

36. Lee, J. H.
Knystautas,R.
Guirao, C. M. Critical Power Density for Direct Initiation of Unconfined Gaseous Detonations, Fifteenth Symposium (International) on Combustion, The Combustion Institute, p.53 (1974).

37. Lee,J. H.
Lee, H.K.
Knystautas,R. Direct Initiation of Cylindrical Gaseous Detonations, Phys. Fluids,Vol.9, p.221 (1966).

38. Bach, G. G.
Knystautas,R. Thirteenth Symposium (International) on Combustion,The Combustion Institute, p.1097 (1971).

39. Knystautas, R.
Lee, J. H. On the Effective Energy for Direct Initiation of Gaseous Detonations, Combustion and Flame, Vol. 27, pp.221-228 (1976).

40. Filler, W.S. Propagation of Shock Waves in a Hydrodynamic Conical Shock Tube, Phys. Fluids, Vol.7, p.664 (1964.).

41. Zel'dovich, Ya. B.
Rauzen, Yu, P. Physics of Shock Waves and High Temperature Hydrodynamic Phenomena, Vol.II, Academic Press, 1967.

42. Glass, I. I.
Hall, J. G. Shock Tubes, Sec.18, Handbook of Supersonic Aerodynamics, Navord, Report 1488 (Vol. 6),1959.

43. Pluckebaum, J. W.
Strauss, W. A.
Edse, R.
Propagation of Spherical Combustion Waves, USAF Report ARL 63-101, 1963.

44. Benoit, A.
Galipeau, J.
Thermodynamic and Combustion Data for Constant-Volume Combustion of Stoichiometric Mixtures of Hydrogen-Oxygen Diluted with Helium or Hydrogen. UTIAS Tech. Note No.85, 1964.

45. Sedov, L.I.
Similarity and Dimensional Methods in Mechanics, Academic Press,1959.

46. Bundy, F. P.
Formation of New Materials and Structures by High Pressure Treatment, ASTM Special Technical Publication No.374.

47. Pugh, H.Ll.D.
The Mechanical Behaviour of Materials Under Pressure, Applied Science Publishers, 1971.

48. Shewmon, P. G.
Zackay, V. S.
Response of Metals to High Velocity Deformation - Proceedings of a Technical Conference held at Ester Park, Colorado, July 11-12, 1960, Interscience Publishers, 1961.

49. Appleton, A. S.
The Metallurgical Effects of Shock Waves, Applied Materials Research, p.195, Oct, 1965.

50. Moffatt, W. G.
Pearsall, G. W.
The Structure and Properties of Materials, Vol. 1, John Wiley and Sons, Inc, New York, 1967.

51. Smith, C. S.
Metallographic Studies of Metals after Explosive Shock, Trans. Amer. Inst. min (metall.) Engrs., 212, p. 574, (1958).

52. Appleton, A. S.
Waddington, J.S.
The Importance in Explosive Loading Experiments. Acta Met., Vol. 12, p.956 (1964).

53. Roig, R. A.
Measurement of Explosively-Driven Implosion Pressures Using Metallurgical Techniques, UTIAS Tech. Note. (to be published).

54. Champion, R. S.
Rhode, R. W.
Hugoniot Equation of State and the Effect of Shock Stress Amplitude and Duration on Hardness of Hadfield Steel, Journal of Appl. Phys. Vol. 41, p.2213 (1970).

55. De Carli, P. S.
Private Communication. (letter dated Feb 12,1976).

TABLE 1

GASEOUS IMPLOSION IMPRINTS ON LEAD TARGETS

RUN NO.	CRATER RADIUS	CRATER DEPTH	REMARKS
1	1.1 mm	------	Depth not measured but lead block melted and re-used for run 2. 0.5 mm - off centre.
2	2.0 mm	1.1 mm	0.25 mm - off centre.
3	2.4 mm	1.2 mm	0.5 mm - off centre.
4	0.8 mm	0.5 mm	Lead block recessed by about 0.5 mm due to machining error 0.2 mm - off centre.

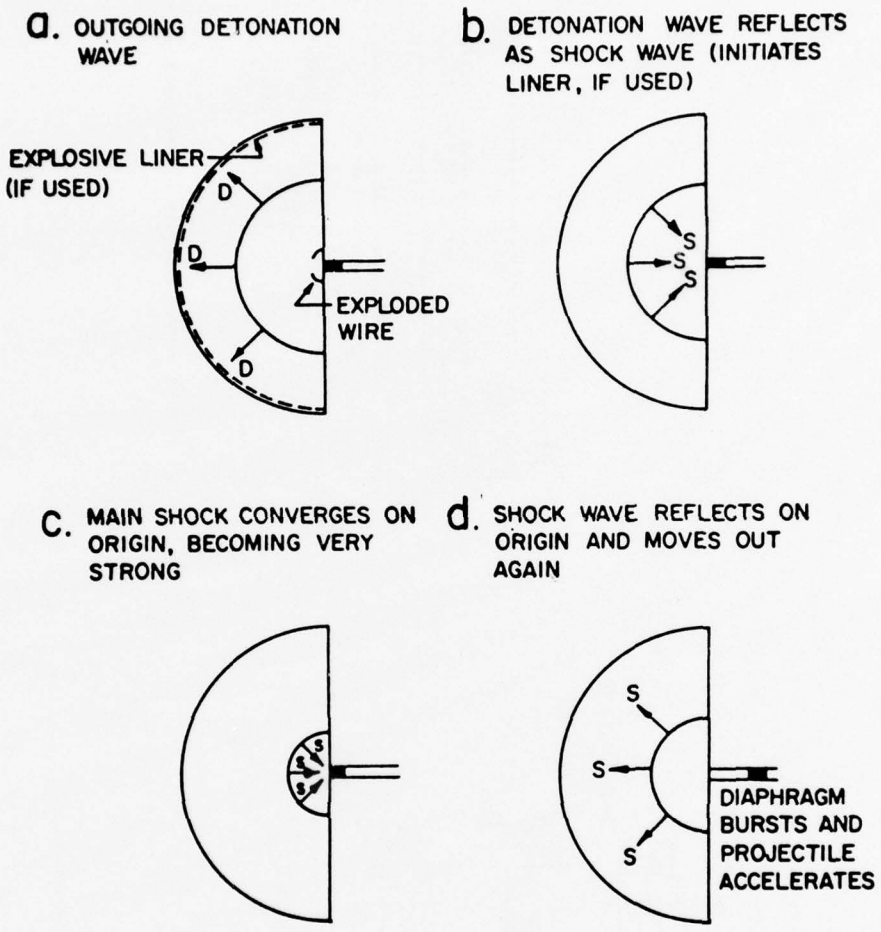

FIG. 1 SCHEMATIC OF IMPLOSION CHAMBER WAVE DYNAMICS (REF. 1)

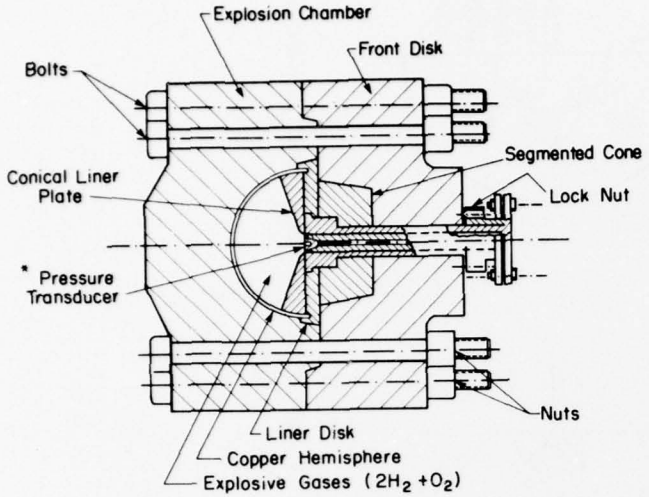

* See details in Figs. 3 and 9

FIG. 2 UTIAS IMPLOSION CHAMBER FACILITY (REF. 35)

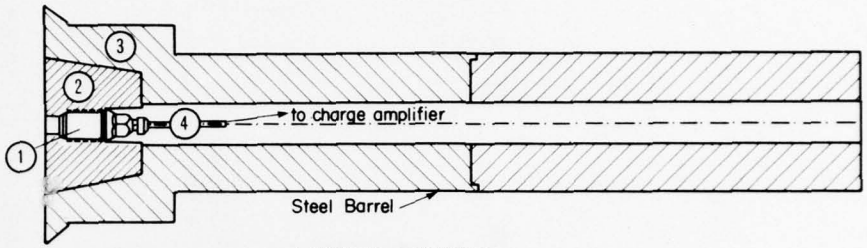

1 PRESSURE TRANSDUCER
2 STEEL INSERT
3 BARREL
4 LOW-NOISE CABLE

FIG. 3 BARREL AND PRESSURE TRANSDUCER IN POSITION

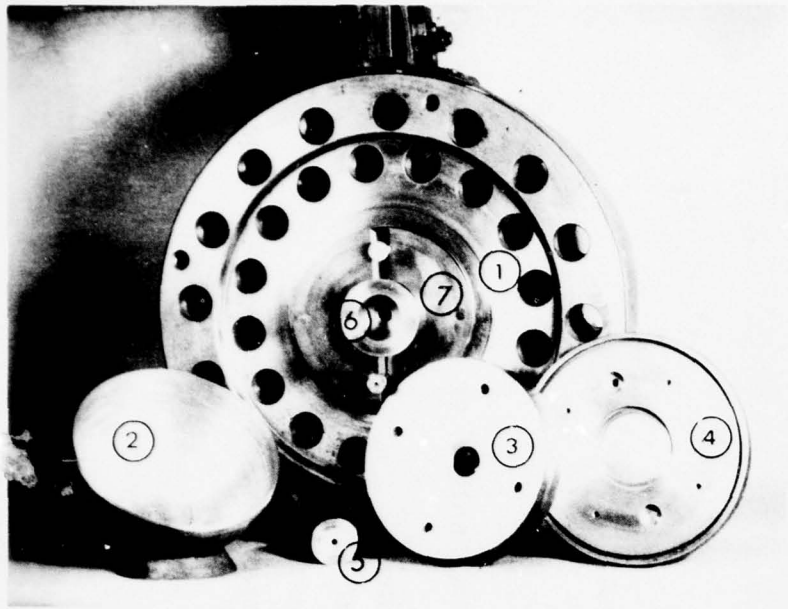

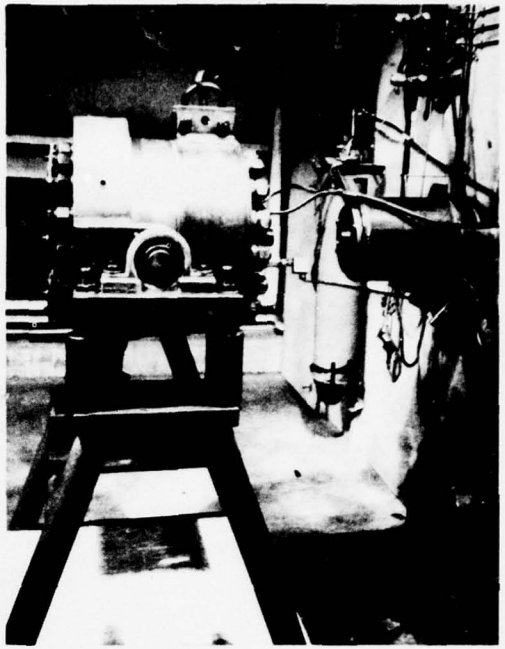

1 FRONT DISC
2 EXPLOSIVE LINER
3 PROTECTOR DISC
4 LINER DISC
5 PRESSURE GAUGE, INSERT
6 BARREL
7 SEGMENTED CONE

FIG. 4 PHOTOGRAPH ILLUSTRATING MAIN PARTS OF UTIAS IMPLOSION CHAMBER FACILITY (REF. 35)

FIG. 5 UTIAS IMPLOSION CHAMBER IN FIRING POSITION

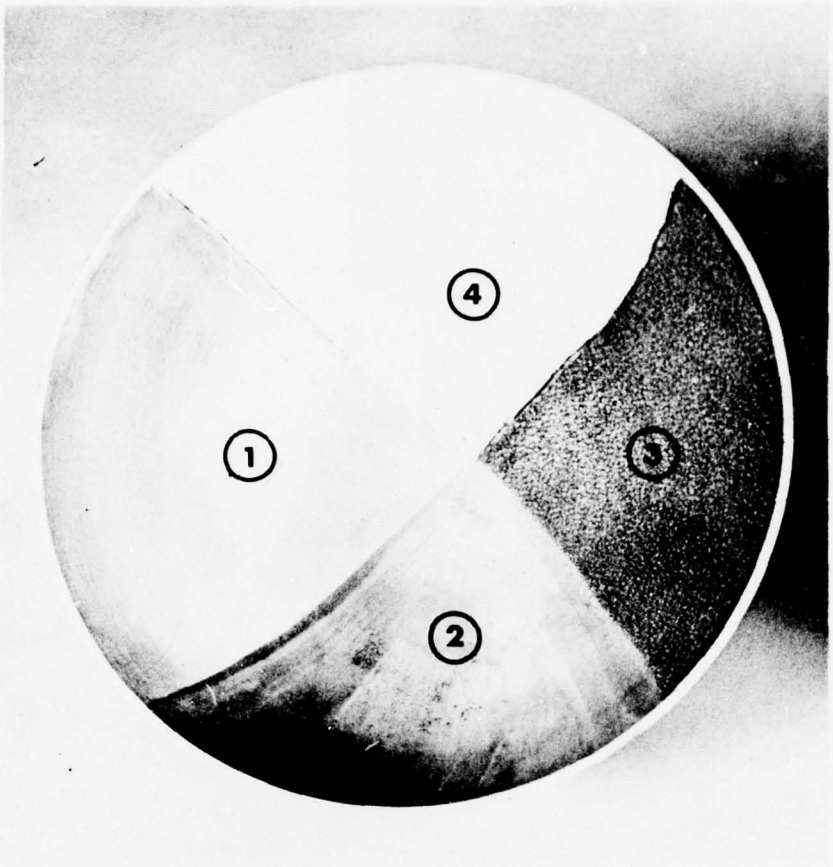

FIG. 6 STEPS REQUIRED FOR PREPARATION OF EXPLOSIVE LINER (REF. 35)

1 POLISHED COPPER LINER

2 THIN COAT OF CEMENT

3 OPEN-CORE FOAM PLASTIC MATRIX

4 PETN + COTTON LINTERS FORCED INTO PLASTIC MATRIX

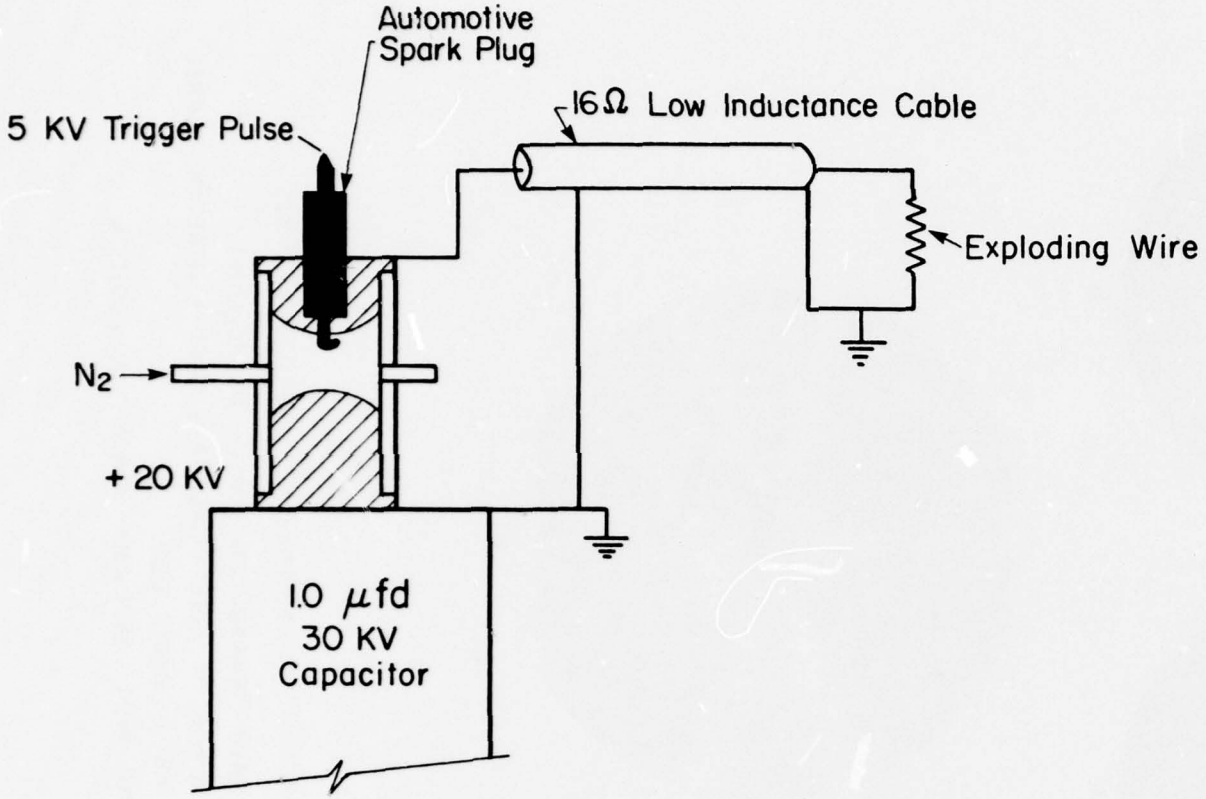

FIG. 7 IGNITION SYSTEM (REF. 15)

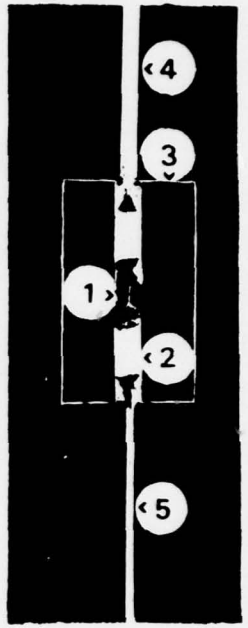

1 EXPLODING WIRE
2 COPPER TAPE
3 POLYETHYLENE SHEET
4 HIGH-VOLTAGE LEAD
5 GROUND LEAD

FIG. 8 EXPLODING WIRE ASSEMBLY

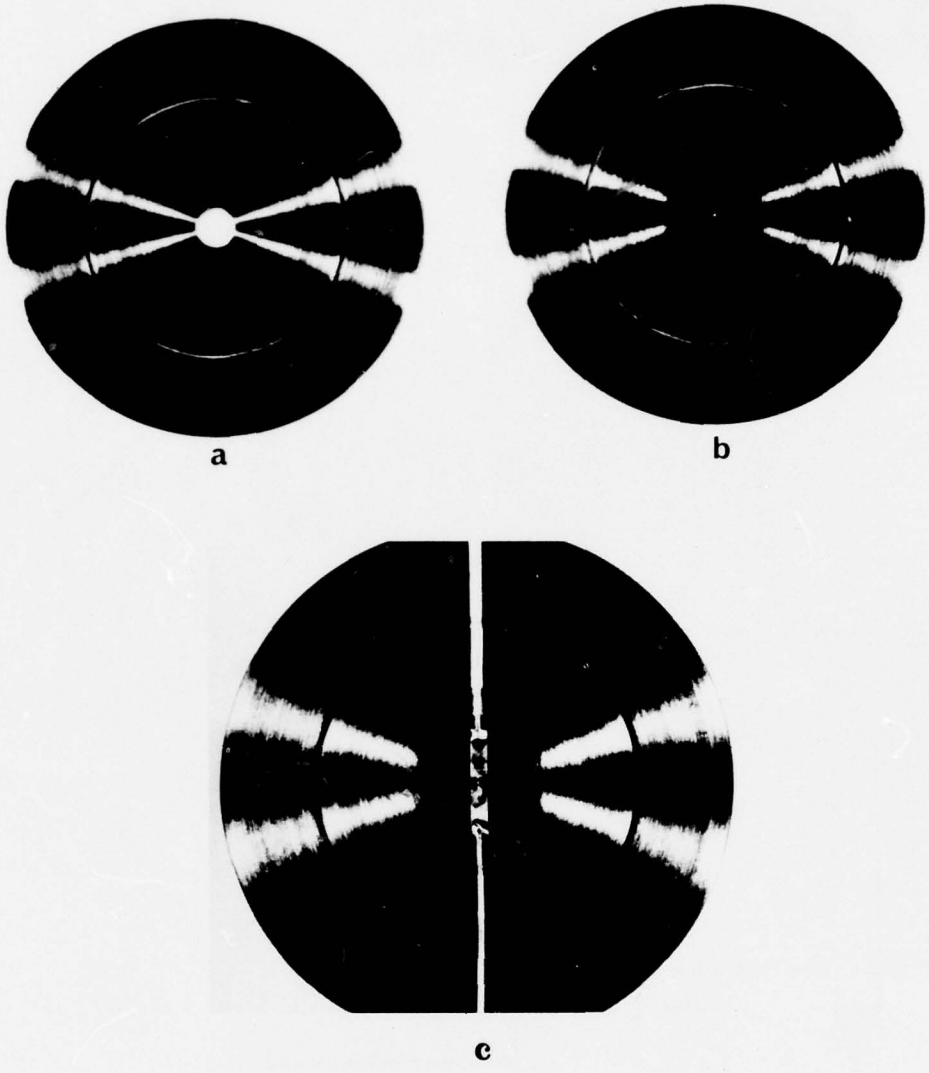

FIG. 9 STEPS INVOLVED IN ASSEMBLING EXPLODING WIRE

a. BARREL WITH TRANSDUCER FIXED IN POSITION

b. THREE LAYERS OF ELECTRICAL TAPE AND CENTRE OF BARREL SHOWN AS A WHITE DOT

c. EXPLODING WIRE ASSEMBLY PLACED IN POSITION

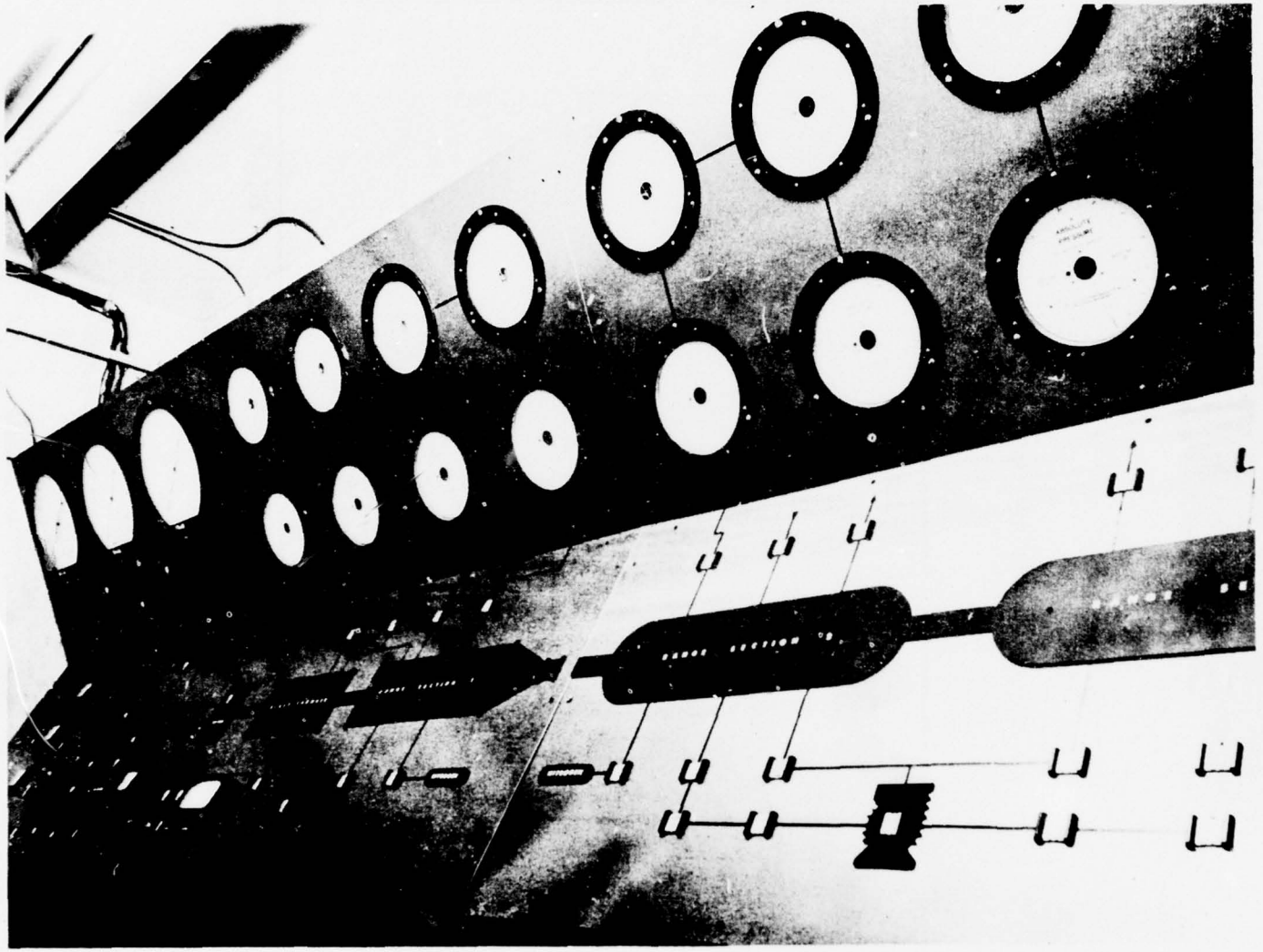

FIG. 10 CONTROL PANEL (REF. 35)

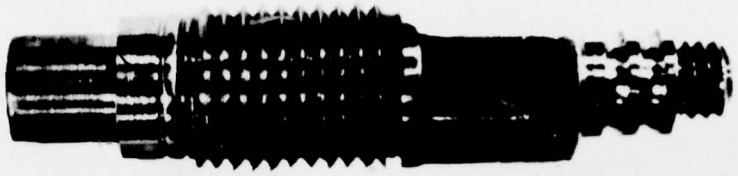

FIG. 11 PRESSURE TRANSDUCER

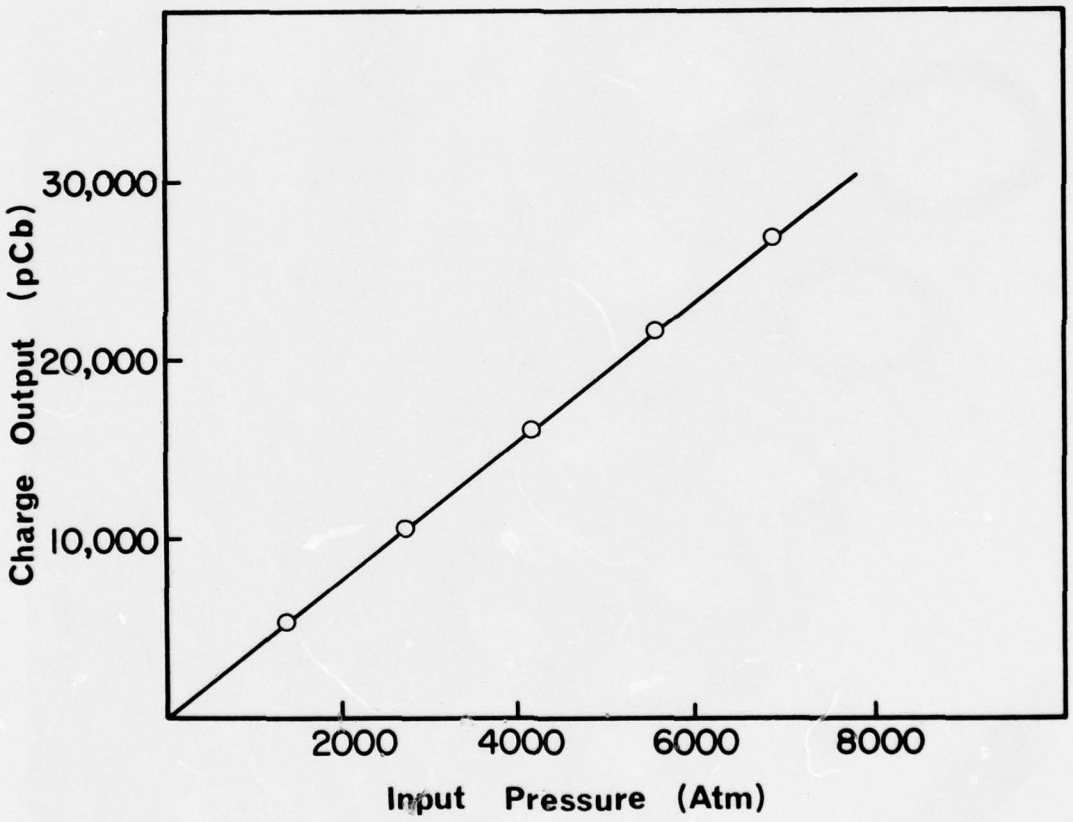

FIG. 12 TRANSDUCER CALIBRATION

a)

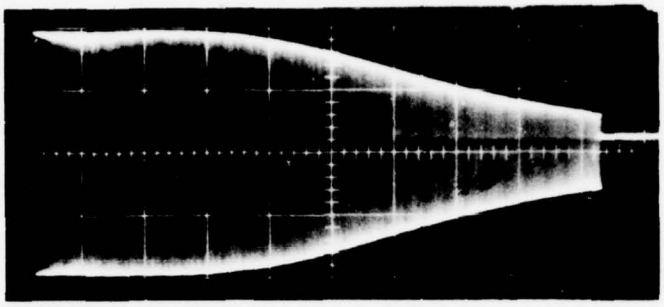

LOW-PASS FILTER SET AT 150 KHZ

HORIZONTAL SCALE : 0·7 HZ - 300 KHZ (LINEAR SWEEP)

VERTICAL SCALE : 200 mV / DIV

b)

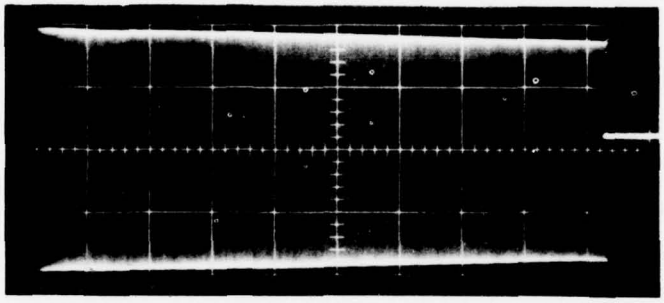

NEW FILTER

HORIZONTAL SCALE : 0·7 HZ - 300 KHZ (LINEAR SWEEP)

VERTICAL SCALE : 200 mV / DIV

c)

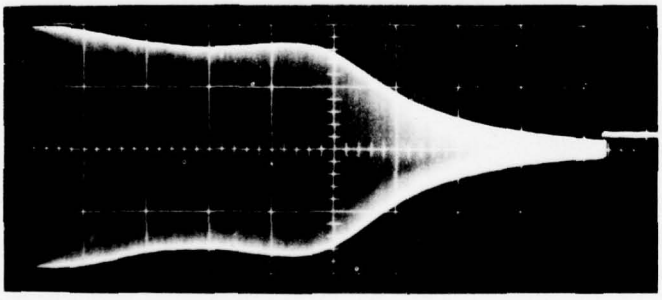

NEW FILTER

HORIZONTAL SCALE : 7 K HZ - 1·5 MHZ (LINEAR SWEEP)

VERTICAL SCALE : 200 mV / DIV

FIG. 13 PERFORMANCE OF CHARGE AMPLIFIER

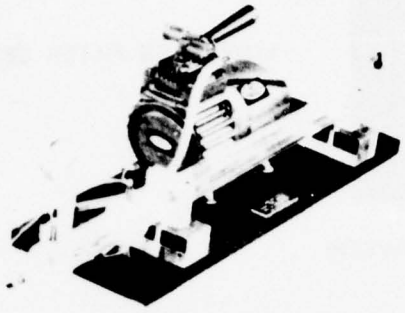

Shock Tube

(a)

DRIVER GAS : AIR

DRIVER PRESSURE : 1 ATM

CHANNEL GAS : AIR

CHANNEL PRESSURE : 15 TORR

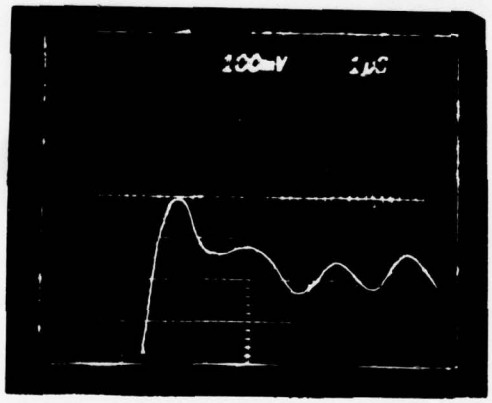

(b)

HORIZONTAL SCALE : 1 μSEC / DIV

VERTICAL SCALE : 103 TORR / DIV

FIG. 14 SHOCK TUBE RUN ILLUSTRATING TIME RESPONSE OF PRESSURE TRANSDUCER

a)

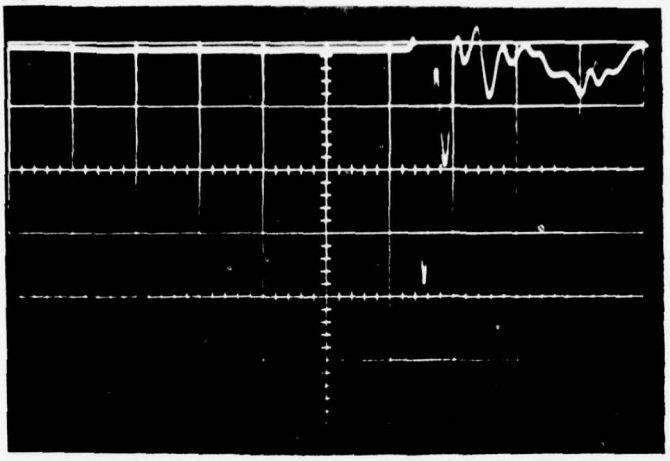

DETONATING COMBUSTION

$2H_2 + O_2$ AT 3·4 ATM

VERTICAL SCALE: 1360 ATM/DIV

HORIZONTAL SCALE: 4 μSEC/DIV

b)

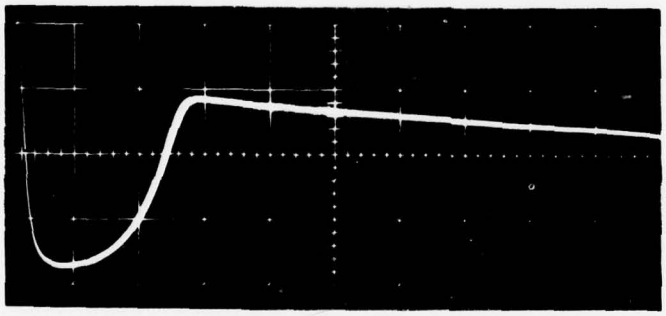

DEFLAGRATING COMBUSTION

$2H_2 + O_2 + 3He$ AT 3·4 ATM

VERTICAL SCALE: 13·6 ATM/DIV

HORIZONTAL SCALE: 1 mSEC/DIV

c)

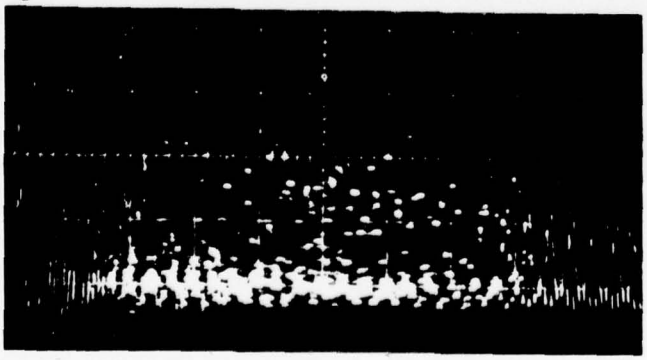

TRANSITIONAL COMBUSTION

$2H_2 + O_2 + 2H_2$ AT 3·4 ATM

VERTICAL SCALE: 13·6 ATM/DIV

HORIZONTAL SCALE: 1 mSEC/DIV

FIG. 15 PRESSURE–TIME RECORDS FOR DIFFERENT TYPES OF COMBUSTION WAVES

DETONATING COMBUSTION OF $2H_2 + O_2$ AT 5·1 ATM

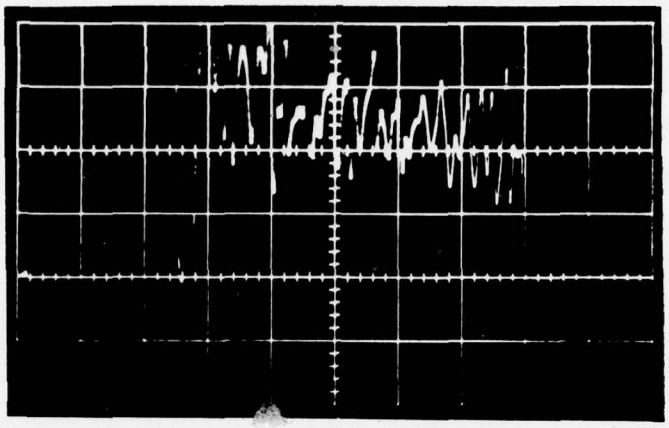

a

HORIZONTAL SCALE: 10 μSEC/DIV

VERTICAL SCALE: 68 ATM/DIV

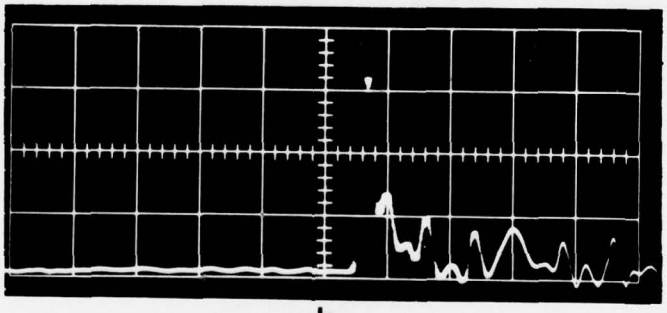

b

HORIZONTAL SCALE: 4 μSEC/DIV

VERTICAL SCALE: 2720 ATM/DIV

FIG. 16 PRESSURE HISTORY AT FOCUS

REPEATABILITY OF PRESSURE MEASUREMENT

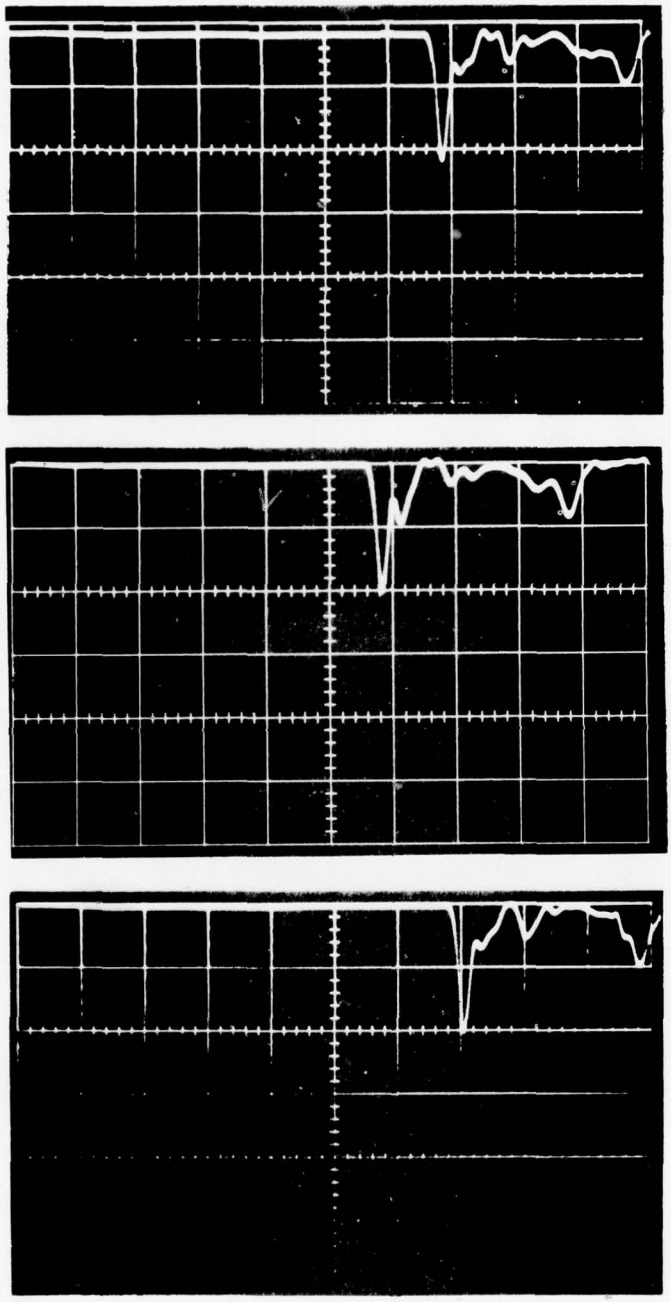

$2H_2 + O_2$ AT 1·7 ATM

HORIZONTAL SCALES: 4 μSEC/DIV

VERTICAL SCALES: 680 ATM/DIV

FIG. 17 REPEATABILITY OF PRESSURE MEASUREMENTS FOR DETONATING COMBUSTION

$2H_2 + O_2$ AT 6·8 ATM

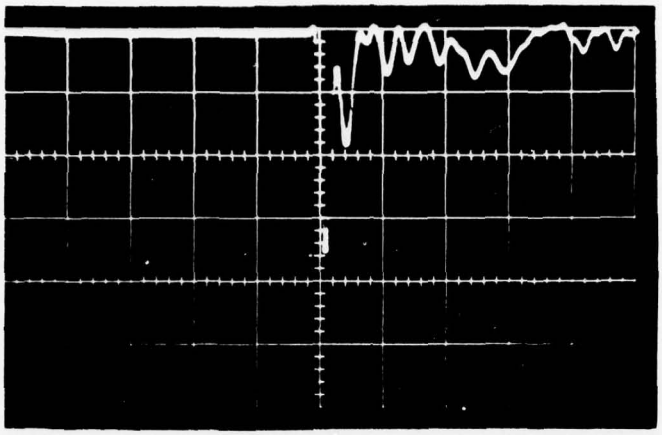

HORIZONTAL SCALE : 4 μSEC/DIV

VERTICAL SCALE: 2720 ATM/DIV

FIG. 18 PRESSURE HISTORY AT FOCUS

$2H_2 + O_2$ AT 5·1 ATM

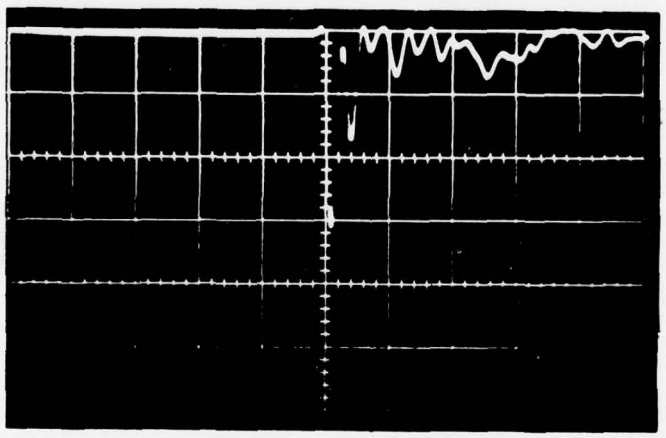

HORIZONTAL SCALE: 4 μSEC/DIV

VERTICAL SCALE: 2720 ATM/DIV

FIG. 19 PRESSURE HISTORY AT FOCUS

$2H_2 + O_2$ AT 3·97 ATM

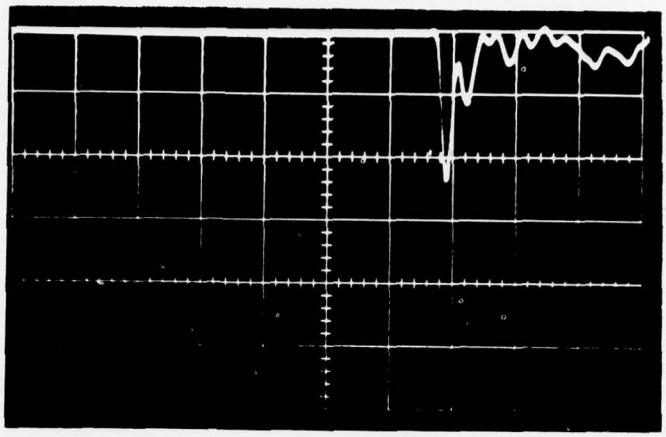

HORIZONTAL SCALE: 4 μSEC/ DIV

VERTICAL SCALE: 2720 ATM/ DIV

FIG. 20 PRESSURE HISTORY AT FOCUS

$2H_2 + O_2$ AT 3·4 ATM

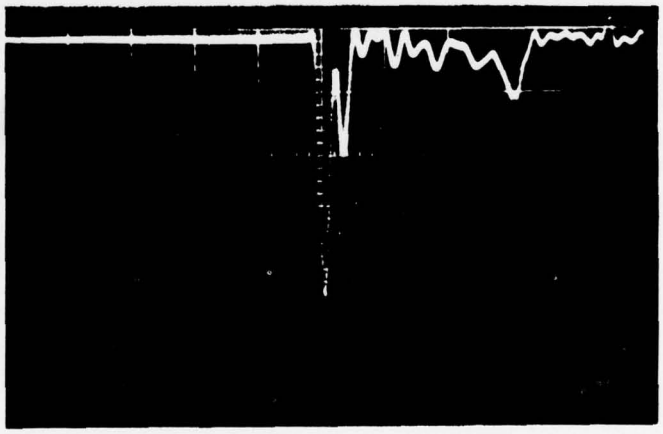

HORIZONTAL SCALE: 4 μSEC/ DIV

VERTICAL SCALE: 1360 ATM/ DIV

FIG. 21 PRESSURE HISTORY AT FOCUS

$2H_2 + O_2$ AT 2·83 ATM

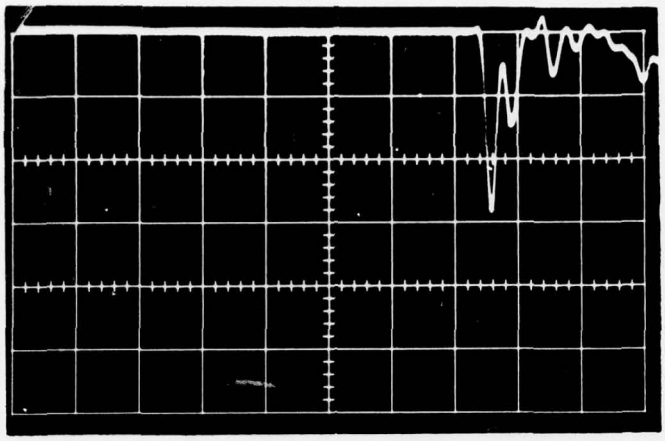

HORIZONTAL SCALE : 4 μSEC/DIV

VERTICAL SCALE: 1360 ATM/DIV

FIG. 22 PRESSURE HISTORY AT FOCUS

$2H_2 + O_2$ AT 2·55 ATM

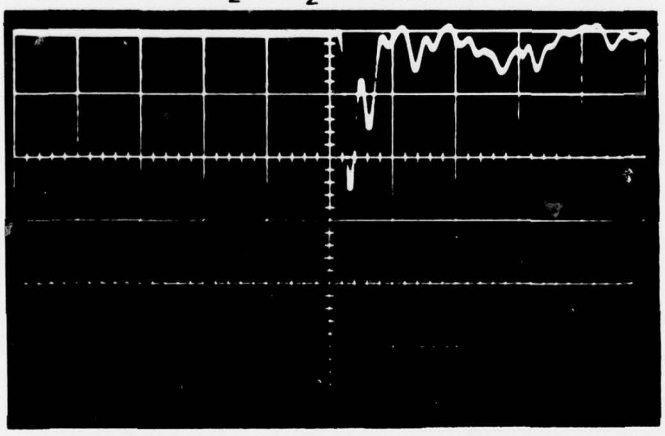

HORIZONTAL SCALE : 4 μSEC/DIV

VERTICAL SCALE: 1360 ATM/DIV

FIG. 23 PRESSURE HISTORY AT FOCUS

$2H_2 + O_2$ AT 2·27 ATM

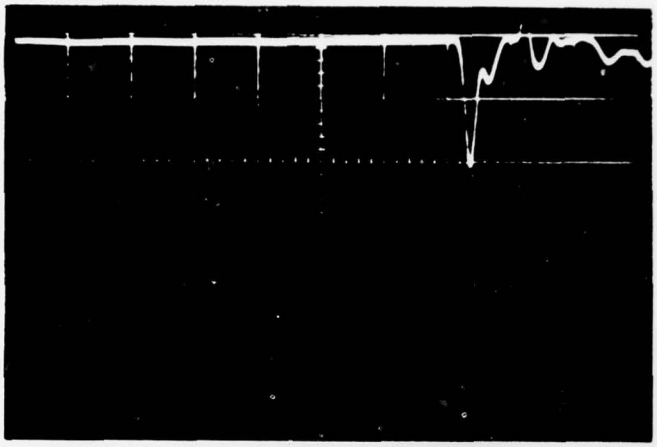

HORIZONTAL SCALE : 4 μSEC/DIV

VERTICAL SCALE: 1360 ATM/DIV

FIG. 24 PRESSURE HISTORY AT FOCUS

$2H_2 + O_2$ AT 1·7 ATM

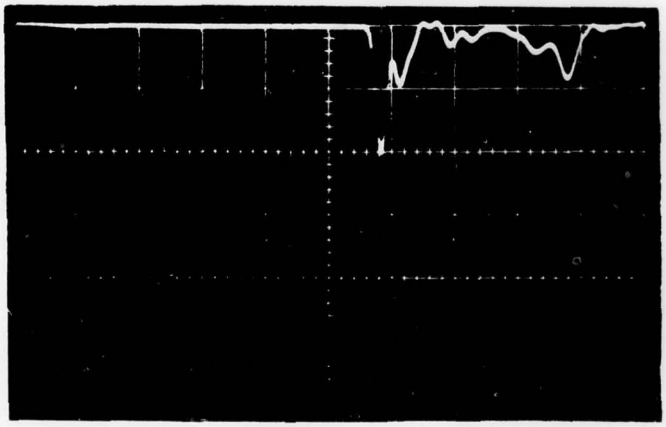

HORIZONTAL SCALE : 4 μSEC/DIV

VERTICAL SCALE: 680 ATM/DIV

FIG. 25 PRESSURE HISTORY AT FOCUS

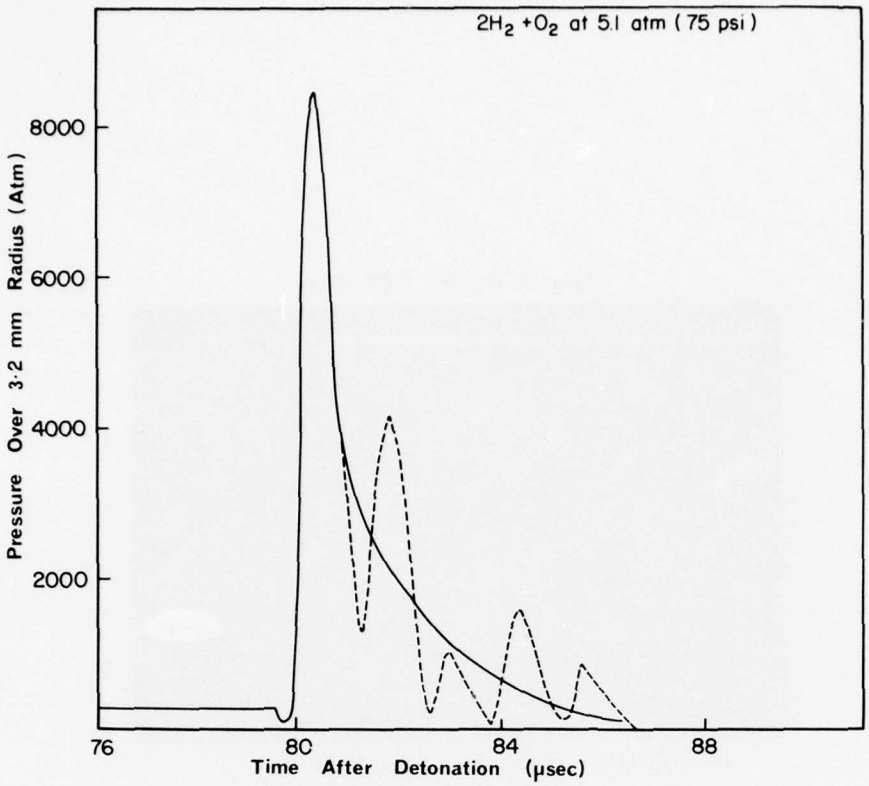

FIG. 26 ESTIMATED DECAY-RATE OF PRESSURE PULSE

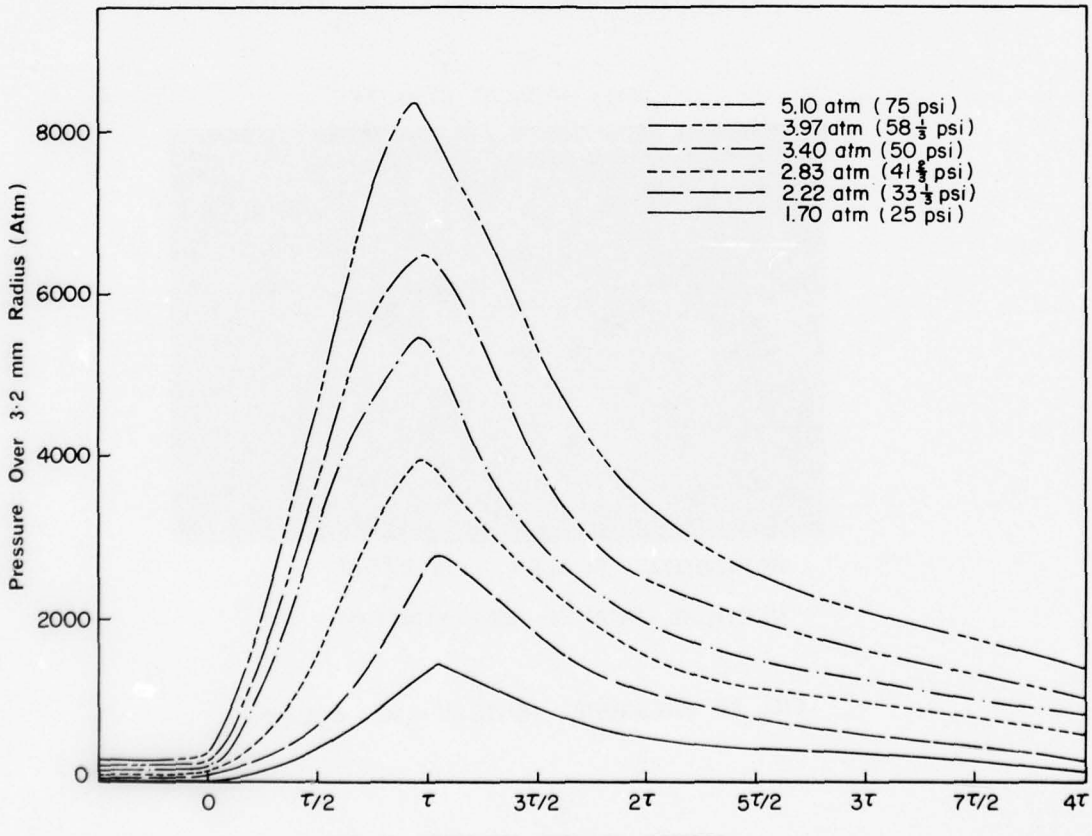

FIG. 27 NORMALISED PRESSURE HISTORIES

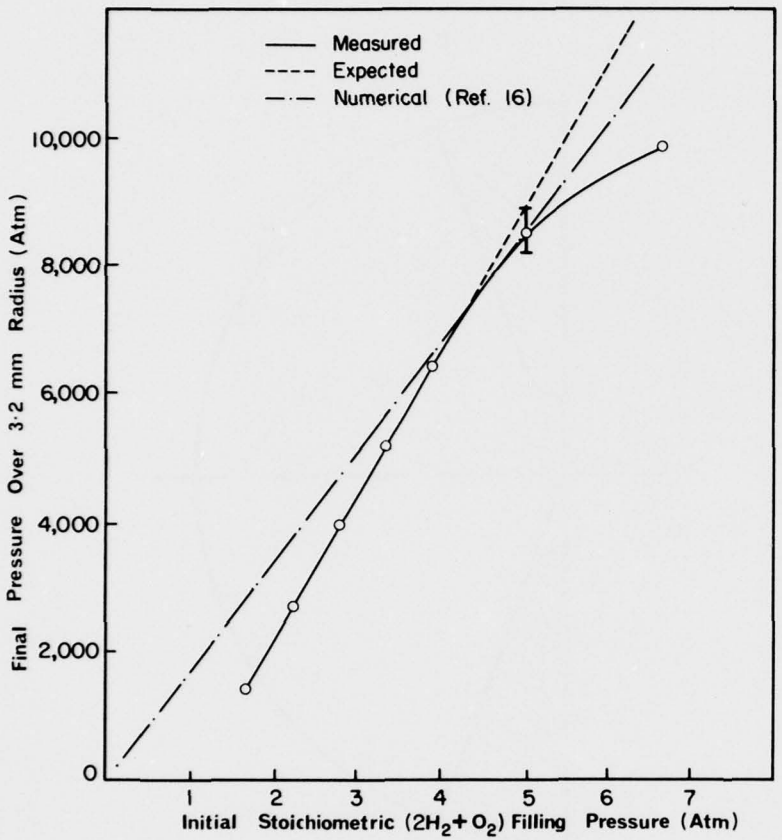

FIG. 28 PEAK PRESSURE VERSUS INITIAL PRESSURE

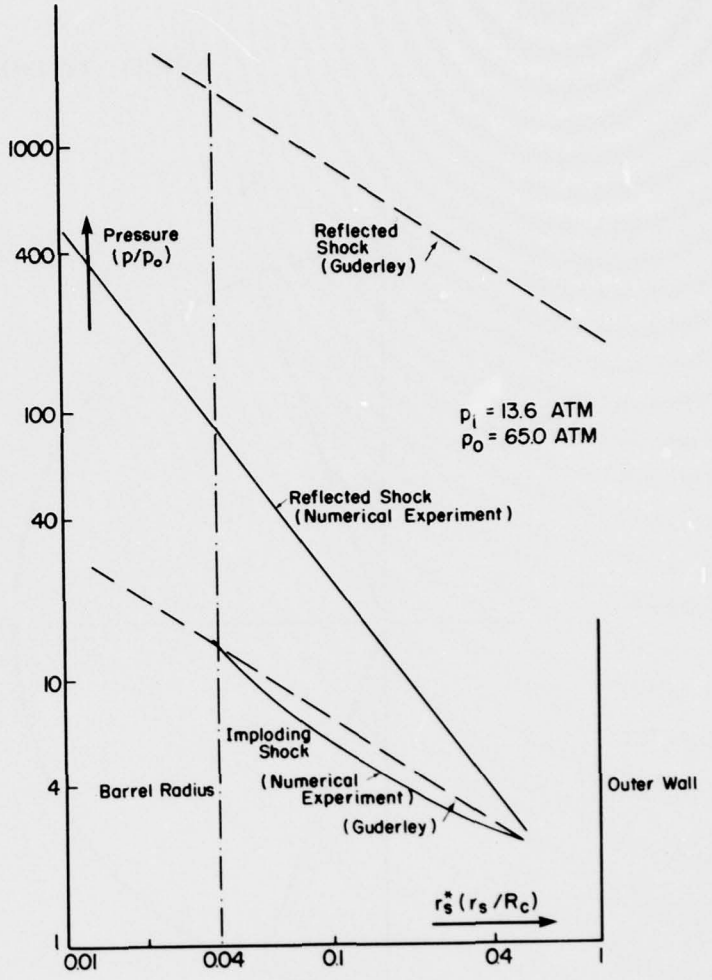

FIG. 29 COMPUTED PRESSURES BEHIND IMPLODING AND REFLECTED SHOCKS (REF.16)

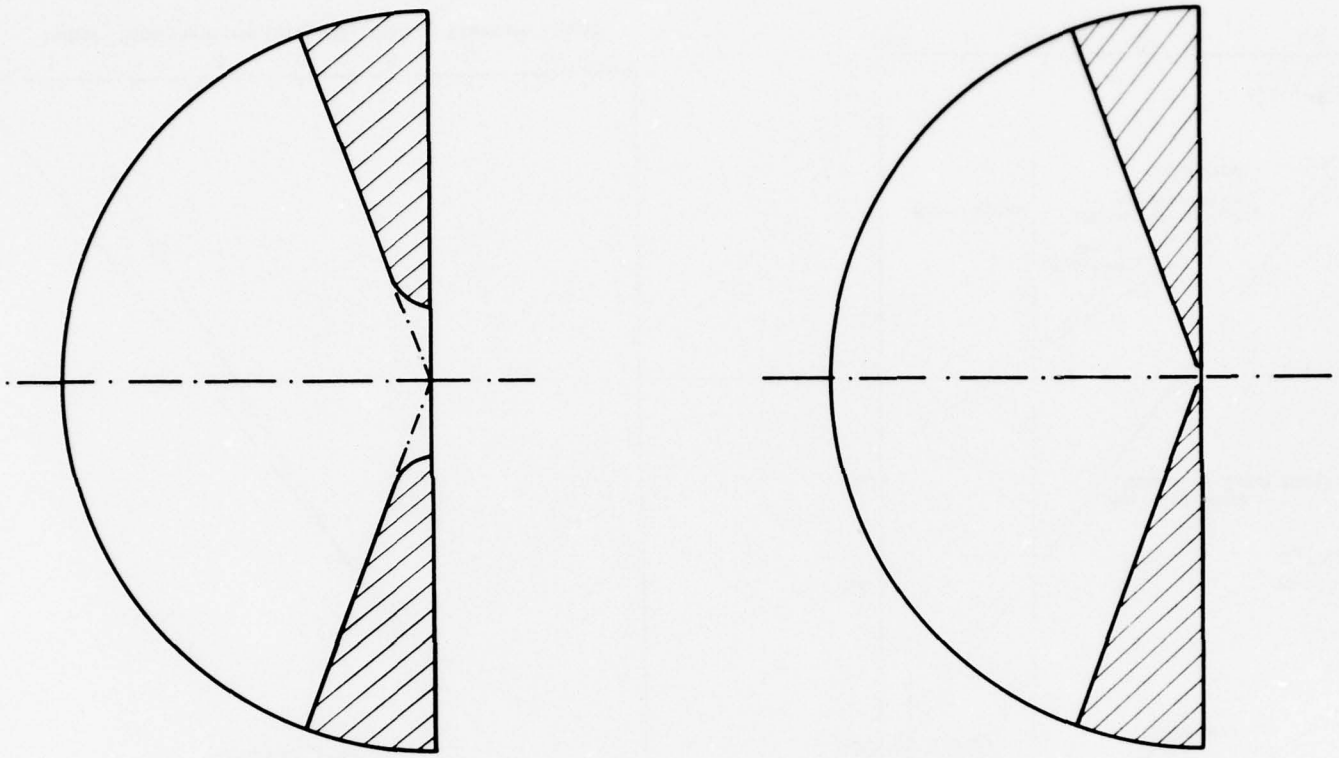

FIG . 30 SCHEMATIC DIAGRAMS OF TWO CONICAL LINERS

$2H_2 + O_2$ AT 3·4 ATM

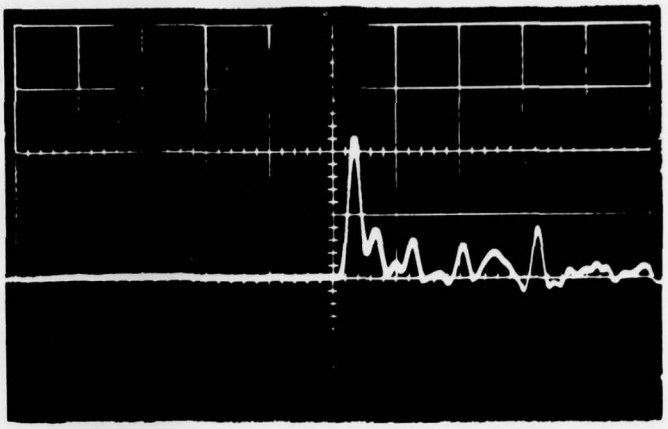

NO LINER

HORIZONTAL SCALE : 4 μSEC/DIV

VERTICAL SCALE: 2720 ATM/DIV

$2H_2 + O_2$ AT 5·4 ATM

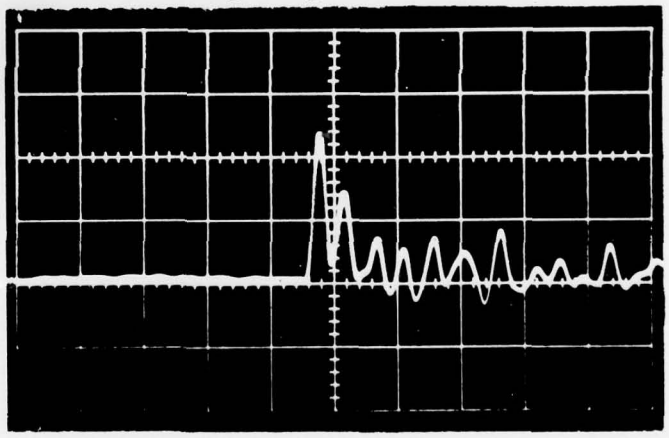

WITH LINER

HORIZONTAL SCALE : 4 μSEC/DIV

VERTICAL SCALE: 1360 ATM/DIV

FIG. 31 PRESSURE HISTORY IN PRESENCE OF A CONICAL LINER

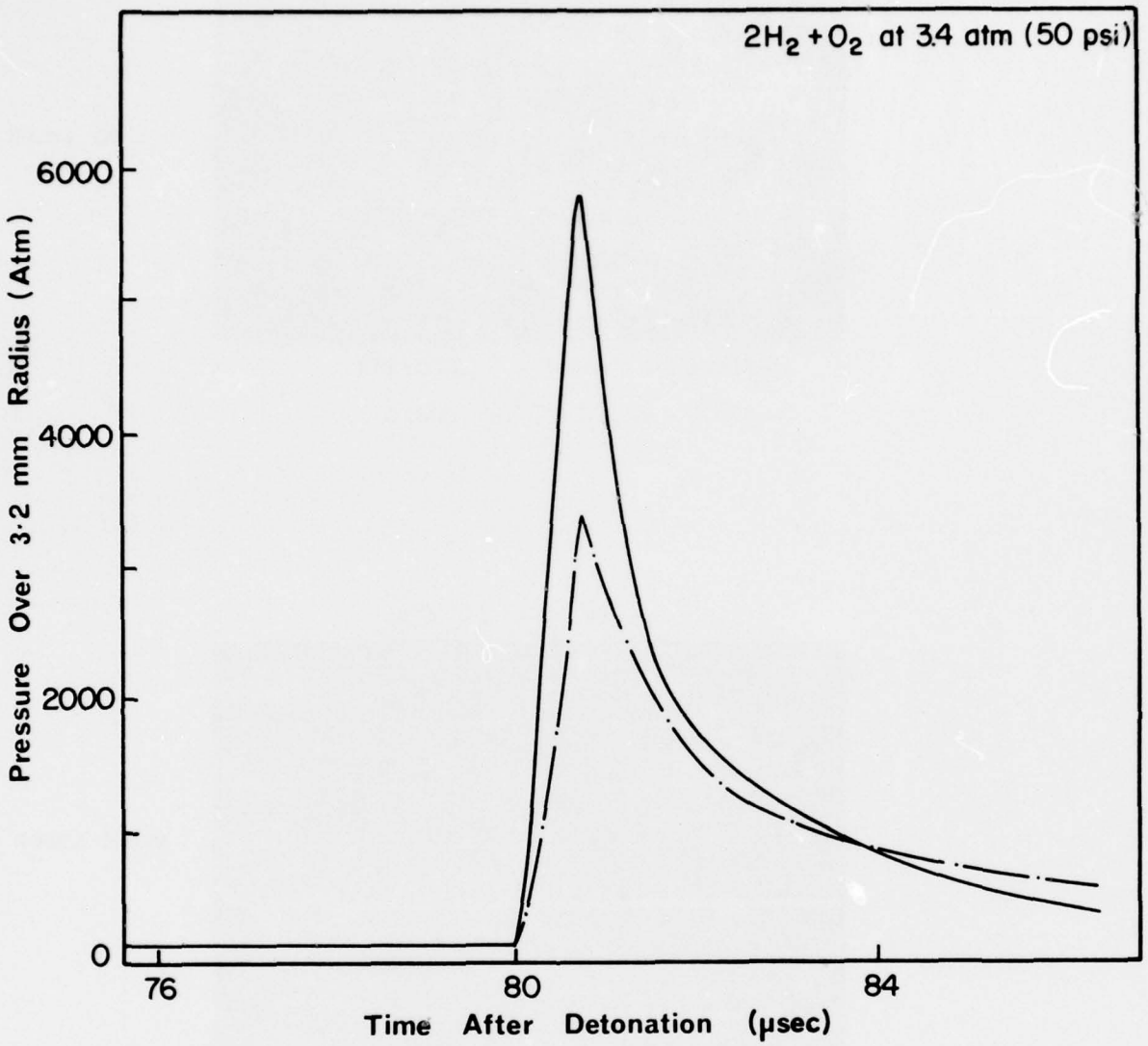

FIG. 32 PRESSURE–TIME HISTORY WITH AND WITHOUT A CONICAL LINER

$2H_2 + O_2$ AT 5·1 ATM

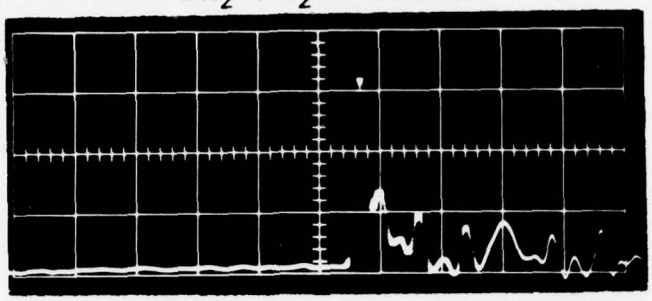

NO LINER

HORIZONTAL SCALE : 4 μSEC/DIV

VERTICAL SCALE: 2720 ATM/DIV

$2H_2 + O_2$ AT 5·1 ATM

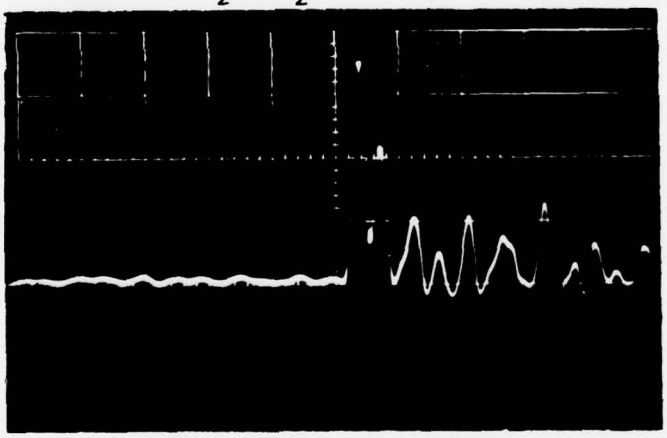

WITH LINER

HORIZONTAL SCALE : 4 μSEC/DIV

VERTICAL SCALE: 1360 ATM/DIV

FIG. 33 PRESSURE HISTORY WITH A LINER

$2H_2 + O_2$ AT 6·8 ATM

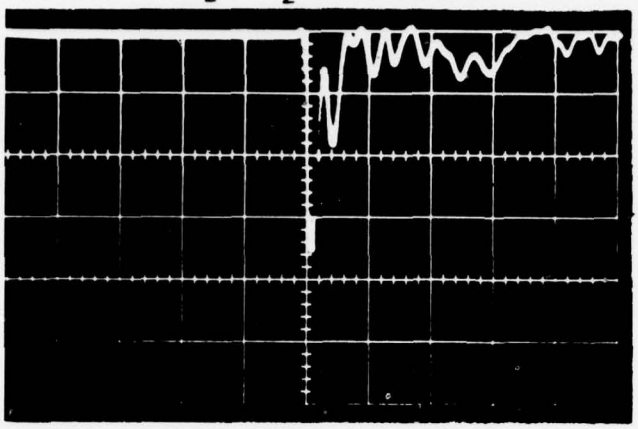

NO LINER

HORIZONTAL SCALE : 4 μSEC/DIV

VERTICAL SCALE: 2720 ATM/DIV

$2H_2 + O_2$ AT 6·8 ATM

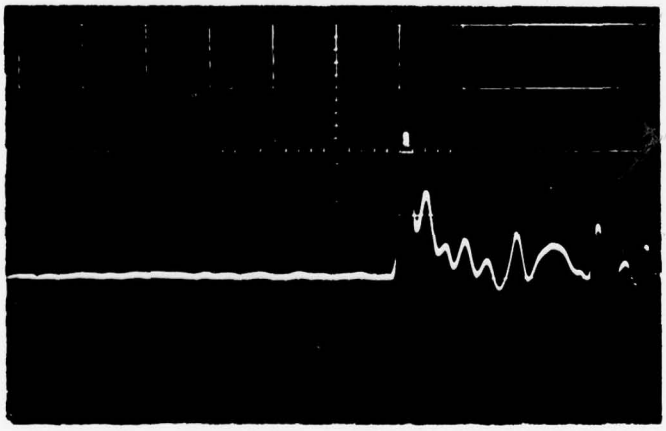

WITH LINER

HORIZONTAL SCALE : 4 μSEC/DIV

VERTICAL SCALE: 2720 ATM/DIV

FIG. 34 PRESSURE HISTORY WITH A LINER

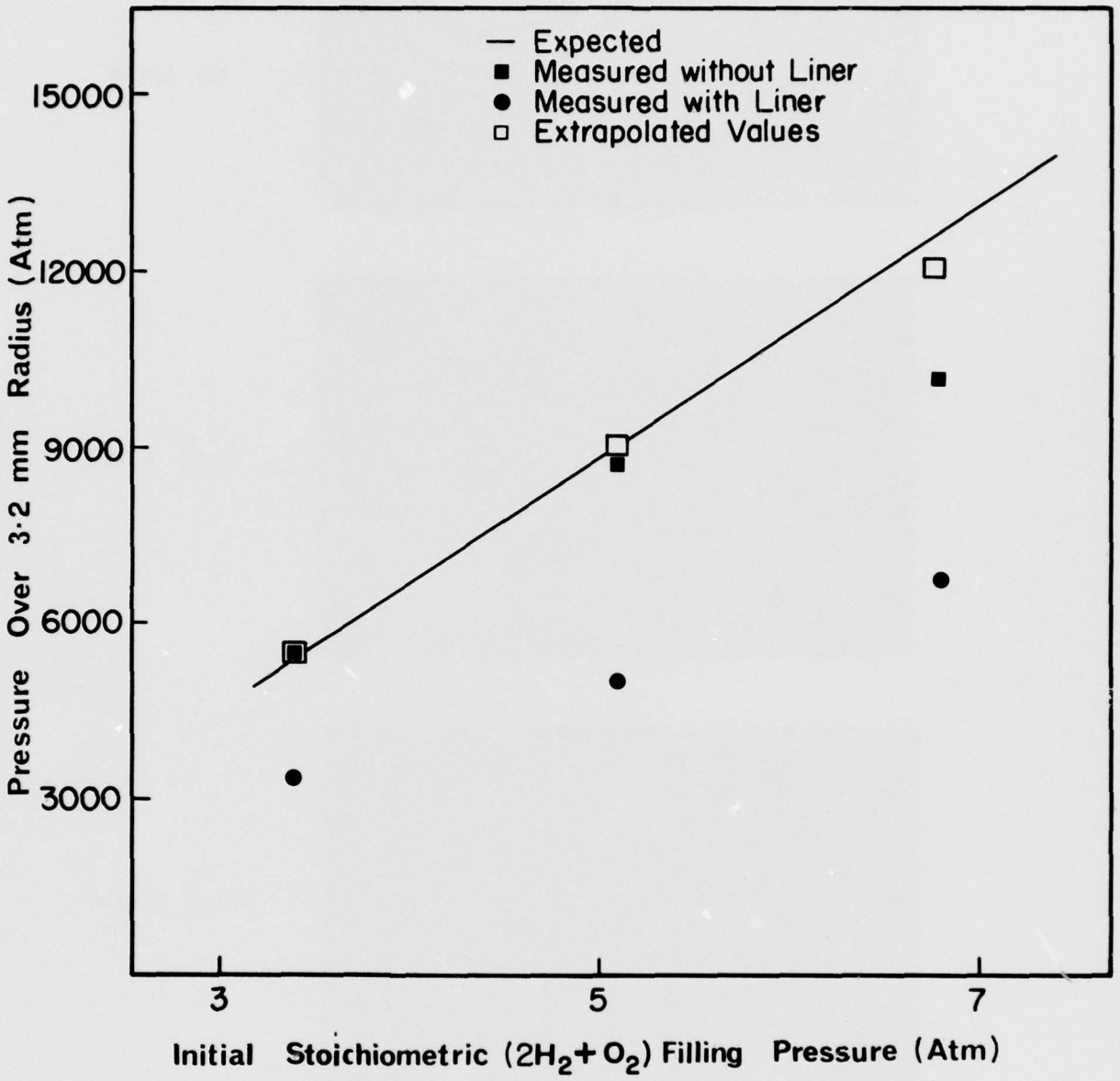

FIG. 35 EFFECT OF CONICAL LINER ON PEAK PRESSURES

$2H_2 + O_2$ AT 5·1 ATM

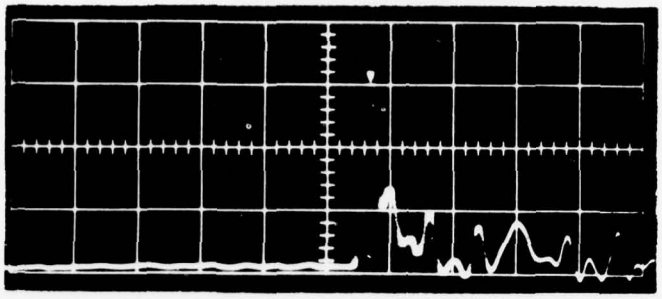

NO LINER

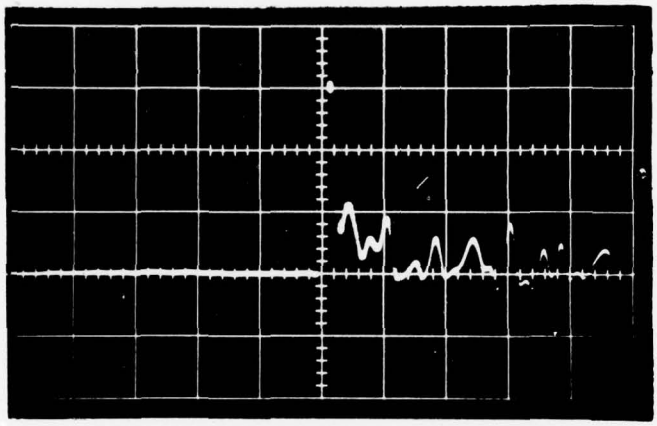

WITH LINER

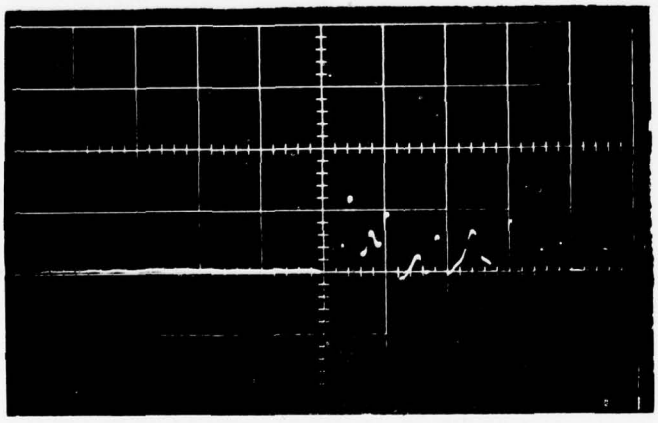

WITH LINER

HORIZONTAL SCALES: 4 μSEC/DIV

VERTICAL SCALES: 2720 ATM/DIV

FIG. 36 PRESSURE HISTORY WITH CONICAL LINER EXTENDED UP TO TRANSDUCER (SEE FIG. 29)

$2H_2 + O_2 + He$ AT 3·4 ATM

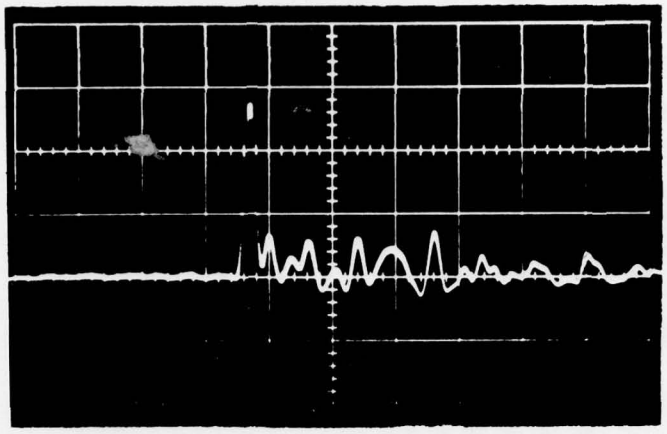

HORIZONTAL SCALE: 4 μSEC/DIV

VERTICAL SCALE: 2720 ATM/DIV

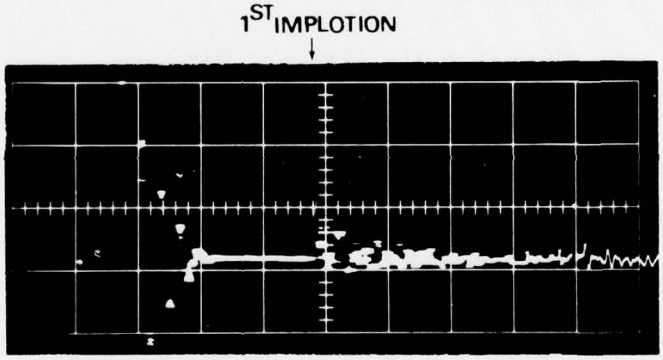

HORIZONTAL SCALE : 20 μSEC/DIV

VERTICAL SCALE: 2720 ATM/DIV

FIG. 37 EFFECT OF HELIUM DILUTION ON PRESSURE HISTORY AT FOCUS

$2\,H_2 + O_2 + 2\,He$ AT 3·4 ATM

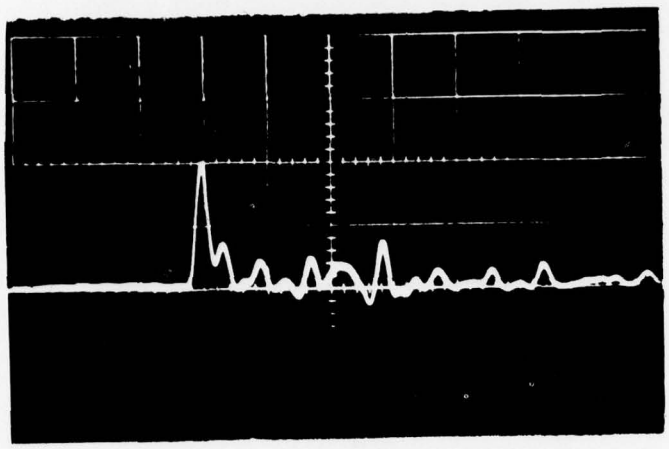

HORIZONTAL SCALE: 4 μSEC/DIV

VERTICAL SCALE: 2720 ATM/DIV

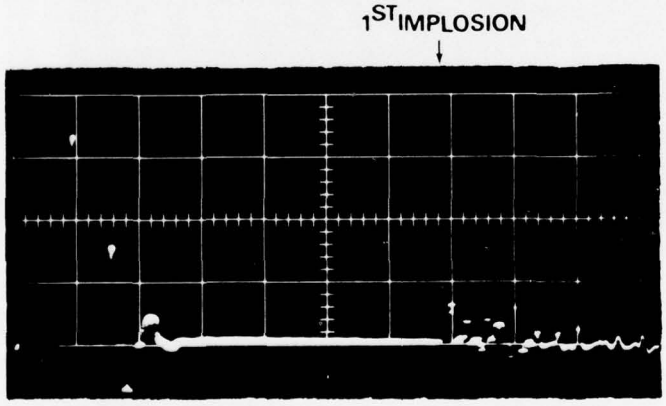

HORIZONTAL SCALE : 10 μSEC/DIV

VERTICAL SCALE: 2720 ATM/DIV

FIG. 38 EFFECT OF HELIUM DILUTION ON PRESSURE HISTORY AT FOCUS

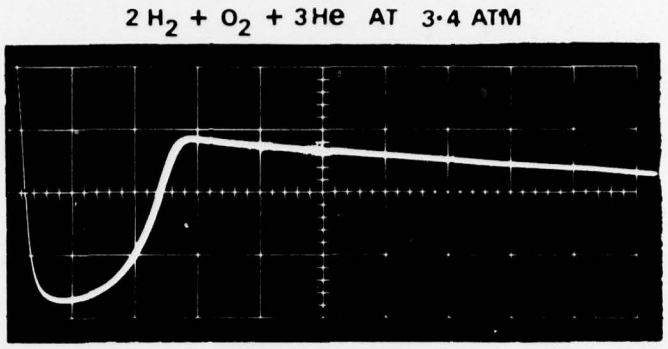

VERTICAL SCALE: 13·6 ATM/DIV

HORIZONTAL SCALE: 1 mSEC/DIV

FIG. 39 DEFLAGRATION PRESSURE HISTORY (HELIUM DILUTION)

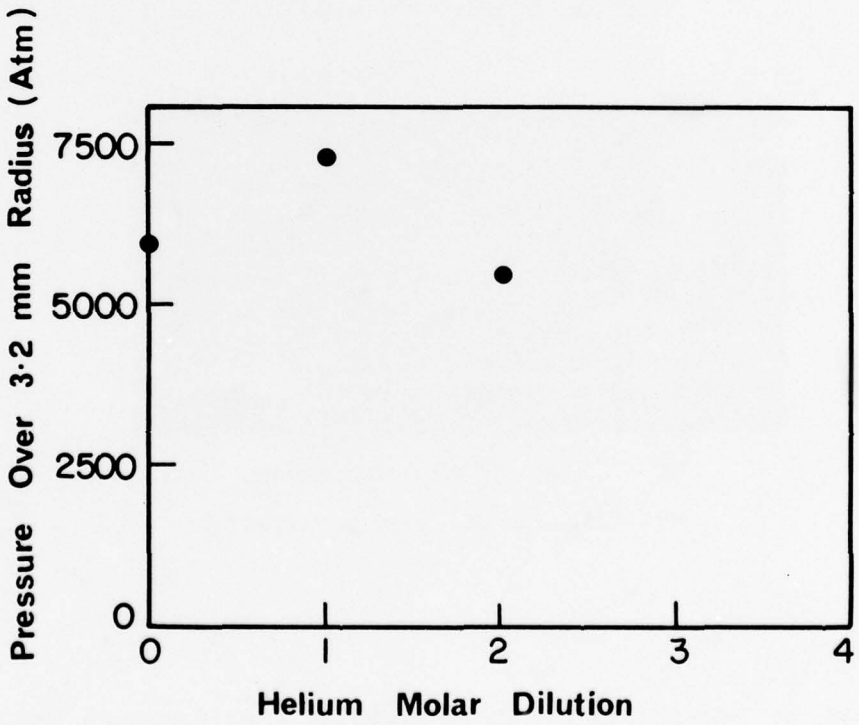

FIG. 40 IMPLOSION PEAK PRESSURES VERSUS HELIUM MOLAR DILUTION

$2H_2 + O_2 + H_2$ AT 3·4 ATM

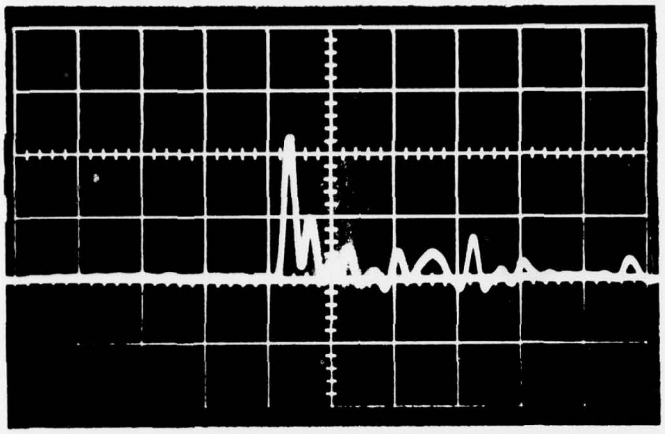

HORIZONTAL SCALE: 4 μSEC/DIV

VERTICAL SCALE: 2720 ATM/DIV

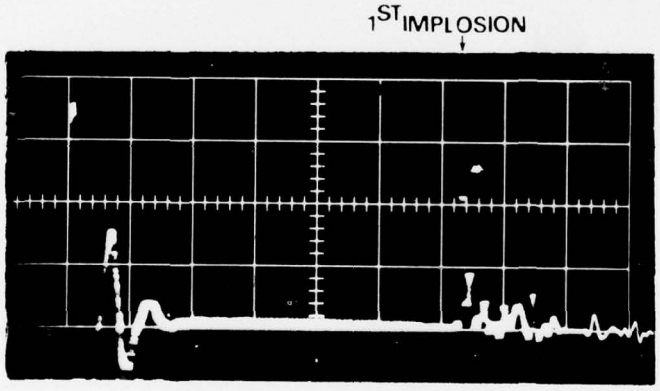

HORIZONTAL SCALE: 10 μSEC/DIV

VERTICAL SCALE: 2720 ATM/DIV

FIG. 41 EFFECT OF HYDROGEN DILUTION ON PRESSURE HISTORY AT FOCUS

$2H_2 + O_2 + 2H_2$ AT 3·4 ATM

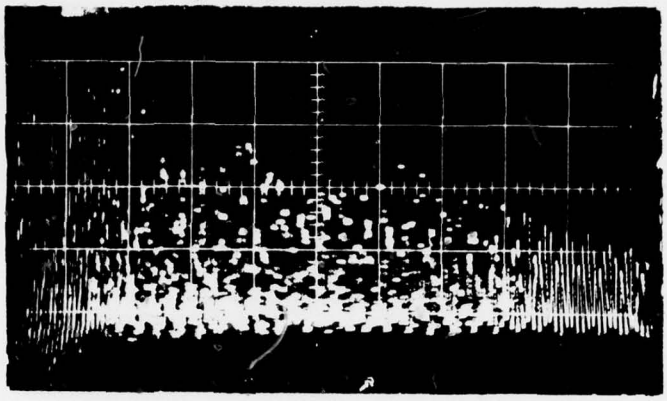

VERTICAL SCALE: 13·6 ATM/DIV

HORIZONTAL SCALE: 1 mSEC/DIV

FIG. 42 PRESSURE HISTORY FOR TRANSITIONAL COMBUSTION (HYDROGEN DILUTION)

$2H_2 + O_2 + 3H_2$ AT 3·4 ATM

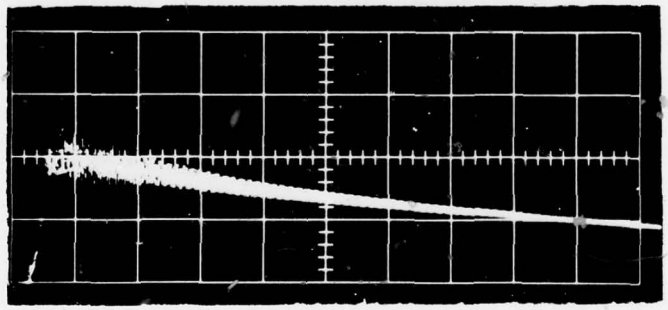

VERTICAL SCALE: 13·6 ATM/DIV

HORIZONTAL SCALE: 2 mSEC/DIV

FIG. 43 DEFLAGRATION (TRANSITIONAL) PRESSURE HISTORY (HYDROGEN DILUTION)

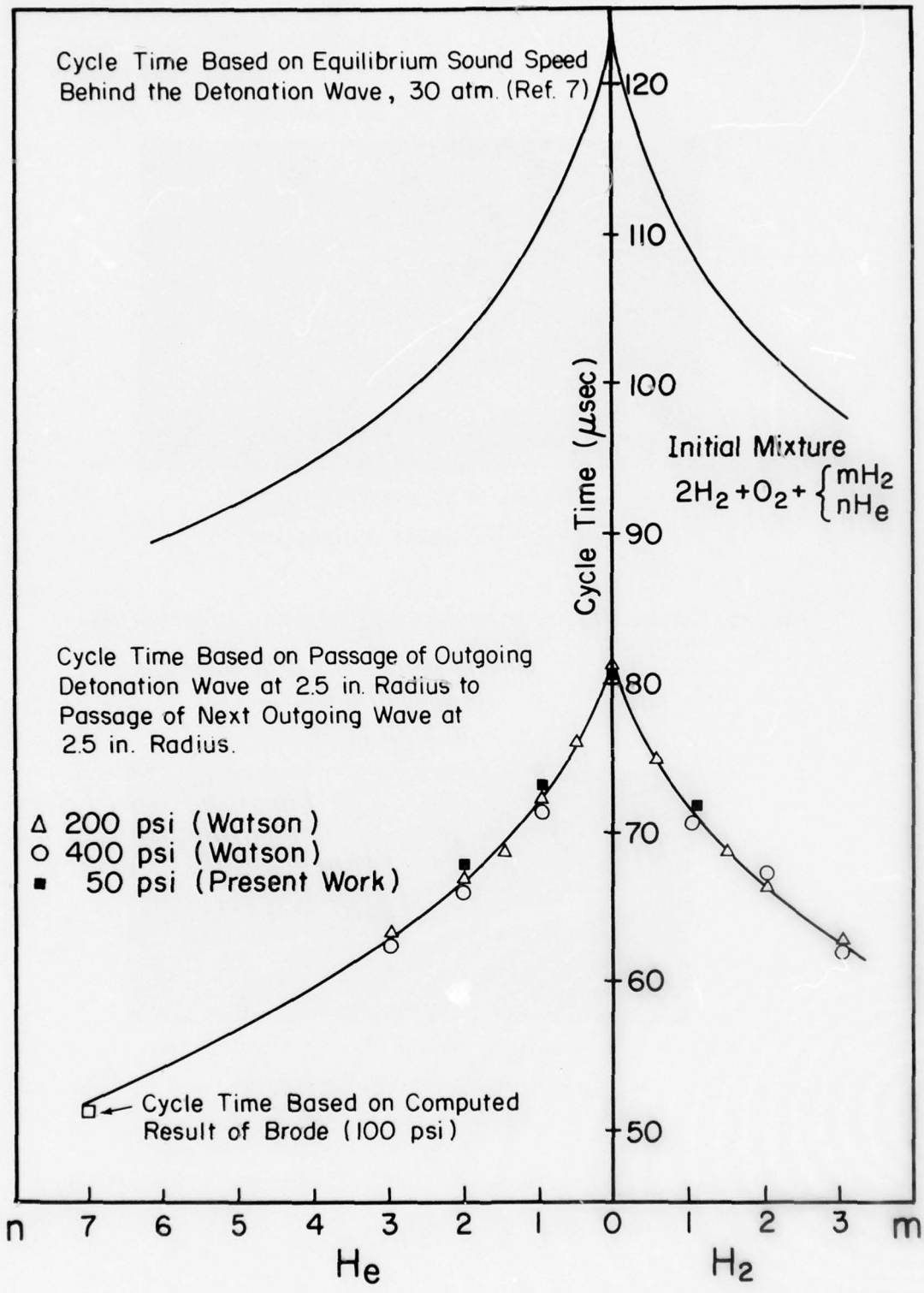

FIG. 44 VARIATION OF CYCLE TIME WITH MOLAR DILUTION

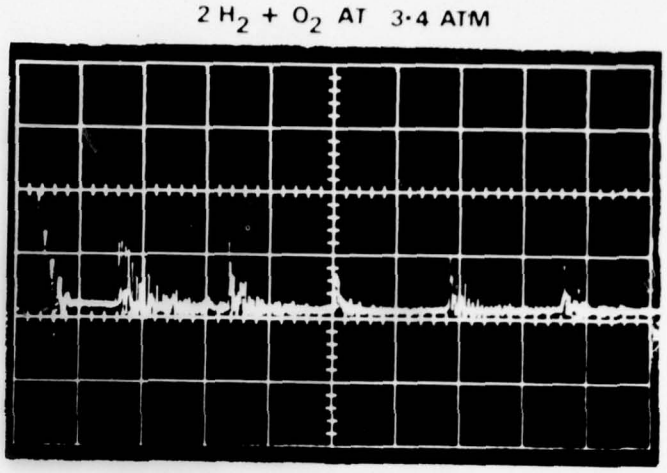

VERTICAL SCALE: 1360 ATM/DIV

HORIZONTAL SCALE: 50 μSEC/DIV

FIG. 45a PRESSURE HISTORY OF SUBSEQUENT IMPLOSIONS

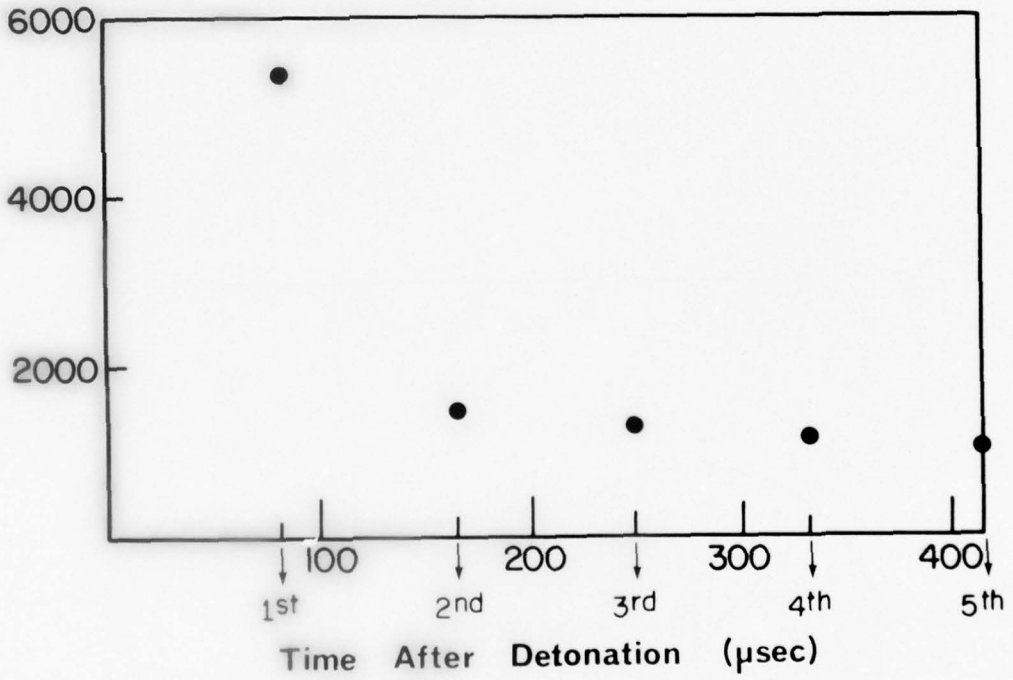

FIG. 45b PEAK PRESSURES FOR DIFFERENT IMPLOSIONS

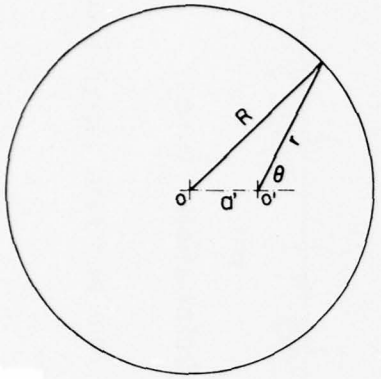

R = RADIUS OF TRANSDUCER
O = CENTRE OF TRANSDUCER
O' = FOCAL POINT OF OFF-CENTRE IMPLOSION

$$r(\theta) = -a'\cos\theta + \left[(a'\cos\theta)^2 - (a^2 - R^2)\right]^{1/2}$$

FIG. 46 ILLUSTRATION OF AN OFF-CENTRE IMPLOSION O'

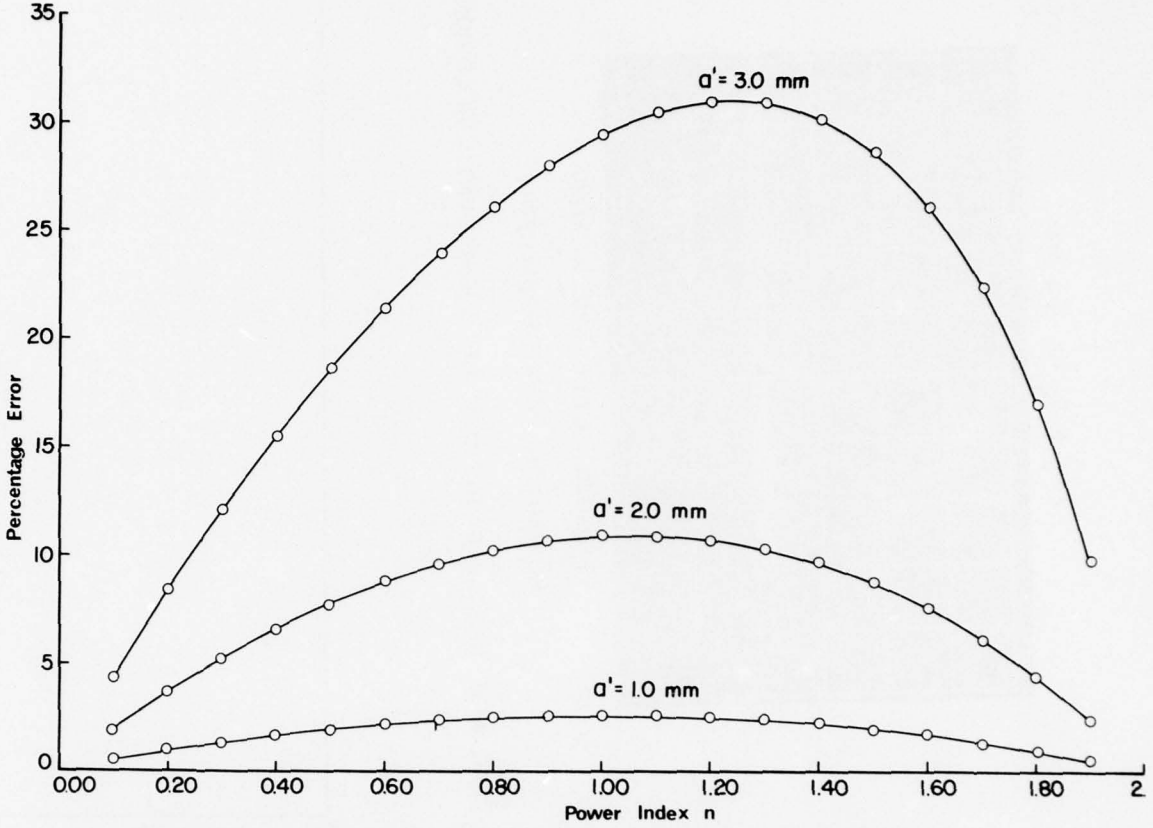

FIG. 47 ERRORS (%) FROM OFF-CENTRE IMPLOSIONS (a') FOR DIFFERENT PRESSURE DISTRIBUTIONS

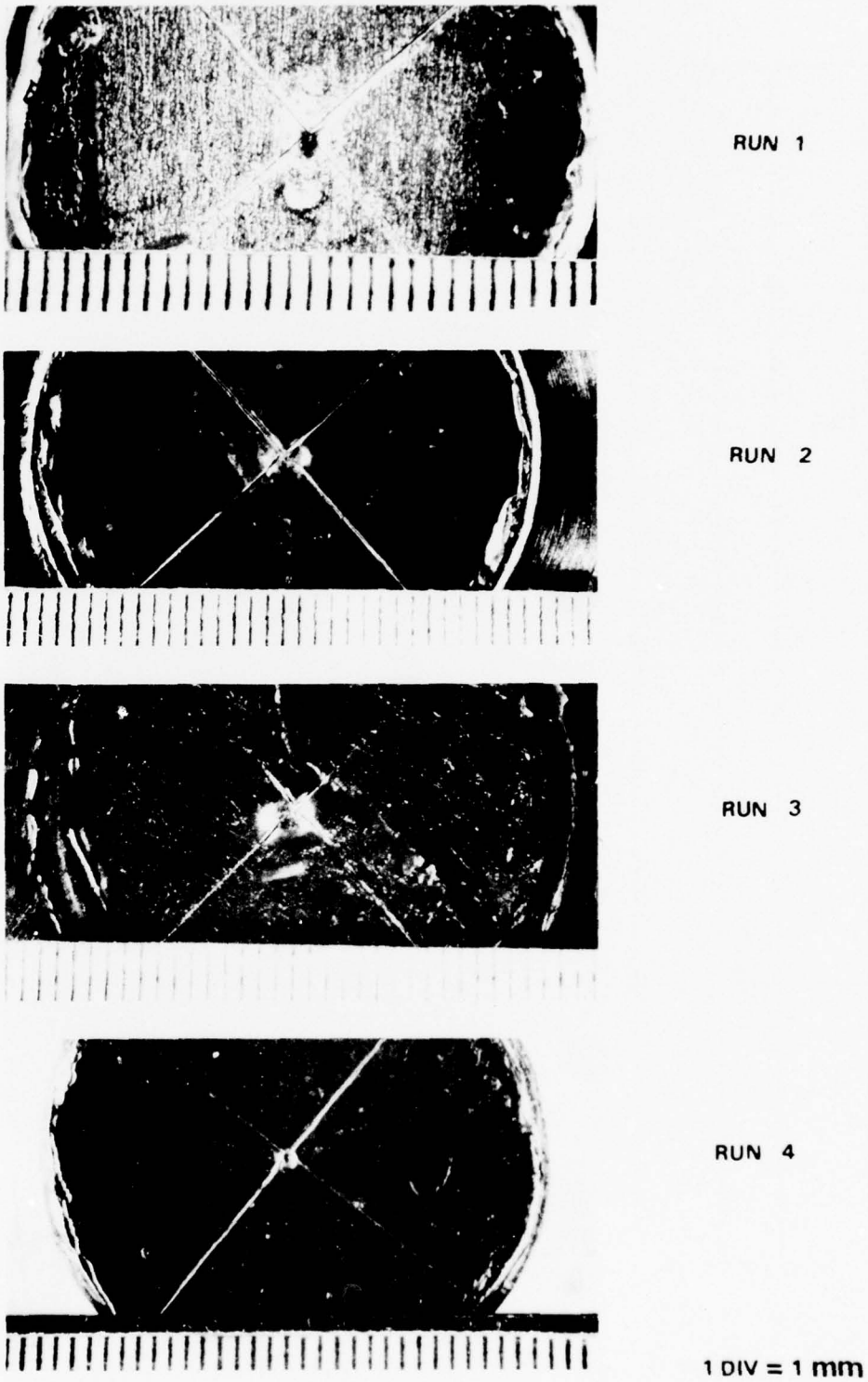

FIG. 48 IMPRINTS OF IMPLOSIONS ON LEAD WITNESS PLATES

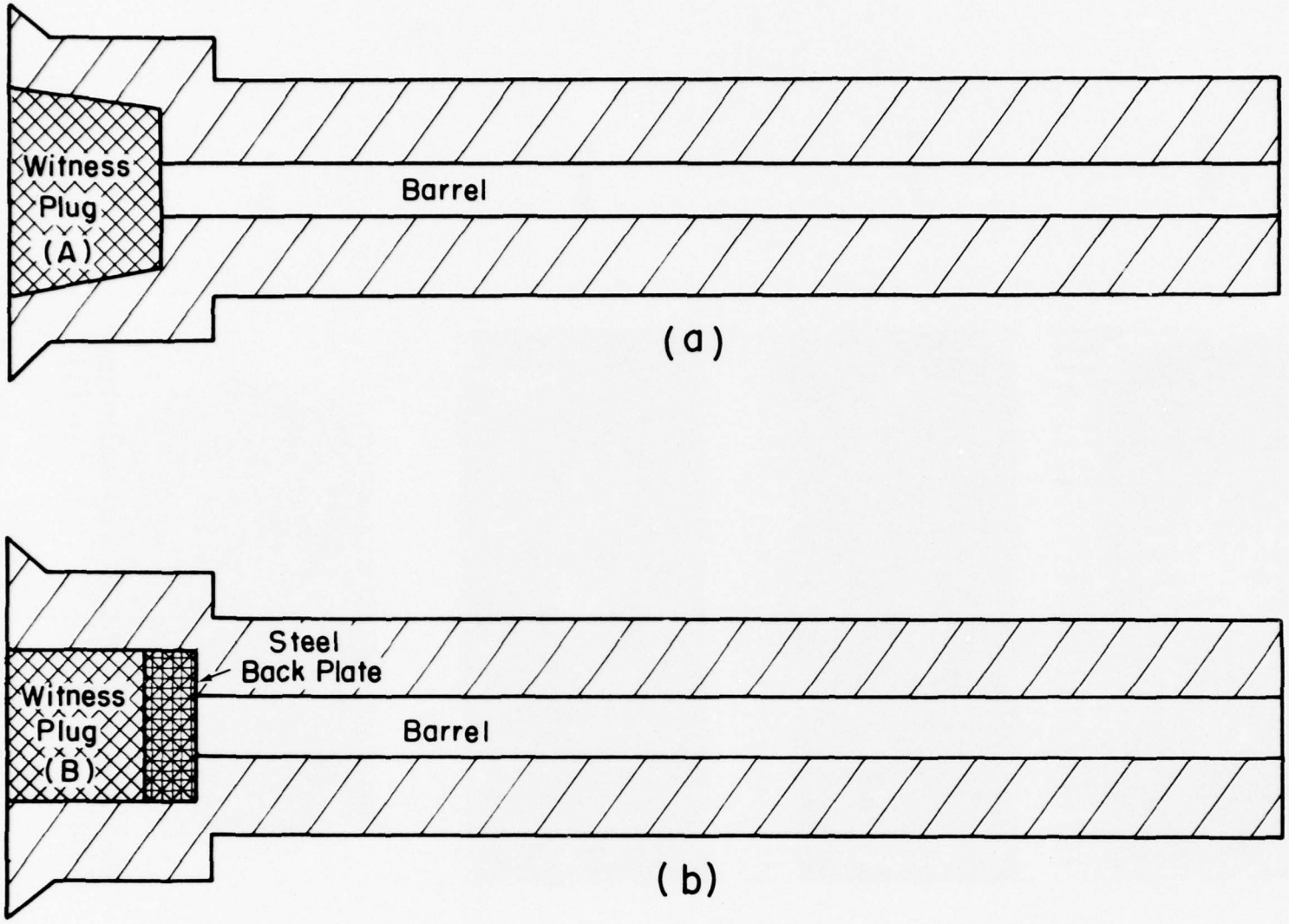

FIG. 49 BOUNDARY CONDITIONS FOR WITNESS PLUGS

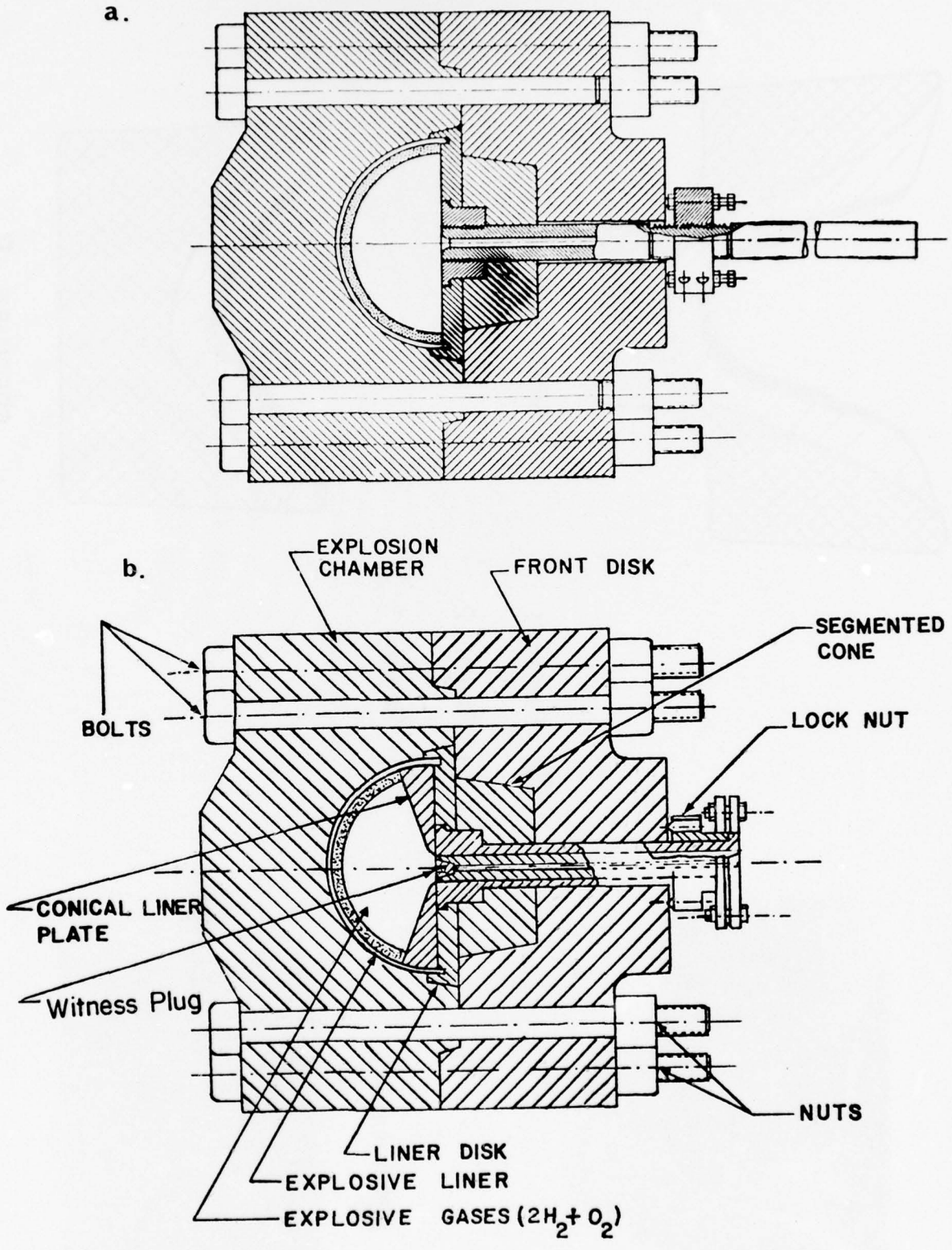

FIG. 50 SECTIONAL VIEW OF IMPLOSION CHAMBER FACILITY

SPECIMEN – A

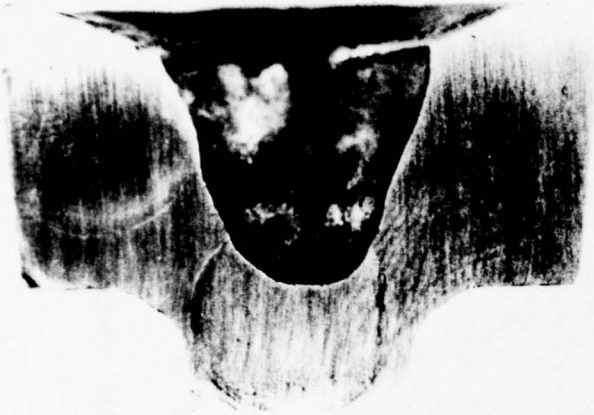

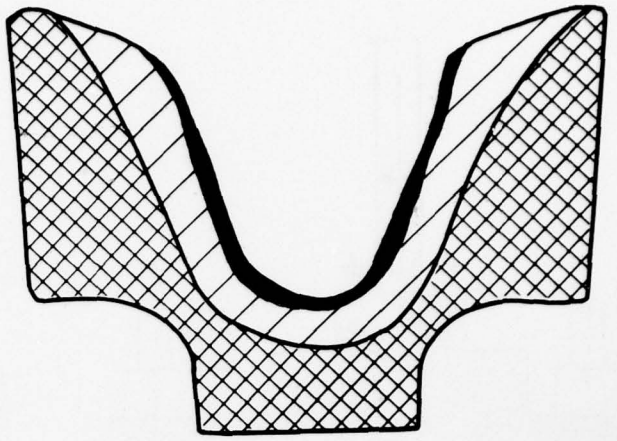

SPECIMEN A

Region 1

Region 2

Region 3

SPECIMEN – B

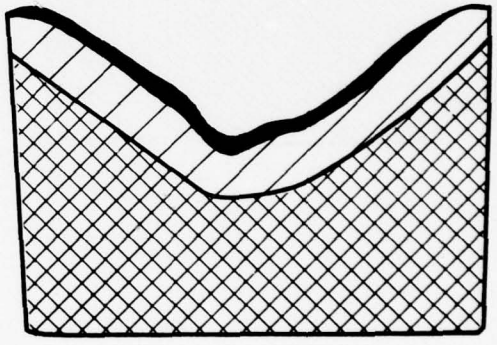

SPECIMEN B

FIGS. 51 & 52 SECTIONS OF SPECIMENS AFTER SHOCK LOADING

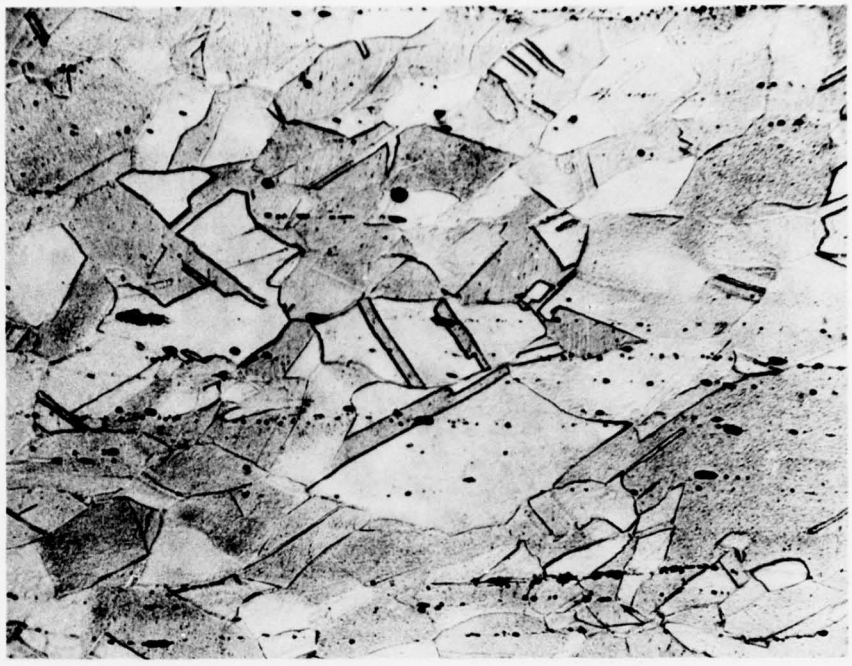

SPECIMEN – A x240

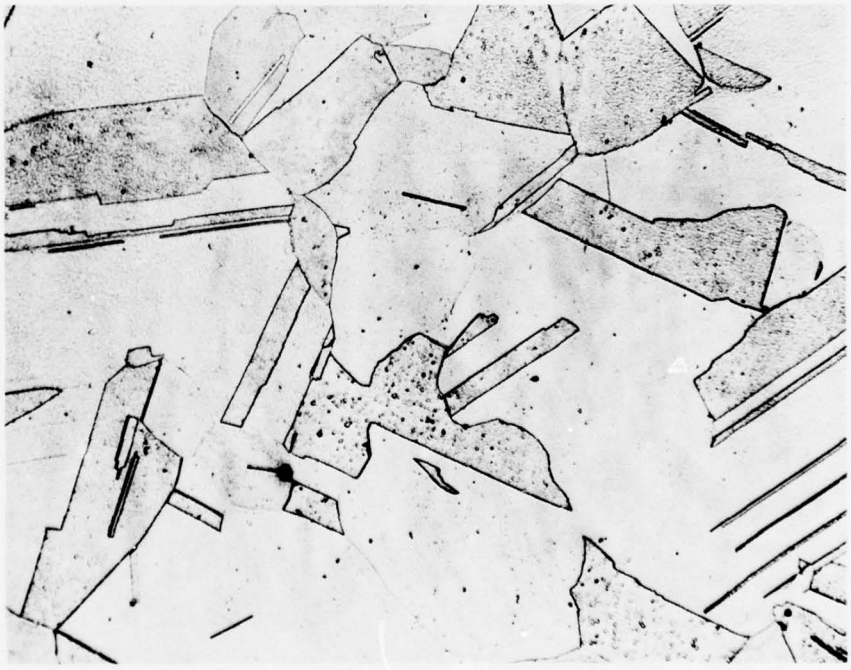

SPECIMEN – B x240

FIG. 53 PHOTOMICROGRAPHS OF UNSHOCKED COPPER

SPECIMEN – A x240

SPECIMEN – B x480

FIG. 54 PHOTOMICROGRAPHS OF SHOCKED COPPER–REGION 1

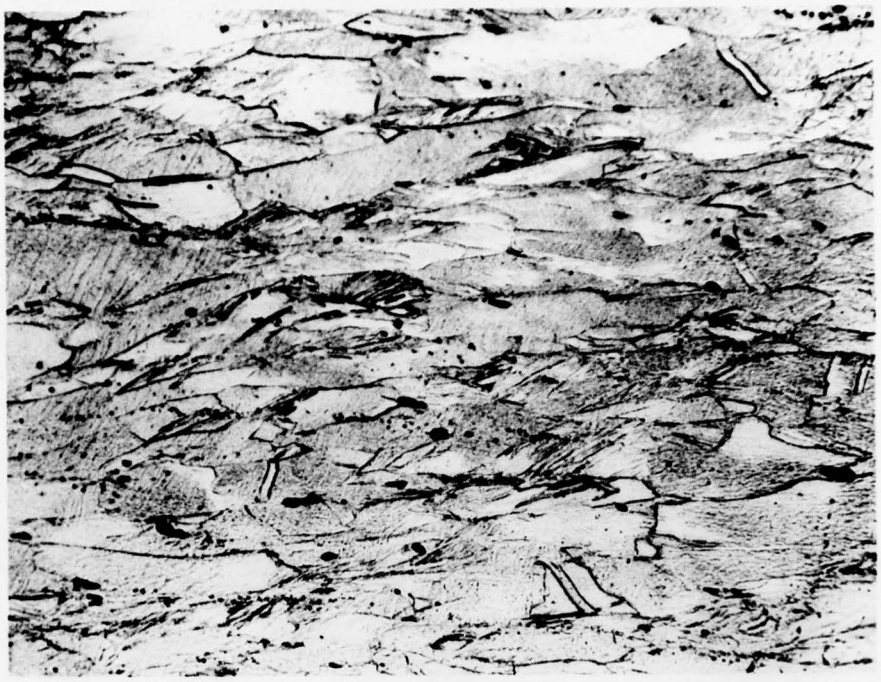

SPECIMEN – A x240

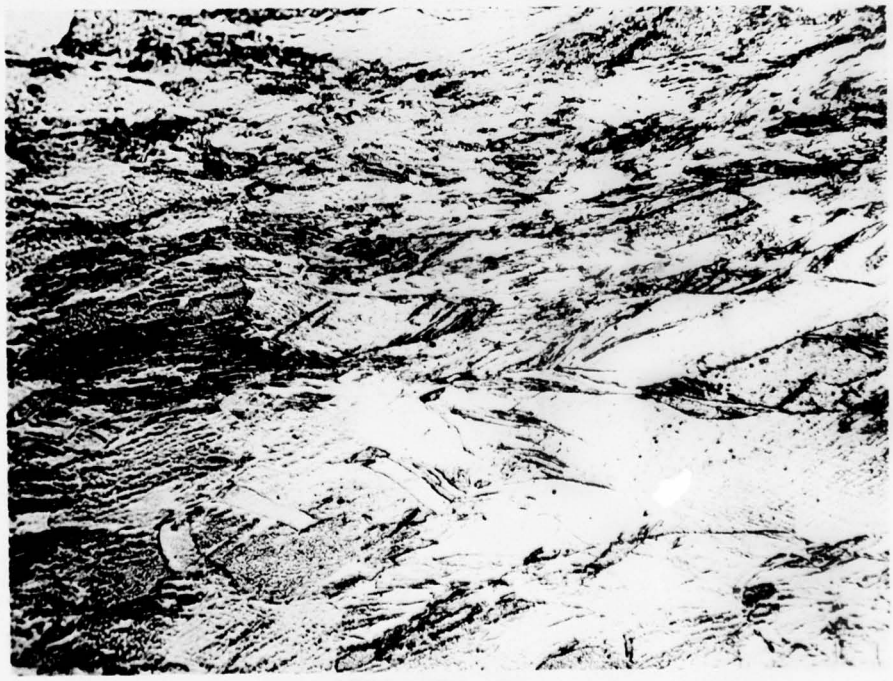

SPECIMEN – B x240

FIG. 55 PHQTOMICROGRAPHS OF SHOCKED COPPER – REGION 2

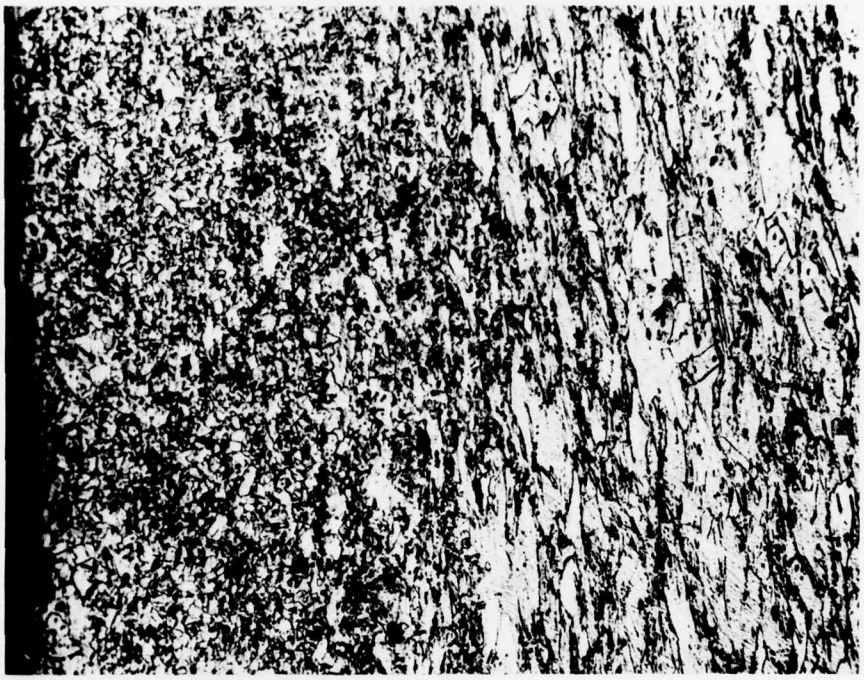

SPECIMEN – A x 95

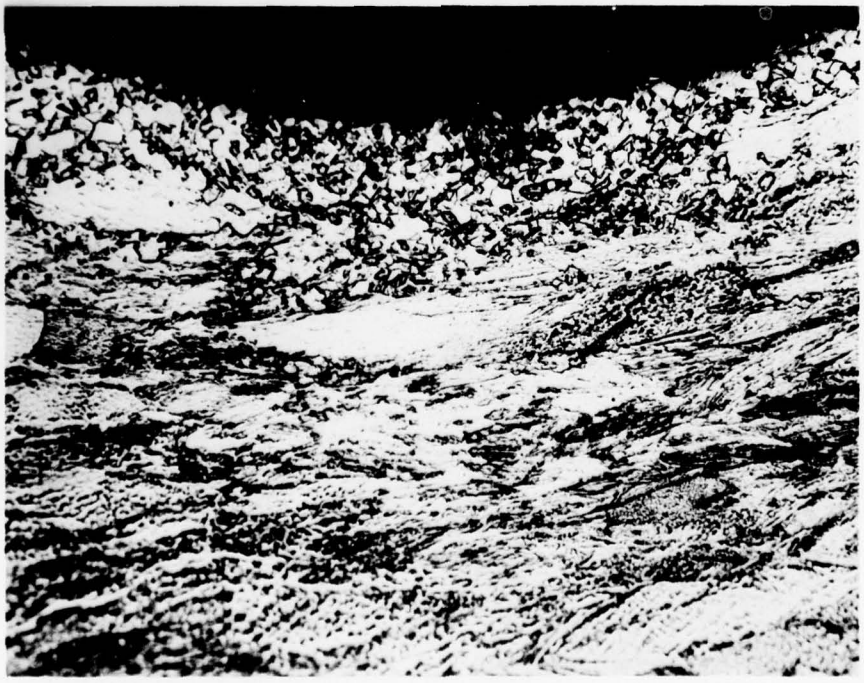

SPECIMEN – B x 240

FIG. 56 PHOTOMICROGRAPHS OF SHOCKED COPPER – REGIONS 1 & 2

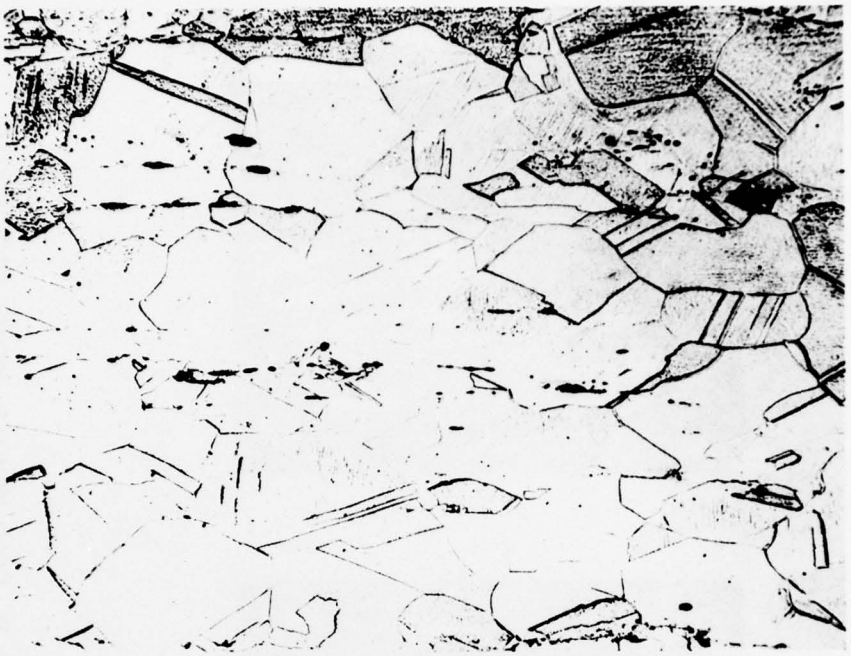

SPECIMEN – A x240

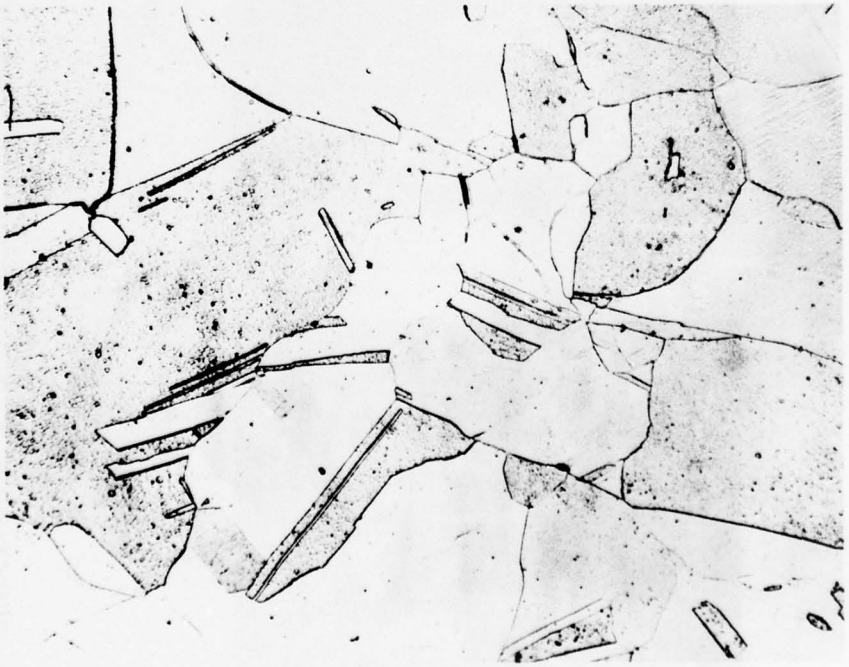

SPECIMEN – B x240

FIG. 57 PHOTOMICROGRAPHS OF SHOCKED COPPER – REGION 3

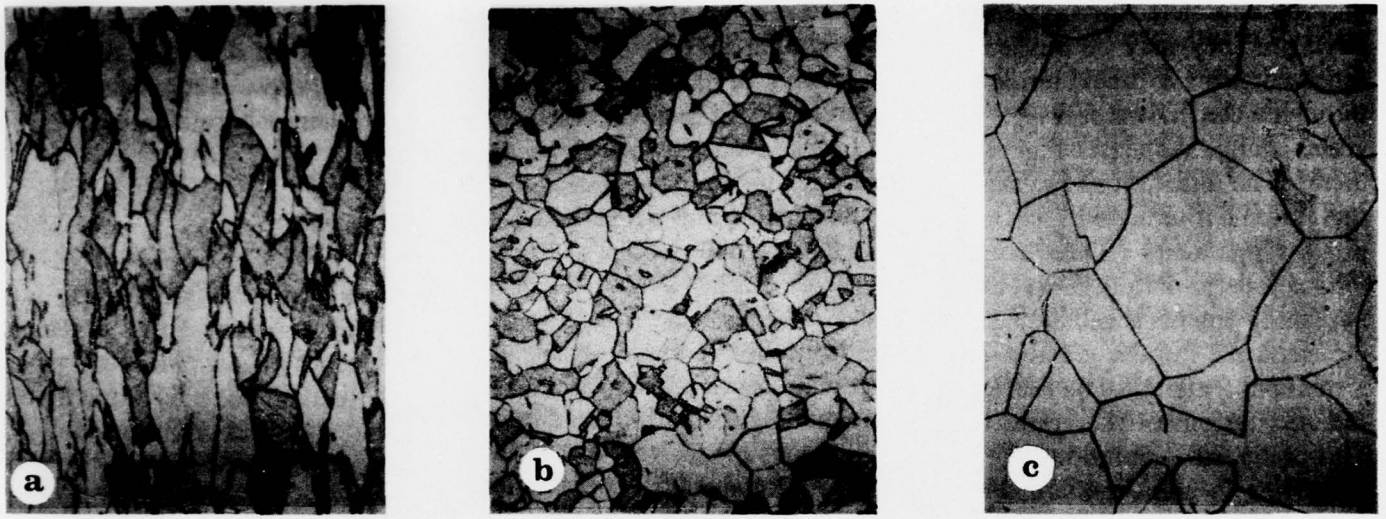

×170

FIG. 58 DEFORMATION, RECRYSTALIZATION AND GRAIN GROWTH IN COLD-WORKED NICKEL(FCC) (REF. 50)

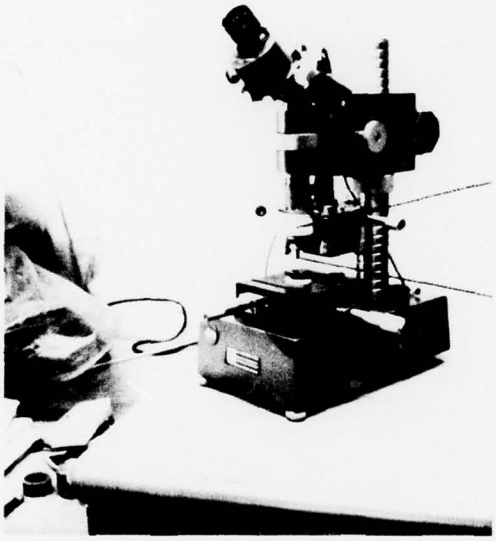

FIG. 59 MINILOAD HARDNESS TESTER WITH SPECIMEN MOUNTED

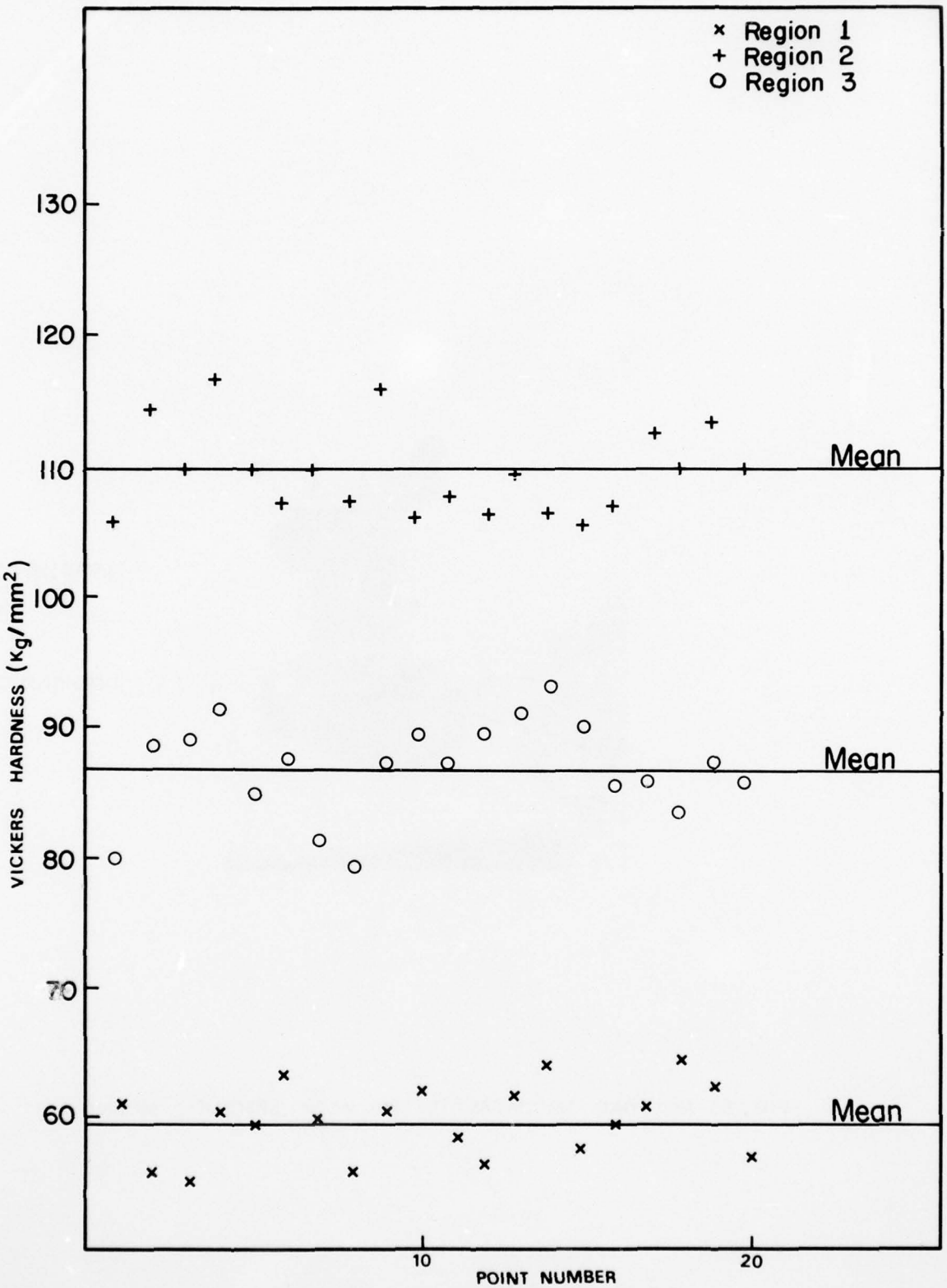

FIG. 60 MICROHARDNESS OF SHOCKED SAMPLE (A)

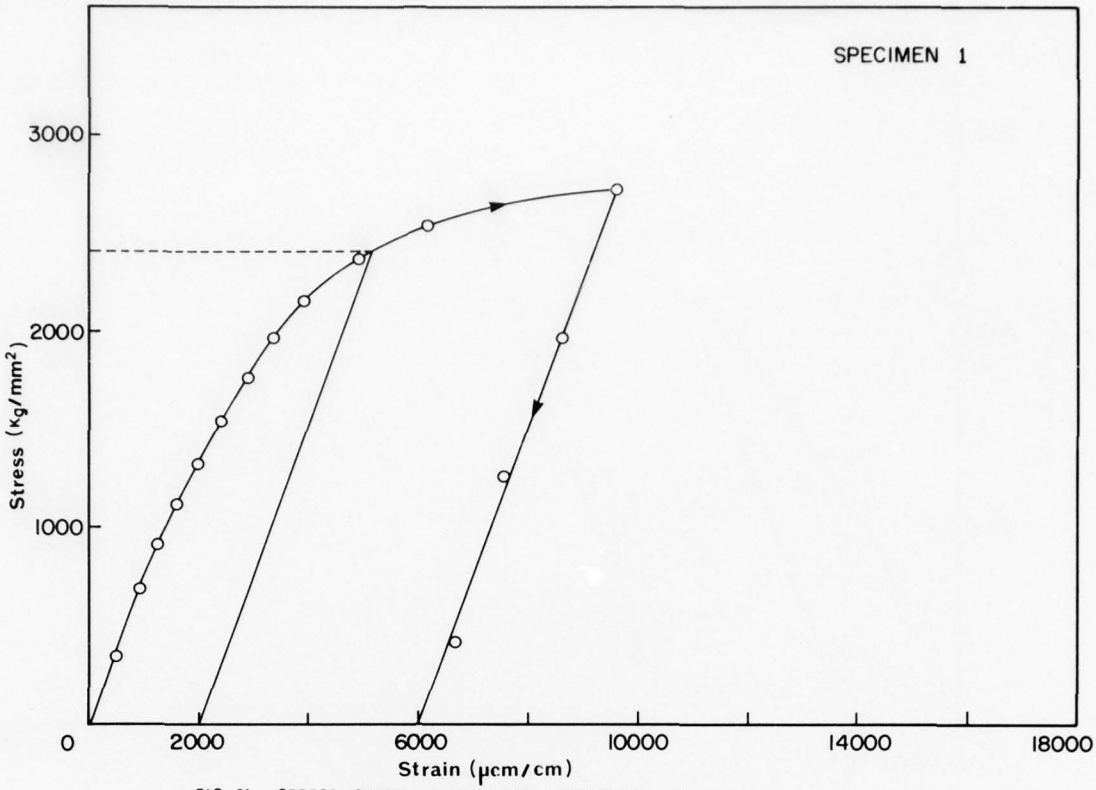

FIG. 61 STRESS-STRAIN CURVE FOR UNANNEALED SAMPLE

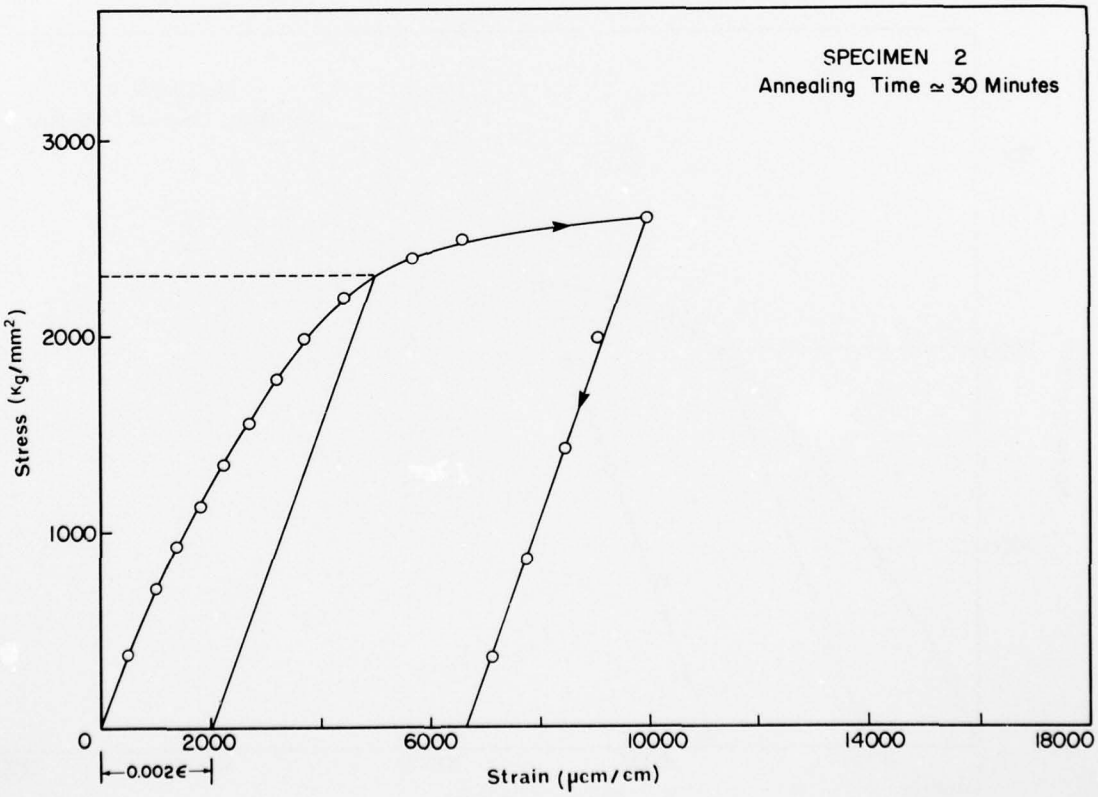

FIG. 62 STRESS-STRAIN CURVE FOR ANNEALED SAMPLE

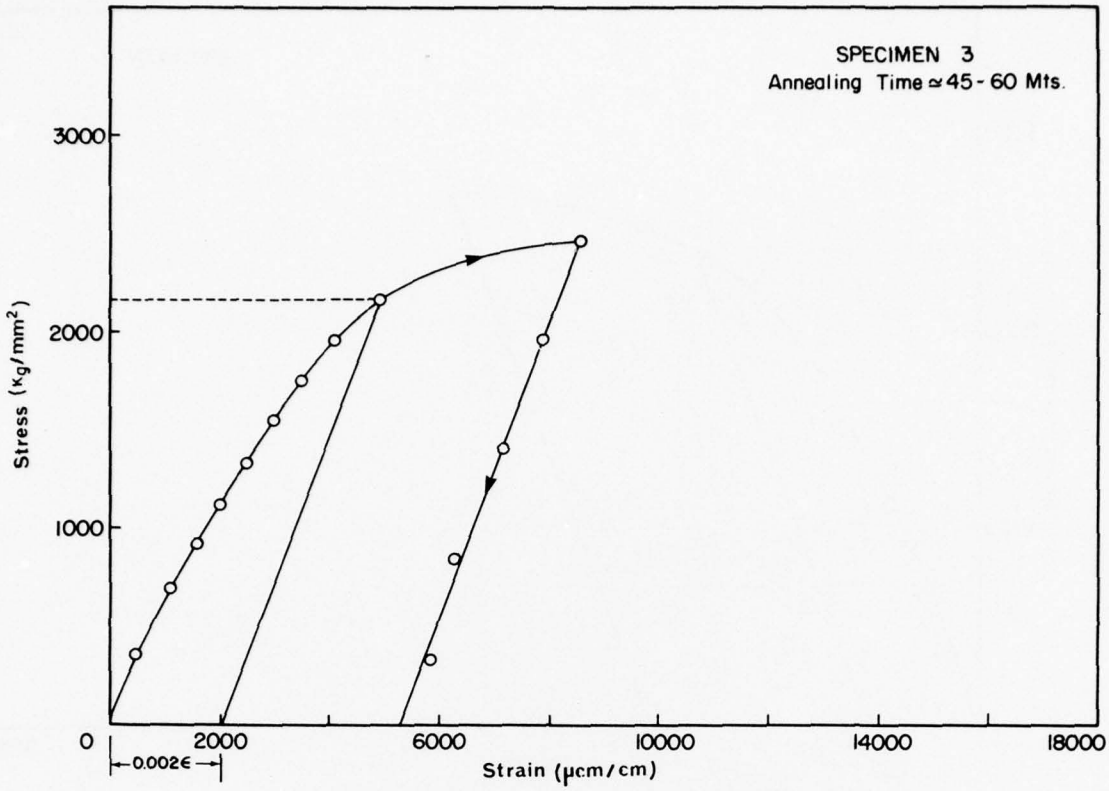

FIG. 63 STRESS-STRAIN CURVE FOR ANNEALED SAMPLE

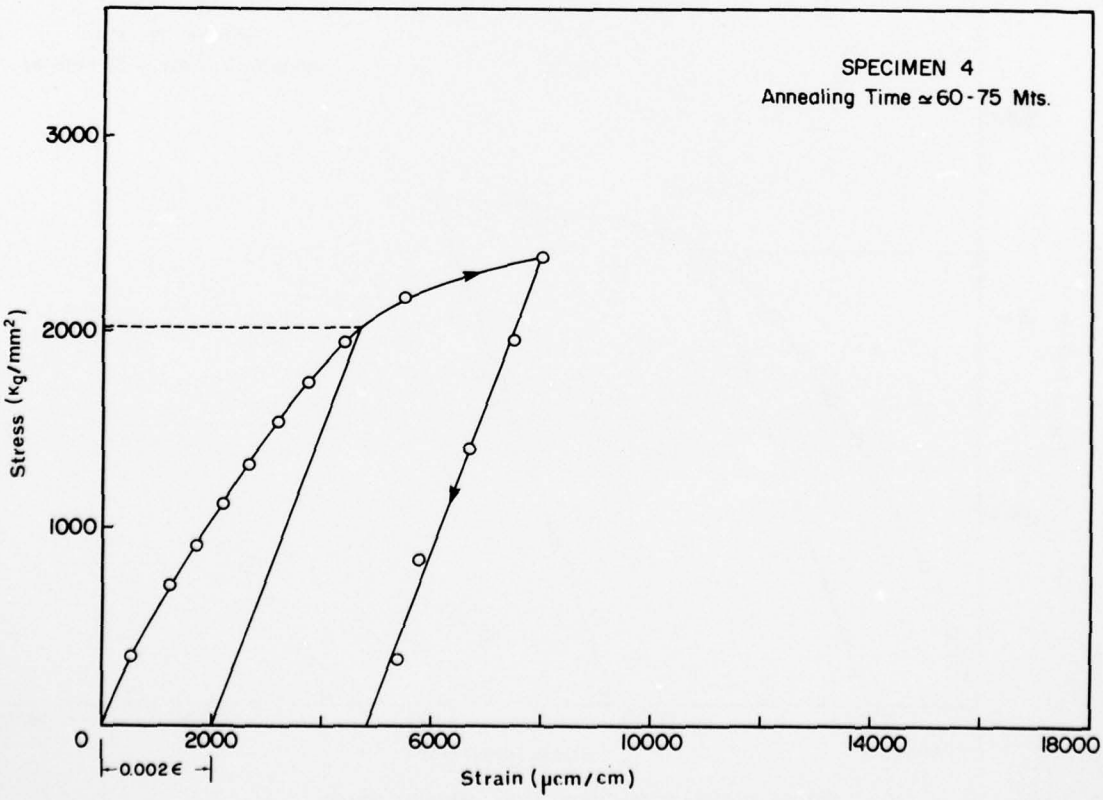

FIG. 64 STRESS-STRAIN CURVE FOR ANNEALED SAMPLE

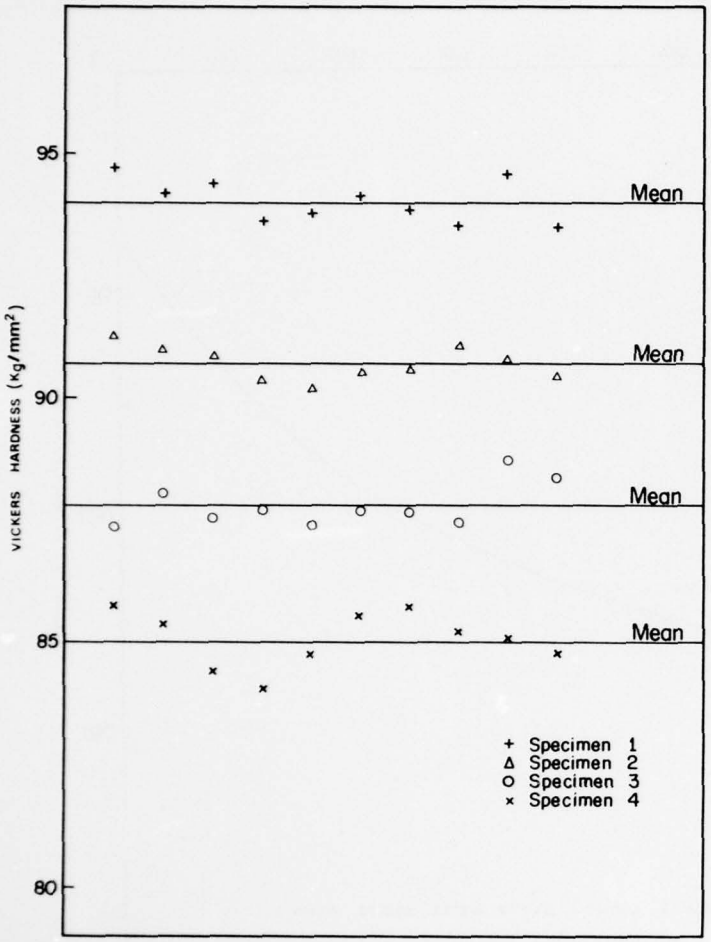

FIG. 65 MICROHARDNESS OF SPECIMENS 1-4

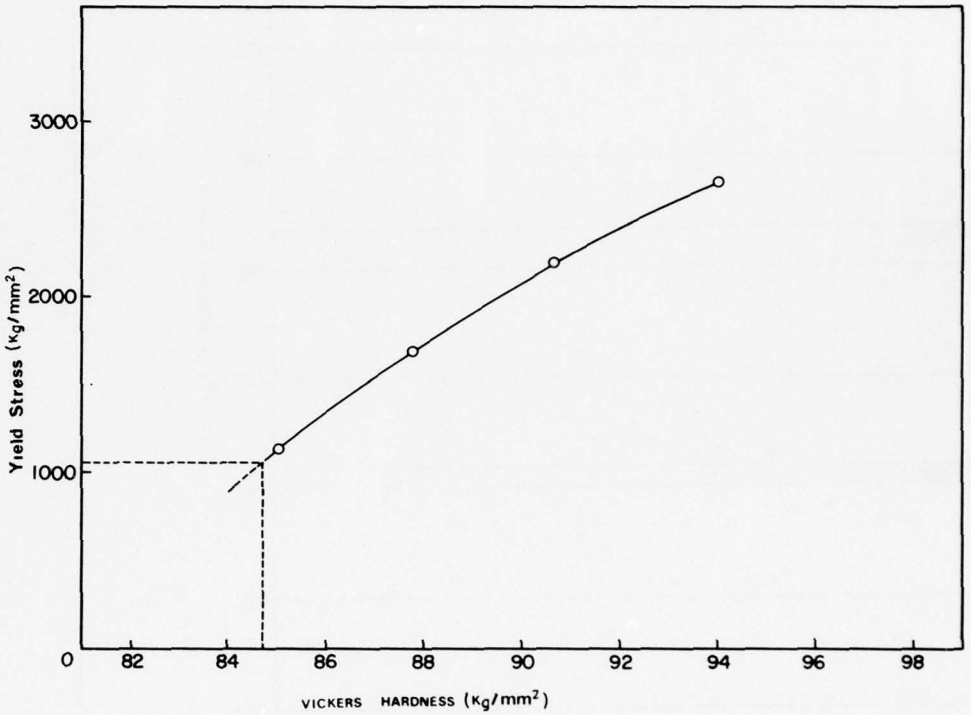

FIG. 66 PLOT OF YIELD-STRESS VERSUS HARDNESS

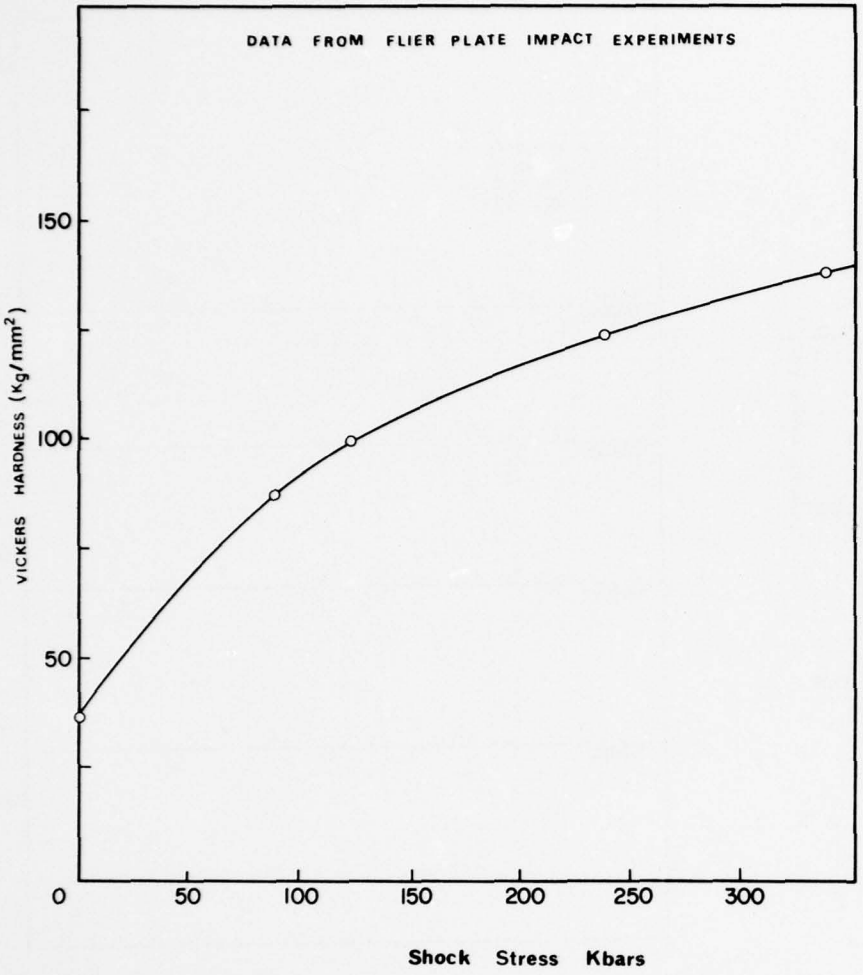

EIG. 67 VARIATION OF HARDNESS WITH. SHOCK STRENGTH (REF. 48)

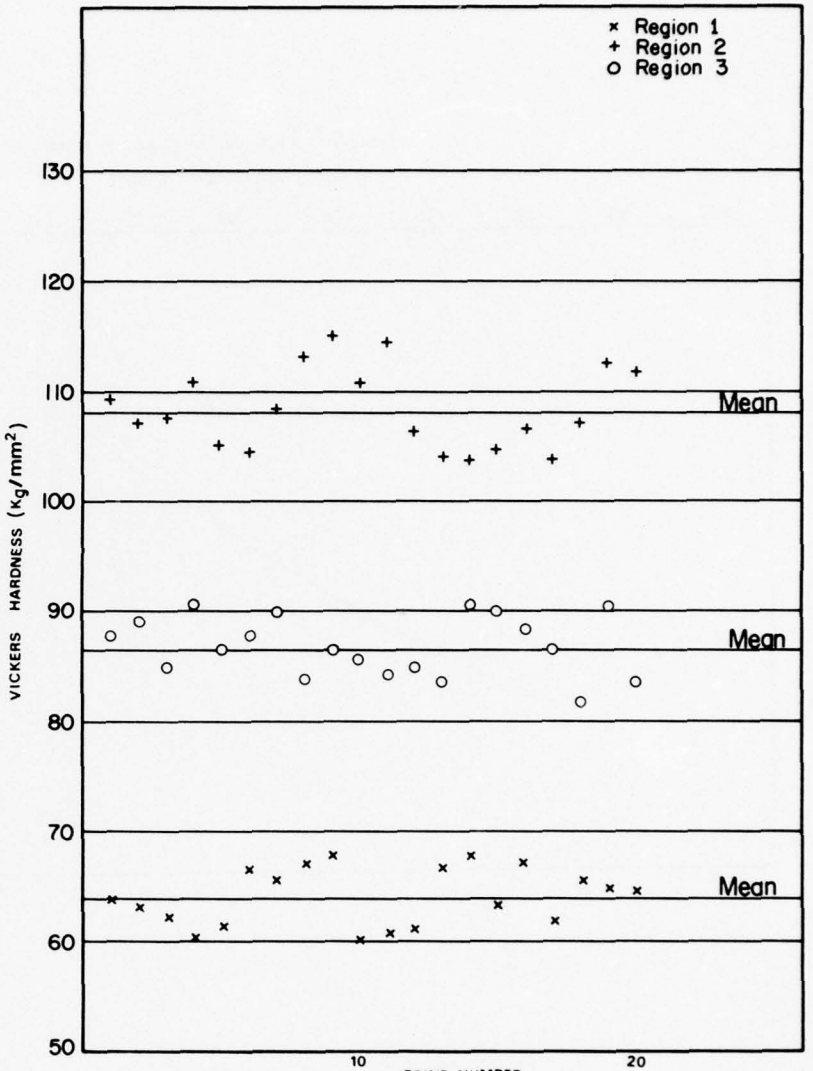

FIG. 68 MICROHARDNESS OF SHOCKED SAMPLE (B)

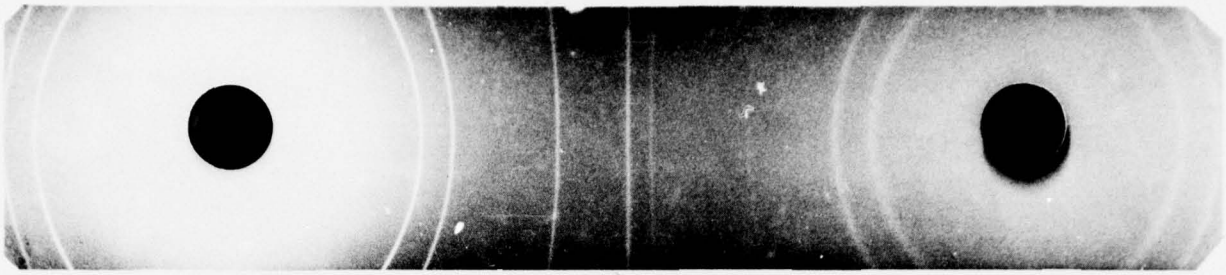

UNSHOCKED COPPER

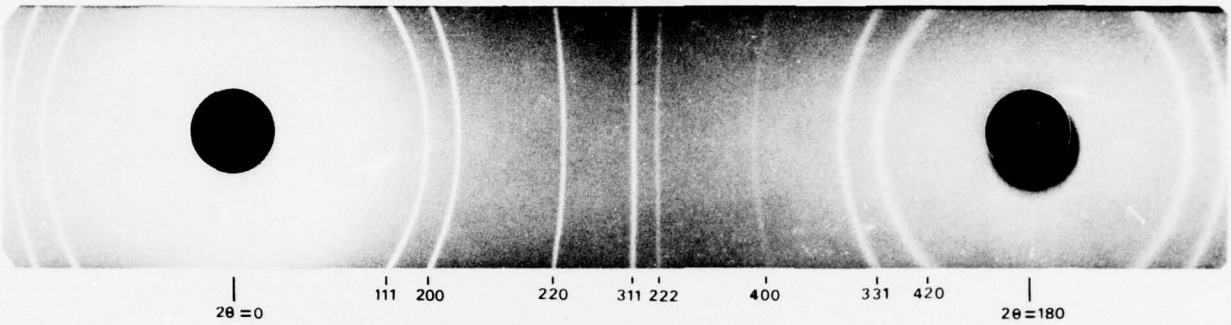

REGION - 1

REGION - 2

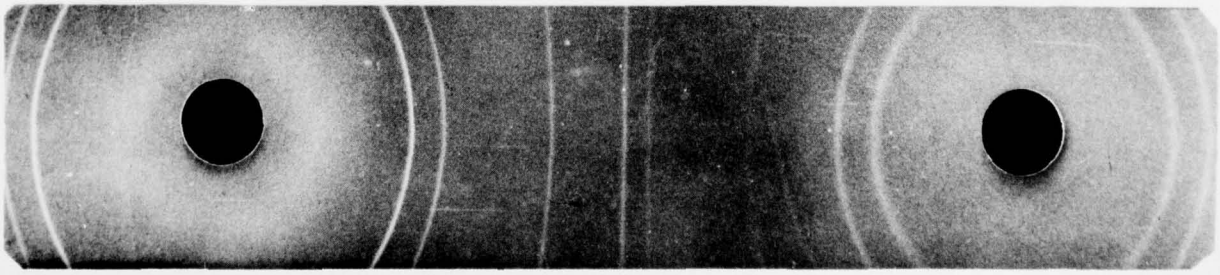

REGION - 3

FIG. 69 X-RAY DIFFRACTION PATTERNS OF COPPER (SPECIMEN B)

APPENDIX A: DESIGN OF A LOW-PASS FILTER TO EXTEND THE OPERATING RANGE OF THE CHARGE AMPLIFIER

Introduction:

The pressure transducer used in the present experiments has a flat response up to 500 KHz according to the manufacturers. But the Kistler charge amplifier used in the early stages of the experimental work was good only up to 150 KHz, because of the presence of a low pass filter. This resulted in serious attenuation of the amplitude of pressures measured. Moreover, the rise-times measured for various initial loading pressures were almost the same, about 1.4 μsec which corresponds with what one would get for a 150 KHz filter. Hence, to actually obtain the real pressure signatures, a low-pass filter of higher cut-off frequency, perhaps as high as 1 MHz was desired. This would make sure that the associated electronics did not limit the measurement capabilities.

Figure A.1 shows the L, R, C circuit for a general low-pass filter:

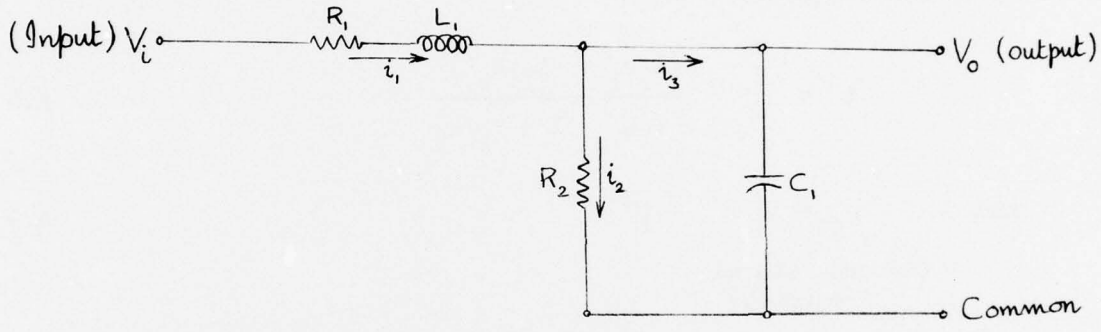

Figure A.1

Basic equations for the circuit are as follows:

$$V_i - V_o = i R_1 + L_1 \, di/dt \qquad \text{A.1}$$

$$V_o = i_2 R_2 \qquad \text{A.2}$$

$$V_o = 1/c_1 \int i_3 \, dt \qquad \text{A.3}$$

$$i_1 = i_2 + i_3 \qquad \text{A.4}$$

Substituting A.2, A.3 and A.4 in A.1, we obtain,

$$\frac{V_o}{V_i} = \frac{1}{(c_1 L_1) D^2 + (R_1 c_1 + \frac{L_1}{R_2}) D + (1 + \frac{R_1}{R_2})} \qquad \text{A.5}$$

where $D = d/dt$

For a general second order system, the solution is given by

$$\frac{V_o}{V_1} = \frac{1}{D^2 + 2 \xi \omega_n D + \omega_n^2} \qquad \text{A.6}$$

Comparing A.5 and A.6

$$\omega_n = \frac{1 + R_1/R_2}{c_1 L_1} \qquad \text{A.7}$$

(natural frequency)

$$\xi = \frac{1}{2} \frac{(R_1 c_1 + L_1/R_2)}{c_1 L_1 \quad 1 + R_1/R_2} \qquad \text{A.8}$$

and $$\omega_d = \omega_n \sqrt{1-\xi^2} \qquad \text{A.9}$$

(damped natural frequency)

In the 150 KHz filter,

$R_1 = 715\ \Omega$; $L_1 = 470\ \mu h$

$c_1 = 1500$ pF ; $R_2 = 15{,}000\ \Omega$

Using Eqns. A.7, A.8 and A.9 yields

$\omega_d = 150$ KHz

as expected.

Now there are two general ways by which the cut-off frequency could be raised to the megabar range.

1. Decreasing the capacitors c_1 or
2. Decreasing the inductance L_1.

In the present work, the capacitance was decreased since capacitors are easily available at almost any given specification and moreover cheap.

The new value of the capacitance c_1 was calculated to be 50 pF using equation A.7, A.8 and A.9 to yield a damped natural frequency of around 1.0 MHz.

APPENDIX B: COMPUTER PROGRAM FOR COMPUTING THE EFFECT OF OFF-CENTRE IMPLOSIONS

```
A=DISTANCE BETWEEN IMPLOSION FOCUS AND THE CENTRE OF TRANSDUCER
R=RADIUS OF THE TRANSDUCER
      DIMENSION X(361)
      R=3.175
      PI=3.1415926
      T=0.1
   60 SUM=0.0
      DUMMY=0.5*PI/180.0
      DO 10 I=1,359
      X(I)=DUMMY
      Y=2.-T
      SUMT=F(X(I),Y)
      SUM=SUM+SUMT
      DUMMY=DUMMY+0.5*PI/180.
   10 CONTINUE
      I=2
      X(I)=0.
      B=F(X(I),Y)*0.5
      I=3
      X(I)=PI
      C=F(X(I),Y)*0.5
      SUMT=PI*(SUM+B+C)/360.
      WRITE(6,50)SUMT
   50 FORMAT(2X,'SUMT=',1F16.8)
      SUM=SUMT
      PAVE=2.*SUM/(Y*PI*R*R)
      WRITE(6,20)PAVE
   20 FORMAT(3X,'PAVE=',1F16.8)
      PACCU=2./(Y*(R**(T)))
      WRITE(6,30)PACCU
   30 FORMAT(3X,'PACCU=',1F16.8)
      ERROR=100.*(PACCU-PAVE)/PACCU
      WRITE(6,40)ERROR
   40 FORMAT(2X,'ERROR=',1F16.8)
      T=T+0.1
      IF(T.GT.1.99)GO TO 70
      GO TO 60
   70 CONTINUE
      STOP
      END
      FUNCTION F(X,Y)
      R=3.175
      A=1.
      B=-A*COS(X)
      C=A*A
      D=COS(X)*COS(X)
      E=C*D
      G=R*R
      H=G-C
      P=E+H
      Q=P**0.5
      F=(B+Q)**Y
      RETURN
      END
```

```
      DIMENSION ERROR(57),T(19),A(3),GLASS(21),RANDY(21)
      READ(5,101)A
      READ(5,102)ERROR
      READ(5,103)T
      WRITE(6,*)A,ERROR,T
      CALL PLOTS(12.0,10.5,2)
      CALL PLOT (0.0,9.5,-3)
      CALL LINEMT(-1)
      CALL AXIS(0.0,0.0,6HT AXIS,-6,10.0,-90.0,0.0,0.2)
      CALL AXIS(0.0,0.0,21HPERCENTAGE ERROR AXIS,21,7.0,0.0,0.0,5.0)
      NPTS=19
      I=1
   20 DO 21 J=1,19
      GLASS(J)=-T(J)
      RANDY(J)=ERROR(I)
      I=I+1
   21 CONTINUE
      GLASS(NPTS+1)=0.0
      GLASS(NPTS+2)=0.2
      RANDY(NPTS+1)=0.0
      RANDY(NPTS+2)=5.0
      CALL LINE(RANDY,GLASS,NPTS,1,1,1)
      IF(I.GT.57)GOTO22
      GOTO20
   22 CALL SYMBOL(6.3,-6.0,0.14,'A=3.0 MM',-90.0,8)
      CALL SYMBOL(6.3,-5.0,0.14,'A=2.0 MM',-90.0,8)
      CALL SYMBOL(6.7,-4.75,0.14,'A=1.0 MM',-90.0,8)
      CALL PLOTND
  101 FORMAT(3F10.0)
  102 FORMAT(6F12.0)
  103 FORMAT(16F5.0)
      STOP
      END
/*
//GO.SYSIN  DD  *
1.0       2.0       3.0
0.47530780  0.89877450  1.27373700  1.60041900  1.87842200  2.10772600
2.28802100  2.41877600  2.50052700  2.53206500  2.51360400  2.44419100
2.32393600  2.15258600  1.92831800  1.65214400  1.32168700  0.93769780
0.49870360  1.90200600  3.62101700  5.16293000  6.52702200  7.71143700
8.71321900  9.52967400  10.15635000 10.58871000 10.82029000 10.84454000
10.65377000 10.23861000 9.58827600  8.69265900  7.53734800  6.10780700
4.38823300  2.36050100  4.31868200  8.3211760   12.02442000 15.43194000
18.54344000 21.35427000 23.85525000 26.03057000 27.85728000 29.30163000
30.31901000 30.84819000 30.80363000 30.09350000 28.56381000 26.03729000
22.27626000 16.97241000 9.72323800
0.1  0.2  0.3  0.4  0.5  0.6  0.7  0.8  0.9  1.0  1.1  1.2  1.3  1.4  1.5  1.6
1.7  1.8  1.9
```

APPENDIX C: METALLURGICAL GLOSSARY

Annealing:- Heating of a material in order to soften it.

Dislocation: - A line imperfection which can be visualized as the boundary between a region of an internal surface over which slip (relative displacement of one part of a crystal relative to another) has occurred and another region over which no slip has occurred.

Point Defect:- A point defect comes about, as a rule, because of the absence of a matrix atom (an atom that would be normally present in a perfect crystal), the presence of an impurity atom, or a matrix atom in the 'wrong' place (a site not occupied in the perfect crystal).

Re-crystallization:

The nucleation of new, strain-free grains in a deformed crystalline matrix.

Stacking Fault:

A surface imperfection which results from the stacking of one atomic plane on another out of sequence, so that the lattices on both sides of the fault have the same orientation but are translated by less than a lattice translation with respect to one another.

Twins: Two regions of a crystal which are mirror images of each other with respect to the plane of the boundary that separates them.

UTIAS TECHNICAL NOTE NO. 209
Institute for Aerospace Studies, University of Toronto
4925 Dufferin Street, Downsview, Ontario, Canada, M3H 5T6

PRESSURE MEASUREMENTS AT THE FOCUS OF COMBUSTION-DRIVEN IMPLOSIONS

Vasudevan, B. Approx.65 pages 69 figures

1. Implosions 2. Detonations 3. Pressure measurements at implosion focus
4. Changes in structure of copper due to implosions

I. Vasudevan, B. II. UTIAS Technical Note No. 209

A detailed experimental investigation was made of time-resolved pressure histories at the focus of combustion-driven implosions in the UTIAS 20 cm diam Implosion Chamber. Gaseous mixtures of stoichiometric hydrogen and oxygen were used in the initial pressure range 1.7 atm (25 psi) to 6.8 atm (100 psi). The gaseous mixtures were detonated using exploding wires. Extended records from a PCB 119M08, 6.3 mm diam piezoelectric pressure transducer gave detailed (averaged) pressure-time histories of initial and subsequent implosions.

A 20-degree conical liner (normally used to protect the front plate of the implosion chamber from damaging off-centred explosive-driven implosions) was used to determine its effect on the pressure histories obtained at the focus of gas-driven implosions. Owing to its deviation from a cone near the apex, the presence of such a liner reduced the peak pressures by about 45%. This fact allowed an indirect estimate of the peak pressure for a 6.8 atm (100 psi) initial pressure run. However, when the conical liner was accurately made, the peak pressures were identical with those without it, as expected from theory.

The actual location of the focal point was determined by taking imprints of implosions on lead witness plates placed at the origin. The imprints were sharp and well-focussed. A maximum degree of off-centredness of about 3/4 mm from the origin, resulted in a reduction of only about 2% in average pressures.

Copper witness plates, subjected to explosive-driven implosions were analyzed using metallurgical techniques. Photomicrographs were taken of the imploded specimen which illustrated the changes in grain size and shape arising from the passage of strong shock waves. Microhardness changes were determined to yield approximate values of peak pressures reached in the specimens.

Available copies of this report are limited. Return this card to UTIAS, if you require a copy.

UTIAS TECHNICAL NOTE NO. 209
Institute for Aerospace Studies, University of Toronto
4925 Dufferin Street, Downsview, Ontario, Canada, M3H 5T6

PRESSURE MEASUREMENTS AT THE FOCUS OF COMBUSTION-DRIVEN IMPLOSIONS

Vasudevan, B. Approx.65 pages 69 figures

1. Implosions 2. Detonations 3. Pressure measurements at implosion focus
4. Changes in structure of copper due to implosions

I. Vasudevan, B. II. UTIAS Technical Note No. 209

A detailed experimental investigation was made of time-resolved pressure histories at the focus of combustion-driven implosions in the UTIAS 20 cm diam Implosion Chamber. Gaseous mixtures of stoichiometric hydrogen and oxygen were used in the initial pressure range 1.7 atm (25 psi) to 6.8 atm (100 psi). The gaseous mixtures were detonated using exploding wires. Extended records from a PCB 119M08, 6.3 mm diam piezoelectric pressure transducer gave detailed (averaged) pressure-time histories of initial and subsequent implosions.

A 20-degree conical liner (normally used to protect the front plate of the implosion chamber from damaging off-centred explosive-driven implosions) was used to determine its effect on the pressure histories obtained at the focus of gas-driven implosions. Owing to its deviation from a cone near the apex, the presence of such a liner reduced the peak pressures by about 45%. This fact allowed an indirect estimate of the peak pressure for a 6.8 atm (100 psi) initial pressure run. However, when the conical liner was accurately made, the peak pressures were identical with those without it, as expected from theory.

The actual location of the focal point was determined by taking imprints of implosions on lead witness plates placed at the origin. The imprints were sharp and well-focussed. A maximum degree of off-centredness of about 3/4 mm from the origin, resulted in a reduction of only about 2% in average pressures.

Copper witness plates, subjected to explosive-driven implosions were analyzed using metallurgical techniques. Photomicrographs were taken of the imploded specimen which illustrated the changes in grain size and shape arising from the passage of strong shock waves. Microhardness changes were determined to yield approximate values of peak pressures reached in the specimens.

Available copies of this report are limited. Return this card to UTIAS, if you require a copy.

UTIAS TECHNICAL NOTE NO. 209
Institute for Aerospace Studies, University of Toronto
4925 Dufferin Street, Downsview, Ontario, Canada, M3H 5T6

PRESSURE MEASUREMENTS AT THE FOCUS OF COMBUSTION-DRIVEN IMPLOSIONS

Vasudevan, B. Approx.65 pages 69 figures

1. Implosions 2. Detonations 3. Pressure measurements at implosion focus
4. Changes in structure of copper due to implosions

I. Vasudevan, B. II. UTIAS Technical Note No. 209

A detailed experimental investigation was made of time-resolved pressure histories at the focus of combustion-driven implosions in the UTIAS 20 cm diam Implosion Chamber. Gaseous mixtures of stoichiometric hydrogen and oxygen were used in the initial pressure range 1.7 atm (25 psi) to 6.8 atm (100 psi). The gaseous mixtures were detonated using exploding wires. Extended records from a PCB 119M08, 6.3 mm diam piezoelectric pressure transducer gave detailed (averaged) pressure-time histories of initial and subsequent implosions.

A 20-degree conical liner (normally used to protect the front plate of the implosion chamber from damaging off-centred explosive-driven implosions) was used to determine its effect on the pressure histories obtained at the focus of gas-driven implosions. Owing to its deviation from a cone near the apex, the presence of such a liner reduced the peak pressures by about 45%. This fact allowed an indirect estimate of the peak pressure for a 6.8 atm (100 psi) initial pressure run. However, when the conical liner was accurately made, the peak pressures were identical with those without it, as expected from theory.

The actual location of the focal point was determined by taking imprints of implosions on lead witness plates placed at the origin. The imprints were sharp and well-focussed. A maximum degree of off-centredness of about 3/4 mm from the origin, resulted in a reduction of only about 2% in average pressures.

Copper witness plates, subjected to explosive-driven implosions were analyzed using metallurgical techniques. Photomicrographs were taken of the imploded specimen which illustrated the changes in grain size and shape arising from the passage of strong shock waves. Microhardness changes were determined to yield approximate values of peak pressures reached in the specimens.

Available copies of this report are limited. Return this card to UTIAS, if you require a copy.

UTIAS TECHNICAL NOTE NO. 209
Institute for Aerospace Studies, University of Toronto
4925 Dufferin Street, Downsview, Ontario, Canada, M3H 5T6

PRESSURE MEASUREMENTS AT THE FOCUS OF COMBUSTION-DRIVEN IMPLOSIONS

Vasudevan, B. Approx.65 pages 69 figures

1. Implosions 2. Detonations 3. Pressure measurements at implosion focus
4. Changes in structure of copper due to implosions

I. Vasudevan, B. II. UTIAS Technical Note No. 209

A detailed experimental investigation was made of time-resolved pressure histories at the focus of combustion-driven implosions in the UTIAS 20 cm diam Implosion Chamber. Gaseous mixtures of stoichiometric hydrogen and oxygen were used in the initial pressure range 1.7 atm (25 psi) to 6.8 atm (100 psi). The gaseous mixtures were detonated using exploding wires. Extended records from a PCB 119M08, 6.3 mm diam piezoelectric pressure transducer gave detailed (averaged) pressure-time histories of initial and subsequent implosions.

A 20-degree conical liner (normally used to protect the front plate of the implosion chamber from damaging off-centred explosive-driven implosions) was used to determine its effect on the pressure histories obtained at the focus of gas-driven implosions. Owing to its deviation from a cone near the apex, the presence of such a liner reduced the peak pressures by about 45%. This fact allowed an indirect estimate of the peak pressure for a 6.8 atm (100 psi) initial pressure run. However, when the conical liner was accurately made, the peak pressures were identical with those without it, as expected from theory.

The actual location of the focal point was determined by taking imprints of implosions on lead witness plates placed at the origin. The imprints were sharp and well-focussed. A maximum degree of off-centredness of about 3/4 mm from the origin, resulted in a reduction of only about 2% in average pressures.

Copper witness plates, subjected to explosive-driven implosions were analyzed using metallurgical techniques. Photomicrographs were taken of the imploded specimen which illustrated the changes in grain size and shape arising from the passage of strong shock waves. Microhardness changes were determined to yield approximate values of peak pressures reached in the specimens.

Available copies of this report are limited. Return this card to UTIAS, if you require a copy.